Title	
Author(s)	Mira, Bulbul
Citation	
Issue Date	2017-06
Type	Thesis or Dissertation
Text version	ETD
URL	http://hdl.handle.net/10119/14753
Rights	
Description	Supervisor: , ,

Doctoral Dissertation

New Reactor Granule Technology for Fabrication of Functionally
Advantageous Highly Filled Nanocomposites

BULBUL MAIRA

Supervisor: Assoc. Prof. Toshiaki Taniike

School of Materials Science

Japan Advanced Institute of Science and Technology

June 2017

1

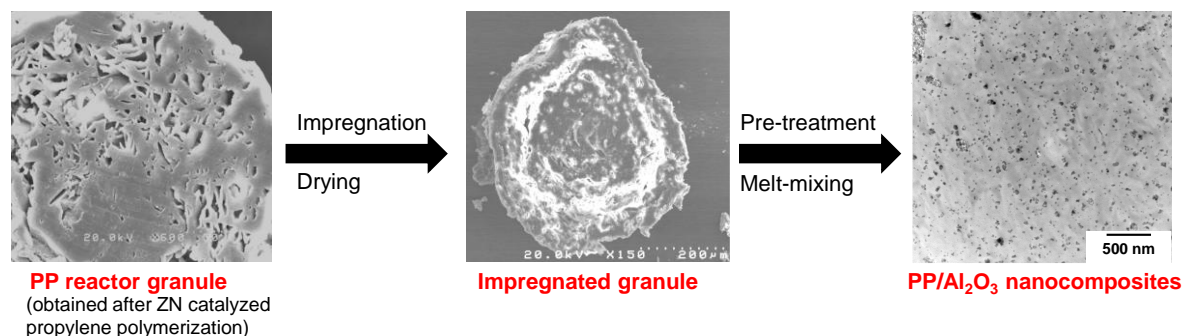# New Reactor Granule Technology for the Fabrication of Functionally Advantageous Highly Filled Nanocomposites

Bulbul Maira

s1440155

Polymer nanocomposites are an emerging class of hybrid materials, where a small fraction of nano-sized filler offers enhancement in properties such as gas barrier, thermal stability, flame retardancy, mechanical properties and so on. A major issue associated with the fabrication of nanocomposites is the dispersion of nanofillers in the polymer matrix because of the great tendency of nanoparticles to agglomeration. Owing to the fact that nano-level dispersion is a prerequisite in realizing the performance of nanocomposites, various strategies such as addition of a compatibilizer or surface modifier have been employed. These dispersants improve the compatibility between nanoparticles (filler) and the polymer, but at the same time result in unfavourable drawbacks such as additional cost, accelerated degradation, processability challenges and so on.

The dispersion problem is extremely challenging in the case of chemically inert polyolefins and also when a relatively high loading of nano-sized filler is required in specific applications such as flame retardancy, thermal conductivity and electrical properties. Ideally, the best approach is to achieve nano-level dispersion without inclusion of any dispersants. Our research group has successfully disclosed a methodology for the fabrication of polyolefin nanocomposites based on an in-situ method *i.e.* in-situ formation of nanoparticles in the presence of the polyolefin [1]. The novelty lies at the fact that it involves the impregnation of metal alkoxides in the porosity of polymer reactor granule and subsequent chemical conversion of the metal alkoxides into inorganic nanoparticles during melt-processing. The reported methodology is known as a new Reactor Granule Technology (RGT) and the concept was firstly exemplified by the preparation of polypropylene (PP)-based nanocomposites with TiO_2 for UV-cut transparent PP. Following this, in this research the RGT was further explored and modified to prepare flame retardant $PP/Mg(OH)_2$ nanocomposites. To achieve flame retardancy, a relatively high filler loading is required and a great challenge existed in controlling the dispersion at a high filler loading. A modified scheme including pre-treatment was invented and it was found that the prepared nanocomposites exhibited uniform dispersion of $Mg(OH)_2$ nanoparticles even at a high filler loading, with which sufficient flame retardancy was facilitated at a filler loading of approximately half compared with the conventional preparation. The results revealed that the modified methodology not only offers uniform dispersion of nanoparticles in a dispersant-free manner but also allows access for the fabrication of highly filled nanocomposites.

Further to generalize the modified RGT to various kinds of highly filled nanocomposites, it was applied for fabrication of functionally advantageous PP nanocomposites with oxide nanoparticles, namely PP/TiO_2 and PP/Al_2O_3 nanocomposites (**Scheme 1**). It was concluded that the reactor granule technology is a versatile approach for the fabrication of polyolefin-based nanocomposites, offering excellent dispersion over a wide range of filler loading and superior properties even without the use of any dispersants. Finally, for maximizing the potential of methodology, the development of heat releasing polyolefin nanocomposites based on modified reactor granule technology was focused. It was found that the interfacial modification of *in-situ* generated Al_2O_3 nanoparticles played a significant role in the improvement of thermal conductivity.

PP reactor granule
(obtained after ZN catalyzed propylene polymerization)

Impregnation / Drying

Impregnated granule

Pre-treatment / Melt-mixing

500 nm

PP/Al$_2$O$_3$ nanocomposites

Scheme 1. Concept of modified reactor granule technology

Keywords: Polyolefins, Highly filled nanocomposites, Reactor granule technology, *In-situ* generation, Dispersant-free

Referee-in-chief: Associate Professor   Toshiaki Taniike

Japan Advanced Institute of Science and Technology

Referees: Professor   Kohki Ebitani

Japan Advanced Institute of Science and Technology

Professor   Masayuki Yamaguchi

Japan Advanced Institute of Science and Technology

Associate Professor   Ken-ichi Shinohara

Japan Advanced Institute of Science and Technology

Professor   Koh-hei Nitta

Kanazawa University

Preface

The present thesis is submitted for the Degree of Doctor of Philosophy at Japan Advanced Institute of Science and Technology, Japan. The thesis is consolidation of results of the research work on the topic "New Reactor Granule Technology for Fabrication of Functionally Advantageous Highly Filled Nanocomposites" under the supervision of Assoc. Prof. Toshiaki Taniike at the School of Materials Sciences, Japan Advanced Institute of Science and Technology during July 2014-June 2017.

First of all, **Chapter 1** is a general introduction according to the object of this research. **Chapter 2** introduces new reactor granule technology for highly filled nanocomposites with focus on fabrication of polypropylene/magnesium hydroxide nanocomposites for effective flame retardation. **Chapter 3** reports the application of reactor granule technology for fabrication of functionally advantageous polypropylene nanocomposites with oxide nanoparticles. **Chapter 4** reports the utilization of reactor granule technology for the development of heat releasing polyolefin nanocomposites. Finally, **Chapter 5** describes the general summary and conclusion of this thesis. To the best of my knowledge, the work is original and no part of this thesis has been plagiarized.

School of Materials Science   Bulbul Maira

Japan Advanced Institute of Science and Technology

June 2017

Acknowledgements

I extend my thanks to my friends Ashutosh Thakur, Neha Sharma and Akanksha Matta for their utmost care and moral support.

I would like to thank God for giving me the strength and wisdom to complete this task and sending all these people in my life.

School of Materials Science   Bulbul Maira

Japan Advanced Institute of Science and Technology

June 2017

Table of Contents

Chapter 1

General Introduction

Chapter 1

1.1 Polymer Nanocomposites

Polymers

   In nature, polymers are the most widespread naturally occurring substances. In fact, there exists a great similarity between the synthetic polymer and the basic molecular structure of all plant and animal life. Natural polymers include materials such as rubber, cellulose, silk and bitumen. However, synthetic polymers are mainly used for engineering design and are often specifically designed by chemical engineers or chemists for some specific purpose. Other engineers (civil, mechanical *etc.*) sometimes work directly with chemical engineers or chemists to synthesize a polymer with particular characteristics or typically design engineering components from the available materials [1]. In our daily lives, polymers play a major role due to their properties such as light weight, ease of processing, low cost, resistance to corrosion, transparency and so on. Due to their long chain molecular structure, many of the useful properties of polymers are in fact unique to polymers. Polymers can be broadly categorized into thermosetting resins and thermoplastics, out of which thermoplastics account for more than 70% of all polymers produced. Depending on their intrinsic properties and applications, thermoplastics can be classified into commodity, engineering and performance plastics. Generally, plastics show a trend towards commoditization both in terms of increasing production volume and decreasing production

cost. Therefore, it is challenging to introduce new polymers into the market for engineering applications. As a consequence, the current focus is at exploring and improving the performance of existing polymers [2]. The properties of polymers are not only affected by the chemical structure but also by the processing step. Additionally, the use of fillers also has a large impact on the performance of polymers. Maximizing the potential of existing polymers by the use of fillers has become a significant topic in the development of polymers.

Polymer Nanocomposites

Polymer nanocomposites, have garnered significant interest since their invention in the late 1990s. As surveyed by Vaia and Maguire, the research and development funding as well as the number of articles and patents, in this area has been growing exponentially [3]. For instance, from 1988 to 2005 the total number of hits for 'polymer nanocomposites' on Scifinder is 9400, where since 1992 the yearly number has roughly doubled every two years. In the last years, this growth has continued:

Years	2006	2007	2008	2009	2010	2011	1988-2011
Number of records	2995	3640	3863	4182	4910	5197	34112

Polymer nanocomposites are the combination of polymers filled with fillers having one dimension smaller than 100 nm. In zero-dimensional (0D) nanocomposites, all three

dimensions of the filler are of the order of 1 nm (metal and metal-oxide nanoparticles, spherical silicate nanoparticles, quantum dots, detonation nano diamonds *etc*.). One-dimensional (1D) nanocomposites contain filler nano-sized in two dimensions (fibers, whiskers or nanotubes) and a two-dimensional (2D) nanocomposite consists of nanometer thickness (graphite, layered silicates *etc.*) [4-14].

Based on application, nanocomposites can be divided into two types: structural and functional. In case of structural nanocomposites, the introduction of filler efficiently enhances their inflammability, durability, barrier properties and processibility. In some cases, the nano-sized fillers with adsorbed substances are able to impart functional properties, for *e.g.* electro conductivity or biocidal properties. Theoretical models of such composites are described by the laws of classical mechanics of solids and viscous fluids. For the fabrication of structural nanocomposites, it is necessary to create stable mixtures in which inorganic nanoparticles are well dispersed throughout the bulk of a polymer matrix, have no tendency for coagulation and in the case of anisodiametric particles are capable of orientation during the preparation. In the case of functional composites, the role of filler is much more significant, since the magnetic, optical and electric properties of materials substantially depend on the characteristics of nanoparticles [15-17]. The interaction between the polymer matrix and filler at the molecular level is of great significance because it leads to synergy of useful properties of the organic and inorganic components of a material [18,19].

Preparation of Polymer Nanocomposites

Several processing techniques have been explored to disperse nanoparticles in to the polymer matrix including *in-situ* method, melt-compounding and solution processing [20-26]. The *in-situ* preparation can be divided into two routes: *in-situ* polymerization in the presence of nanoparticles and *in-situ* synthesis of nanoparticles in the polymer matrix [24-28]. In the *in-situ* polymerization method, the particles are first dispersed in the monomer(s) followed by the polymerization. Yang *et al.* has reported this method for the preparation of poly(amide-6) /silica nanocomposites [24]. Firstly, the silica particles were with ε-caproamide followed by addition of the appropriate polymerization initiator. The mixture was then polymerized at elevated temperature under a nitrogen atmosphere [24]. Well dispersed particles with a particle size of ~50 nm were obtained, but aggregation occurred on using particle sizes of ~12 nm [26]. The aggregation was explained to be originated due to increased surface energy of smaller particles.

Ash *et al.*[29] and Siegel *et al.*[30] obtained well dispersed alumina nanoparticles in the PMMA matrix. They firstly added alumina nanoparticles to methylmethacrylate (MMA) and dispersed them through sonication with subsequent addition of the initiator and the chain transfer reagent. The *in-situ* synthesis of nanoparticles in the polymer matrix was reported by Jain *et al.* who combined a solid-state modification of isotactic poly(propylene) (iPP) and an *in-situ* sol-gel reaction for the preparation of iPP/silica nanocomposites [31]. Well dispersed particles having size in the range of 20-50 nm were obtained.

Another frequently used technique for the dispersion of nanoparticles is the solution processing. Vollenberg *et al.* dissolved poly(imide) and the clay particles in polar solvent for several hours and then the mixture was solvent casted to allow for the solvent to evaporate [20]. They were able to produce well-dispersed poly(imide)-organophilic clay nanocomposites. Bansal *et al.* achieved excellent dispersions via a toluene solution mixing of polystyrene with untreated or low molar mass PS-grafted silica nanoparticles [32]. They showed that the nanoparticle dispersion was strongly affected by the choice of the solvent [33].

The majority of synthetic polymers were prepared via melt-compounding [34]. Chan *et al.* prepared iPP/CaCO$_3$ nanocomposites through melt-mixing of iPP with CaCO$_3$ nanoparticles [22]. They obtained reasonably well-dispersed nanocomposites at filler loading of 4.8 and 9.2 vol%, but at 13.2 vol% excessive aggregation of nanoparticles occurred. Zhou *et al.* combined *in-situ* nanoparticle surface modification with melt-mixing whereas Rong *et al.* [35] melt-compounded iPP with pre-treated silica nanoparticles to study the influence of interfacial interactions in iPP/silica nanocomposites while Zhou *et. al.*[36] combined the in-situ nanoparticle surface modification with melt-mixing. They concluded that an effective way to improve interfacial interaction is to carry out grafting and cross-linking of nano-silica during melt-mixing with iPP.

Due to different physical and chemical characteristics of the used components, it is difficult to use a universal approach for the fabrication of polymer nanocomposites. Moreover, different processing techniques in general do not yield similar results. Each system requires

a special set of processing conditions based on the desired processing and material properties. It can be concluded from above that one of the key issues in choosing processing technique is how well the nanoparticles can be dispersed in the polymer matrix.

State of Dispersion

The advantages of nanocomposites can be exploited if the state of dispersion of nanoparticles can be controlled. In some cases, a perfectly homogenous dispersion is required, while in other cases such as carbon nanotubes filled systems for electro conductive properties, a percolative network is necessary, which can be achieved by controlled aggregation of nanoparticles [37]. Mediocre performance of nanocomposites can be attributed to number of factors such as poor dispersion, poor alignment, poor interfacial load transfer to the interior of filler bundles, process related deficiencies and fractal nature of filler clusters [38].

The filler geometry is an important factor that influences the state of dispersion of nanoparticles [39]. In general, 3-dimensional fillers are easier to disperse than low dimensional fillers. The difference is due to the fact that 3-dimensional quasi-spherical particles exhibit only point to point contacts whereas in case of 1-dimensional rods or tubes increased particle-particle interaction arises due to contact along the full length of the cylinder. 2-dimensional sheets even have a larger contact area. The increased particle contact area as well as resulting interaction makes homogeneous dispersion even more

difficult. Considering these factors, 3-dimensional fillers such as spherical particles are easier to disperse than either rods or sheets.

In addition to the filler geometry, the relative size of the polymer and the nanoparticles also affects the final state of dispersion. Mackay *et al* [40] showed that that the thermodynamic stability of the nanocomposites was enhanced if radius of gyration (R_g) of the linear polymer is greater than the radius of the nanoparticles. If R_g of the polymer is smaller than the radius of the nanoparticles, the surface energy mismatch between the polymer chains and the nanoparticles is larger, leading to aggregation of the nanoparticles. Other groups observed a more complex behavior *i.e.* the state of dispersion can be poor or good with increasing R_g [41-43].

Another parameter that affects the final dispersion state of dispersion of nanoparticles is the polymer-nanoparticle interactions.

Polymer-Filler Interactions

In a polymer-filler system, even at a low concentration, a considerable portion of the polymer is affected by the filler due to polymer-filler interactions. The type of interaction between polymer segments and filler surfaces can be divided into two categories [44]:

i) interfaces in which the segment-to-surface interactions are weak and dispersive, and the polymer are physisorbed at the interfaces. *e.g.* isotactic PP on graphite.

ii) interfaces in which the segment-to-surface interactions are strong and specific, and the polymer are chemisorbed at the interfaces. *e.g.* PMMA on aluminium.

In polymer nanocomposites, even very weak interaction between a single monomeric unit and particle surface can be magnified into powerful attractive or repulsive forces. This is because polymer having high molar mass have many units, which can interact with the nanoparticle surface. Despite of a certain intramolecular order, a linear chain in the polymer melt can be considered as random coil. If such a chain approaches an impermeable surface, it changes to a train-loop-tail structure [45] (**Fig. 1**). The number of adsorbed units along the linear chain anchored to the particle surface depends on both the molar mass of the linear chain and the surface to polymer interaction energy. Generally, the number of adsorbed units to the particle surface increases if the molar mass of the polymer chain or number of repeating units increases.
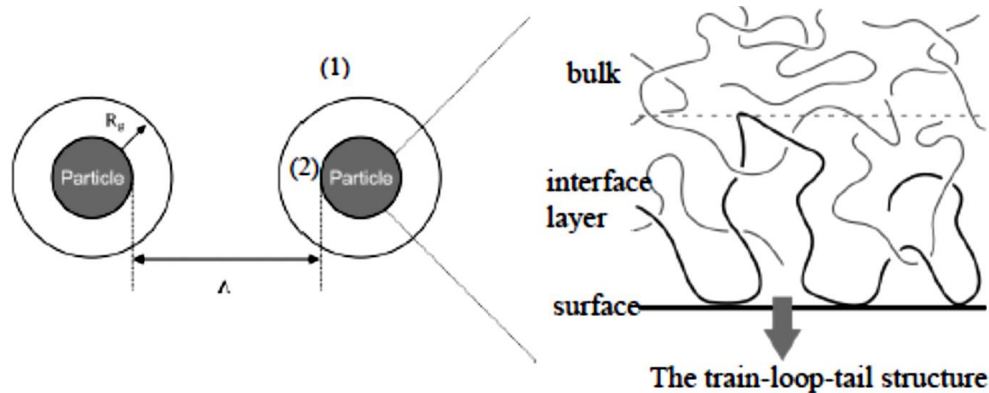

Figure 1. Representation of ideal composite structure, where two polymers are considered (1) mobile bulk polymer and (2) immobilized 'effective' phase (interface layer + particle surface) [46].

In addition to the two-dimensional trains, which are anchored to the surface, the rest of the chain is in the vicinity of the surface in the form of loops and tails with their segments extending into the liquid phase. The relative sizes of loops, trains, and tails depend on the flexibility and length of the chain [47]. Even at low particle concentrations, individual polymer chains can physically attach to multiple particles, forming bridging networks [48]. An assumption for the adsorption process is that the polymer chains initially attach very rapidly to the bare nanoparticle surface and with the increasing coverage the attachment process slows down proportionally. The adsorption energy of the polymer chains and the molar mass distribution has an effect on the adsorption process [49-53]. For polymers with a broad molar mass distribution, the surface is assumed to be saturated with a macromolecular monolayer, composed of low molar mass species. Later, the lower molar mass chains are substituted by the high molar mass chains due to an entropic reason. This adsorption process is irreversible, since many points along the chain are attached to the nanoparticle surface. The polymer matrix becomes a non-continuum medium, if the polymer chains are strongly adsorbed on the nanoparticles surface. The nanoparticles surrounded by the polymer chains or interfacial chains form new filler particles with an increased effective filler volume. These particles consist of a hard core surrounded by an immobilized soft polymer shell and are regarded as core-shell particles. The thickness of the polymer shell is related to the molar mass. Generally, the adsorption process of the polymer chains to the filler surface is complicated to have a quantitative analysis. Different adsorption processes affect the properties of the polymer matrix.

Chapter 1

Potential Applications and Future Perspective of Nanocomposites

Nanocomposites could achieve dramatic commercial importance in the field of advance composites. Particularly, in case of cross-ply composites, due to low strength and modulus of the matrix phase, carbon reinforced composites have a limit on achievable properties. Modification of the matrix phase with carbon nanotubes at the lower scale of dimensions and carbon nanofibers at a higher dimension scale would allow for significant increase in the strength and modulus contributions of the matrix to the overall composite properties. This could offer dramatic improvement in cross-ply composites which are the major type of composite structure utilized in advanced composite applications. These improvements are key to wind energy turbine and future aircraft applications.

Translation of secret of nature's methodology for optimization of material properties by nano-level construction (biomimetics) to polymer nanocomposites could allow great advances. Nanostructures surfaces have been observed to yield exceptional adhesion (gecko foot) and super hydrophobic character (lotus leaf). The combination of the biological and polymer material science disciplines often involves the design of nanoscale polymeric composite materials to mimic the biological systems.

It is expected that the fundamental and applied research in the field of polymer nanocomposites will facilitate the development of innovative materials with enhanced properties involving components not yet foreseeable or of novel applications for existing materials with suitably tailored properties.

1.2 Theoretical Background

<u>Surface activity and surface energy</u>

   Surface forces play an important role in the preparation and performance of polymer nanocomposites, as they influence the adhesion between the polymer and the nanoparticles. The reinforcement of elastomers by particulate fillers is dependent on the physical interactions between the filler and rubber matrix. The surface activity is related to the number and type of active functional groups and the surface energy. The surface activity determines the compatibility between the filler and a specific elastomer and the ability of an elastomer to adhere to the inorganic phase. Generally, it is attributed to the distribution of active sites on the surface of reinforcing fillers for the adsorption of polymer segments. Even though a filler possesses high aspect ratio and a high surface, it can offer relatively poor reinforcement when its specific surface possesses low activity. Carbon black (CB) is a good example of a filler which displays high surface activity due to the variety of chemical groups such as phenols, quinone, carboxylic acid groups present on the filler surface. Due to the presence of numerous active sites on the surface of CB, it is compatible and interacts strongly with the elastomers as well as non-polar rubbers such as NR and SBR, without the need of any surface modifiers.

   In contrast to CB, silica is hydrophilic with silane (Si-OR) and acidic silanol (Si-OH) groups attached to the surface. Due the highly polar surface, silica does not interact well with non-polar elastomers such as SBR. The presence of silanol groups on the surface leads to strong filler-filler interactions, resulting in high level of interparticle interaction and finally

in agglomeration. This indicates that CB being less polar than silica is better suited for the reinforcement of non-polar hydrocarbon elastomers. The surface of non-black fillers, such as silica should be modified to decrease their hydrophilicity and polarity and increase their compatibility with elastomers for improved reinforcing capabilities.

One of the most convenient and sensitive techniques for the characterization of surface activity of fillers is inverse gas chromatography (IGC) at infinite dilution. It is based on the adsorption and desorption kinetics of the gas molecules in the flow of an inert carrier gas and is widely used to determine the surface energy as well as the highly active present on the filler surfaces. A good match of surface energies indicates polymer-filler interactions and greater compatibility of the rubber and filler. For instance, a high degree of agglomeration in the rubber matrix results from the large energy differences between the polymer and filler, strong interparticle forces and high filler loadings. The surface energy of the filler gives the measure of the compatibility with the rubber. The surface energies of fillers are much higher than that of organic polymers. Most fillers have surface energies greater than 100 mJ/m^2, whereas polymers typically have surface energies of approximately 35 mJ/m^2.

Wang and coworkers utilized IGC to compare the surface energies of a wide range of commercial CB and silica. The surface energy of fillers can be described by the following simple equation (**Eq. 1**):

$$\gamma_S = \gamma_S^D + \gamma_S^{SP} \quad \textbf{(1)}$$

where γ_s is the surface energy, γ_s^D is the dispersive component and γ_s^{SP} is the specific or polar component. Fillers with with high filler-filler interaction will have high specific component of the free surface energy (γ_s^{SP}), and fillers with high rubber-filler interaction will have high dispersive component of the surface free energy (γ_s^D). CB possesses a high γ_s^D, which is related to stronger interactions between the hydrocarbon rubber and the filler. In contrast, silica is characterized by a lower γ_s^D, and a higher specific component of the surface free energy, represented by a high S_f, which is related to stronger filler-filler interactions.

The surface characteristics of silica can be altered by surface modification, thereby decreasing the specific component of the surface free energy and consequently, increasing interactions between the rubber and silica. The resulting material exhibits improved dispersion and remarkably enhanced processability. In addition, other types of fillers such as double layered hydroxides, montmorillonite and graphene have been modified by various types of organic compounds to control the filler surface energy, reduce hydrophilicity and increase the interlayer distance. This has resulted in enhanced contact between the rubber and filler.

Wetting and Spreading

The wetting parameter is important in the bonding or adherence of the filler to the polymer and depends on the filler hydrophilicity or polarity and the available polar groups of the polymer. Wetting depends on the energies (or surface tensions) of the interfaces

involved such that the total energy is minimized. The degree of wetting is determined by the

contact angle Θ_c, at which the liquid-gas interface γ_{LG} meets the solid-liquid interface γ_{SL}.

A contact angle of 90° or greater, generally characterizes the surface as non-wetttable, called

hydrophobic and interact through van der waals forces and have lower or no capacity to form

hydrogen bonds. On the other hand, if the contact angle is less than 90°, the fluid will spread

to cover a large area of the surface and the wettable surface may be termed as hydrophilic.

Hydrophilicity means that molecule can transiently bond to water through hydrogen bonding.

The spreading parameter S is useful for gauging wetting and is given by **Eq. 2**:

$$S = \gamma_{SG} - (\gamma_{SC} + \gamma_{LG}) \quad \textbf{(2)}$$

When S < 0, there is partial wetting, when S > 0, the liquid wets the surface completely.

<u>Adhesion</u>

The degree of adhesion between the filler and polymer matrix influences the mechanical

properties of nanocomposites. However, due to several factors such as the specific

combination of materials, inherent properties of constituents or the conditions under which

the composites are used, the adhesion is not always perfect. This can be predicted

theoretically, although it is difficult to prove experimentally. The first criterion for good

adhesion is intimate contact, *i.e.* good wetting of the surface. Wetting is a necessary, but not

sufficient condition for good adhesion. The simple case is to consider the work of adhesion

to be associated to non-polar (London forces) between the materials. This is the case when at least the adhesive (polymer melt) or adherand (filler surface) is non-polar. So, for thermoplastics such as polytetrafluoroethylene (PTFE), PP, and PE this simple case is applicable.

The work of adhesion (W_a) in the case of non-polar system is expressed in **Eq. 3**.

$$W_A = 2\sqrt{\gamma_S \gamma_L} \quad \textbf{(3)}$$

where γ_s and γ_L refer to the surface energies of the solid and liquid respectively.

This implies that the work of adhesion can be maximized for a given adherand by maximizing the surface energy of the adhesive. However, it is also known that wetting is required and the surface tension of the adhesive must not exceed that of the adherand. The ideal case is when the surface tension of the polymer melt is high as possible, but without exceeding that of the filler surface, so that the spontaneous spreading still occurs. This has been experimentally verified for a range of polymeric adhesives on a set of surface with controlled surface energy.

Later, it was realized that polar interactions could also play a role in wetting and adhesion. The surface energy term was divided into non-polar and polar components and new equation was proposed to include the factor of polar interactions across the interface (**Eq. 4**). From this equation, it is expected that the maximum adhesion will occur when the ratio of polar to non-polar surface energy is the same for the adhesive and the adherand.

$$W = W_A^d + W_A^p = 2\sqrt{\gamma_s^d}\gamma_c^d + 2\sqrt{\gamma_s^p}\gamma_c^p \quad \textbf{(4)}$$

Further the importance of Lewis acid and base interactions were considered for calculating the work of adhesion (**Eq. 5**).

$$W_A = W_A^d + W_A^p + W_A^{AB} \quad \textbf{(5)}$$

Schreiber and coworkers used plasma treatment to alter the lewis acid–base balance of fillers and then compounded with LLDPE and poly(ethylene-vinyl acetate) [EVA], which is based on PE, but contains some (28 mole %) acetate groups, which are found to be lewis acid. They then assessed the effect of adhesion on mechanical performance of the composites by measuring tensile modulus and elongation at break. The maximum modulus and adhesion were obtained when the filler was plasma treated with methane to make the surface non-polar, same as that of polymer.

In the case when filler was plasma treated with ammonia, the results obtained are different for both LLDPE and EVA. In case of EVA, the highest modulus and least elongation to break were recorded due to enhanced adhesion from the bonding between the lewis acidic groups in the polymer and the lewis basic sites introduced on the surface of the filler. On the other hand, in LLDPE, lower modulus and higher elongation at break was obtained due to reduced adhesion between the non-polar polymer and polar filler surface.

Percolation in Composites

Percolation represents the standard model for structurally disordered systems [54-56]. For explaining this, a cubic lattice is considered where each site is randomly occupied with probability p or is empty with probability 1-p (**Fig. 2**).
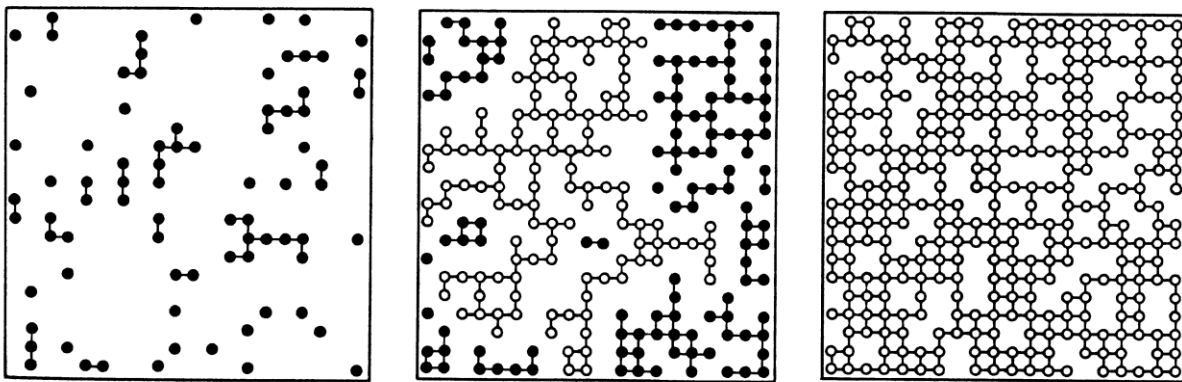

Figure 2. Illustration of site percolation for three different concentrations: p = 0.2, 0.59 and 0.80. The occupied sites are represented by small circles. Open and close circles mark large infinite and finite clusters respectively [54]. The lines connect the nearest neighbour cluster sites.

Empty or occupied sites may stand for very different physical properties. If it is assumed that occupied sites behave as electrical conductors and empty sites as insulators, then the electric current can flow between neighbor conductor sites. At low concentration, the conductor sites are either isolated or form small clusters of nearest-neighbor sites. If the two conductor sites are connected by a path of nearest neighbor-conductor sites, then the current can flow between them and the conductor-sites are considered to belong to the same cluster. At low values, the mixture behaves as an insulator, since no conducting path connecting

opposite edges in the lattice exist. On the other hand, at large values, the mixture behaves as conductor, where electric current can flow, due to the existence of many conducting paths between opposite edges. At some concentration in between, a threshold concentration must exist where for the first time electrical current can percolate form one edge to the other. Below this, there is insulator and above that is conductor. The threshold concentration is called the 'percolation threshold' or the 'critical concentration' since it separates the two different phases. This percolation transition is refereed as geometrical phase transition which is characterized by the geometric features of large clusters in the neighborhood of p_c. At low values of p, only small clusters of occupied sites exist. At increased concentration, the average size of the clusters increases. At the critical concentration, a large cluster appears which connects opposite edges of the lattice.

This cluster is called as infinite cluster, since it diverges in the thermodynamic limit. When p is increased further, the density of the infinite cluster increases, since more and more sites become part of the infinite cluster, and the average size of the finite clusters, which do not belong to the infinite cluster decreases. Trivially, at p = 1, all sites belong to the infinite cluster. The percolation transition is characterized by the geometrical properties of the clusters near p_c. The probability P_∞ that a site belongs to the infinite cluster is zero below p_c and increases above p_c as represented by **Eq. 6**:

$$P_\infty = (p-p_c)^\beta \quad \textbf{(6)}$$

Fig. 3 illustrates this behavior. The linear size of the finite clusters, below and above p_c is characterized by the correlation length ξ. The correlation length is defined as the mean distance between two sites on the same finite cluster and represents the characteristic length in percolation. When p approaches p_c, ξ increases as represented by **Eq. 7**:

$$\xi = |p\text{-}p_c|^{-\nu} \quad \textbf{(7)}$$

with same exponent ν below and above the percolation threshold. While p_c depends explicitly on the type of the lattice, the critical exponents β and ν are universal and depend only on the dimension of the lattice and not on the type of lattice.
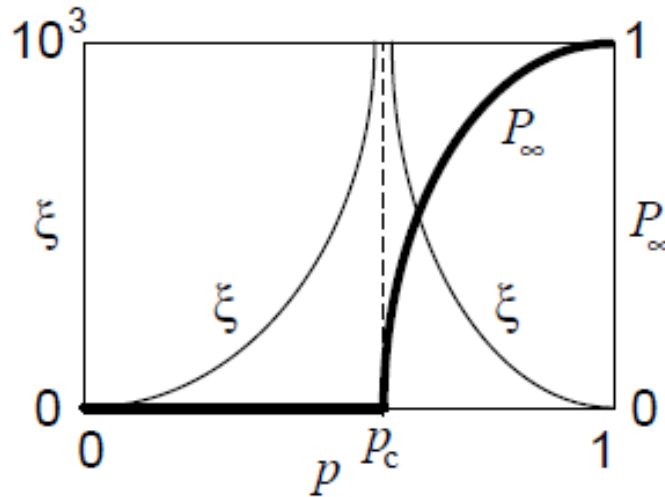

Figure 3. Schematic representation of the probability P_∞ (Eq. 6, bold line) and the correlation length ξ (Eq. 7, thin line) versus the concentration p of occupied sites [57].

Application of Percolation Theory

The percolation theory [58,59] is considered as most appropriate for the description of an abstract model of the conducting polymer composite materials. Since majority of the polymers are typical insulators, the probability of transfer of current carriers between two conductive points isolated from each other by an interlayer of the polymer decreases exponentially with the growth of gap I_g (tunnel effect) and is other than zero only for $I_g < 100$ Å. Because of this reason, the transfer of current through macroscopic distances can be affected via the contacting-particle chains. The importance of percolation theory lies in the calculation of the probability of the formation of such chains. It is also important to be noted that the concept of contact is not only for the particles in direct contact with each other but apparently implies convergence of the particles to distances at which the probability of transfer of current carriers between them becomes other than zero. The main concept of percolation theory is the so called percolation threshold C_p – minimum concentration of conducting particles C at which a continuous conducting chain of macroscopic length appears in the system. For the determination of this magnitude, the Monte Carlo method or the calculation of expansion of coefficients of C_p by powers of C is used for different lattices in the knots of which the conducting particles are located. The value of the percolation threshold for a continuous 3-dimensional medium equals $C_p \sim 0.15$.

Calculation of dependence of conductivity on the conducting filler concentration is a very complicated multifactor problem, as a result it depends primarily on the shape of the filler particles and their distribution in a polymer matrix. According to the nature of distribution of

the constituents, the composites can be divided into matrix, statistical and structurized systems. In matrix systems, one of the phases is continuous for any filler concentration. In statistical systems, constituents are spread at random and do not form any regular structures. In structurized systems, constituents form chain-like, flat or 3-dimensional structures. In the matrix systems, the maximum values of the percolation threshold are obtained because the filler doesn't form chain-like structures till large concentrations. In practice, statistical or structurized systems are preferred because they become conductive at relatively smaller concentrations of the filler. The deviation of the percolation threshold form the values of C_p to either side for a statistical system (~0.15) can be used to judge the nature of the filler distribution.

The composite obtained by pressing a mixture of the polymer powders and metal with radii of R_p and R_m, respectively ($R_p > R_m$) is an example of structurized system [60]. When the powders are being mixed, metal particles stick around polymer granules and if the pressing temperature is lower than the polymer melting temperature, the metal particles do not penetrate inside the granules. As the volume of the material accessible for the filler is artificially reduced, conducting chains are formed at lesser concentrations and the larger the R_p/R_m ratio, the more reduced is the percolation threshold.

The composites with the conducting fibers may also be considered as the structurized system. The fiber with diameter d and length l may be considered as a chain of contacting spheres with diameter d and chain length l. Thus, comparing the composites with dispersed

and fibre fillers, it can be said that N= 1/d particles of the dispersed filler are as if combined in a chain. From this qualitative analysis, it follows that the lower the percolation threshold for the fibre composites the larger must be the value of 1/d. This conclusion is confirmed both by the experimental data and the calculations for model systems. For 1/d ~10^3, the value of the threshold concentration can be reduced to between 0.1 and 0.3 percent of the volume.

Halpin-Tsai Equations

A set of empirical relationships that enable the property a composite material to be expressed in terms of the properties of the matrix and reinforcing phases, taking into account their respective proportions and geometry are termed as halpin-tsai equations [61]. Among, the various micromechanics relationship available, the most widely used are the Halpin-Tsai equations because of their relatively simple form of expression and their ability to describe experimental data with reasonable accuracy [62]. **Eq. 8** represents the general form:

$$P = HS(P_f, P_m, V_f, \xi_p) = P_m \frac{1+\xi_p n_p V_f}{1-n_p V_f} \text{ where } n_p = \frac{P_f - P_m}{P_f + \xi_p P_m} \quad \textbf{(8)}$$

Here the Halpin-Tsai relationship is represented by the function HS. The equivalent fiber and matrix values of the property to be determined are represented by P_f and P_m, respectively. ξ_P represents the contiguity factor which describes the influence of the phase arrangement of the reinforcing phase on the particular property, identified by the subscript.

Although, there is no formal derivation for Halpin-Tsai equations, but they exhibit resemblance to certain elasticity-based expressions for elastic properties of mixtures of materials. In some special cases, they are also reduce to some well-known analytical expressions. $\xi_P = 0$ and $\xi_P = \infty$ are the most extreme cases. In these cases, the Halpin-Tsai equations for modulus reduce to the lower and upper bound expressions respectively, **Eqs. 9 and 10**.

$$E_1 = E_f V_f + E_m V_m \quad \textbf{(9)}$$

$$E_2 = \left(\frac{V_f}{E_f} + \frac{V_m}{E_m} \right)^{-1} \quad \textbf{(10)}$$

Values of the ξ_P for Halpin-Tsai equations are given in **Table 1**. To enable the most accurate fit to be obtained to each particular set of experimental data, it is permissible to adjust ξ_P due to empirical nature of Halpin-Tsai equations. In case of fibers that are themselves anisotropic *i.e.* carbon and aramid, it is necessary to use the appropriate P_f value for the determination of specific property (*i.e.* the fiber transverse modulus should be used when calculating the ply transverse modulus). The same applies for shear moduli.

Table 1. Values of the contiguity factor for Halpin-Tsai equations [63].

Case	ξ_P
Perfectly aligned continuous fibres. Young's modulus, E_{11}, parallel to fibers	$\xi_{11} = \infty$ (equivalent to Eq.3)
Imperfectly aligned (or wavy) continous fibres. Young's modulus, E_{11}, parallel to fibres.	$\xi_{11} < \infty$ (often in the range, 100-1,000, adjusted to allow for lack of perfect fiber alignment)
Aligned discontinuous fibres, length, L and diameter D. Young's modulus, E_{11}, parallel to fibres.	$\xi_{11} = 2L/D$
Aligned continous or discontinuous fibres. Young's modulus, E_{12}, perpendicular to fibres.	$\xi_{22} = 2$ or value to achieve best fit to data
Aligned continous or discontinuous fibres. Shear modulus, G_{12}, for shear parallel to fibres. The same expression also applies for G_{13}.	ξ_{12} (or ξ_{13}) = 1 or value to achieve best fit to data
All, the above, principal Poisson's ratio, v_{12}	$\xi_{v12} = \infty$ (equivalent to Eq.4)

The Halpin-Tsai relationships can be used to derive all the elastic constants for laminate possessing a particular reinforcement content and architecture, when the elastic constants of the polymer matrix are known. For this, the relationships between the elastic constants for an isotropic material are useful (**Eq. 11**).

$$G = \frac{E}{2\,(1+v)}\,, K = \frac{E}{3\,(1-2v)} \text{ and } G = \frac{3K\,(1-2v)}{2\,(1+v)} \quad \textbf{(11)}$$

These relationships are applicable for all isotropic matrix and fiber materials (*i.e.* all resins and glass fibers, but not carbon or aramid). Only, the value of young's modulus is frequently known. In this case, the shear modulus may be found by assuming a particular value for the Poisson's ratio, 0.35 is a typical value for resins and 0.28 for glass fiber. When the resin is above its glass transition temperature, the Poisson's ratio becomes large, eventually approaching the value of 0.5, often assumed for rubbers. The effect of the value chosen for Poisson's ratio is not very large.

Thermal conductivity of polymers

Polymers have low thermal conductivity. The thermal conductivity of insulating polymeric materials is usually 3 to 5 orders lower than that of metals and ceramics. Due to the chain-like structure, the heat capacity of polymers consists of the contribution from two mechanisms: i) lattice vibrations and ii) characteristic vibrations, originating from internal motions of the repeating unit. The lattice (skeleton) vibrations are acoustic vibrations, which mainly contribute to the thermal conductivity at low temperature. The optical vibrations, which are characteristic vibrations of the side groups become visible above 100 K. Generally, in case of amorphous polymers thermal conductivity increases with increasing temperature, if the temperature is in glassy region and remains constant or decrease slowly in the rubbery region.

Numerous applications in the field of electrical engineering such as insulating materials for power equipment, electronic packaging and encapsulations and other areas where good

dissipation is needed require thermal conductivity. Thermal conductivity improvement in polymers may be achieved either by addition of highly heat conductive fillers or by molecular orientation of polymer. The main approach to improve the low thermal conductivity of polymers is to fill them with particles with high thermal conductivity. Industrial companies specializing in the production of polymer-based insulating materials, use a fill grade up to 60 wt% of alumina or silica. The thermal conductivity of these fillers is not so high but the price is low.

Modeling of thermal conductivity in nanocomposites

It is difficult to evaluate the properties of final composites due to almost infinite number of possible material compositions such as weight fraction of filler, kind of polymer matrix, type of thermally conductive filler *etc*. Therefore, during the process of screening appropriate compositions for the selection of the more favorable ones, theoretical predictions and modelling play a significant role. By the application of modelling, firstly dependence of thermal conductivity of composite on the matrix and filler thermal conductivity can be determined. Secondly, ideal thermal conductivity of many materials such as polymers, ceramic particles, carbon nanotube and graphite can be predicted by modeling such as molecular dynamics simulations. Other factors such as morphology of the filler (percolated network, fractal clusters, individual particles, aggregates), anisotropy (for filler particles having non-spherical morphology), effects of processing history and properties of filler–matrix interfaces (**Fig. 4**).
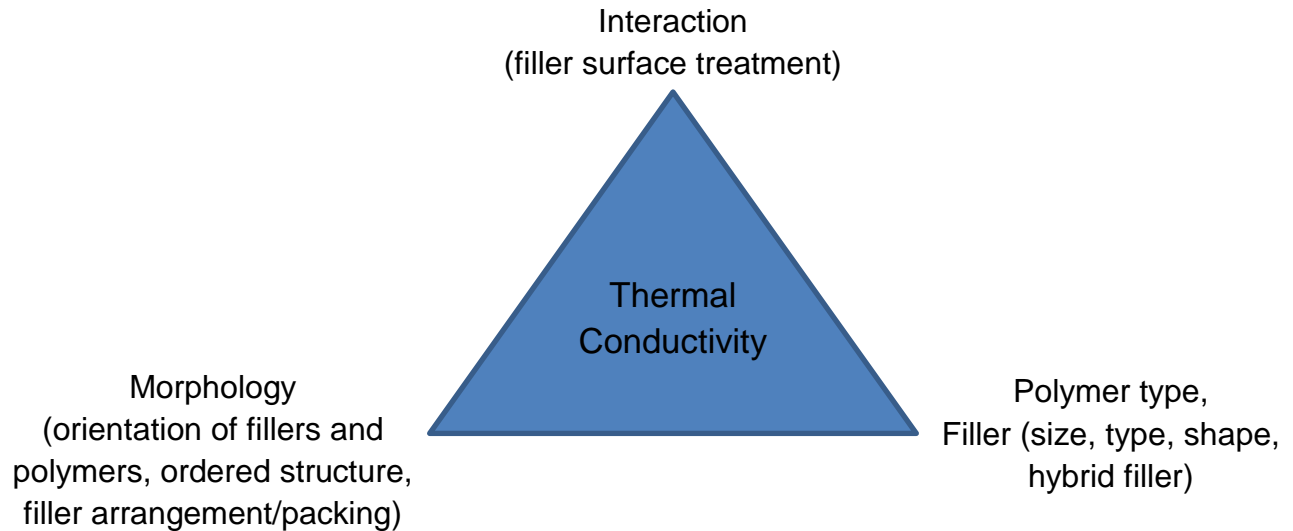
Interaction
(filler surface treatment)

Thermal
Conductivity

Morphology
(orientation of fillers and
polymers, ordered structure,
filler arrangement/packing)

Polymer type,
Filler (size, type, shape,
hybrid filler)

Figure 4. Factors influencing the thermal conductivity of composites [64].

Mainly, models for composites can be divided into two classes – finite element simulations and analytical micromechanical models. Usually, finite element models offer higher opportunity for the calculation of thermal conductivity of composites accurately by taking into consideration both the possible interfacial resistance and realistic composite morphology but they are usually time-consuming and are mainly used to test predictions of consecutive models. Analytical micromechanical models provide closed-form expressions for the thermal conductivity of composites as functions of the thermal conductivity of filler materials and the matrix. The assumptions of these models usually include ideal matrix-filler interfaces (no thermal resistance for phonons) and idealized morphology (uniform dispersion of filler particles). However, the predictions are usually qualitative, as a result of which these models can offer quicker estimates of the dependence of thermal conductivity of

composites on the filler loading and the thermal conductivity of both the filler and the matrix. As a result, these models can provide very quick estimates of the dependence of composite thermal conductivity on the filler loading and thermal conductivity of filler and the matrix.

Consecutive (micromechanical) modeling

The simplest approach to estimate the thermal conductivity of the composites is the rule of mixture (parallel and series model).

In the parallel model, the overall thermal conductivity constitutes the contribution from the matrix and filler independently, corresponding to their relative volume fractions (**Eq. 12**).

$$\lambda_c = \phi \, \lambda_f + (1\text{-}\phi) \, \lambda_m \quad \textbf{(12)}$$

The series model is applicable in the case where there is a uniform dispersion of fillers in the matrix and there is no percolation even at high filler concentrations (**Eq. 13**). .

$$\frac{1}{\lambda_c} = \frac{\Phi}{\lambda_f} + \frac{1-\phi}{\lambda_m} \quad \textbf{(13)}$$

In all the formulas λ_c, λ_f and λ_m represents the composite, filler and matrix thermal conductivities respectively. ϕ is the volume fraction of the filler.

The parallel or series models are applicable only when the filler particles are either in parallel or series with respect to the heat flow. Since the particles are randomly distributed

and are not perfectly aligned in the direction of heat flow in the polymer. Therefore, parallel

and series model are normally not effective in prediction of the thermal conductivity of the

composites. The series model is usually closer to the experimental data, therefore many

different models are developed from the basic series model as compared to parallel model.

[65]. These models generally introduce some more complex volume fractions and weighted

averages on thermal conductivities of polymer and matrix. These models are based on the so

called effective medium theories or effective medium approximations. Two commonly used

models based on effective medium approximation methods are the Maxwell-Garnett [66] and

the Bruggeman [67].

Maxwell-Garnett derived the expression (**Eq. 14**) for the thermal conductivity of

randomly distributed and non-interacting homogenous nanoparticles in a homogenous

medium.

$$\lambda c = \lambda m \frac{[2\,\lambda m + \lambda f + 2\,\Phi\,(\lambda f - \lambda m)]}{[2\,\lambda m + \lambda f + \Phi\,(\lambda f - \lambda m)]} \quad \textbf{(14)}$$

Fricke extended Maxwell-Garnett's model for ellipsoidal particles in a continuous phase.

In the effective medium approach, the basic assumption of separated particles for highly

filled composites is not valid, where contacts are likely to occur, possibly leading to

thermally conductive paths. For these types of composites, a much better description is

provided by the Bruggeman model. In this model, mean field approach is used to capture the

interactions among the randomly distributed fillers. For this model, there is no limitation on

the concentration of inclusions. As a result, it is widely used for particle percolation in

suspensions, i.e. particle clustering effect. For a binary composite containing spherical fillers and matrix, the Bruggeman model yields the following **Eq. 15:**

$$1 - \Phi = \left(\frac{\lambda f - \lambda c}{\lambda f - \lambda m}\right) \cdot \left(\frac{\lambda m}{\lambda c}\right)^{1/3} \quad \textbf{(15)}$$

Bruggeman and Maxwell-Garnett models give quite similar predictions for low filler loadingcomposites. The Maxwell-Garnett model significantly underestimates the thermal conductivity for high filler loading and in systems where thermally conductive fillers form percolated pathways, while the Bruggeman model can well describe the experimental data. Hence, the Maxwell-Garnett model is used to approximate the thermal conductivity of composites and Bruggeman model is used to predict the effective thermal conductivity of particle clusters [68]. The representation of this combination approach is depicted in **Fig. 5**.
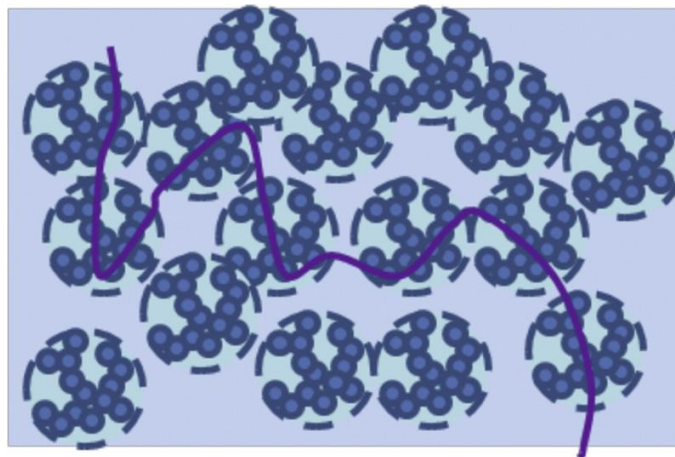

Figure 5. Representation of well-dispersed aggregates in composites. Solid line represents the thermally conductive path [64].

<u>Finite element modeling</u>

The aforementioned approaches based on consecutive modeling offer quick estimation of the trends expected upon changes in loading of filler or filler type, but they are applicable to some very specific situations (*e.g.* perfectly aligned ellipsoidal fillers in a homogenous matrix or monodisperse spherical fillers in a homogenous matrix). Usually, there is more complication in case of composite morphology, in which numerical based approaches such as finite difference modeling or finite elemental analysis could be more suitable. In general, within finite elemental analysis approach, the morphology of a composite material is considered and then the stationary equation of heat transfer in solids (**Eq. 16**) is solved.

$$\nabla(k(\mathbf{r})\nabla \mathrm{T}(\mathbf{r})) = 0 \quad \textbf{(16)}$$

Subjected to the boundary condition,

$$k\frac{\partial T}{\partial \boldsymbol{n}} = -J \quad \textbf{(17)}$$

where, $\partial \mathrm{T}/\partial \mathbf{n}$ denotes the normal derivative at the boundary condition. If at the boundary X = 0, the heat flux J is applied, while the boundary $\mathrm{X} = \mathrm{X_0}$ is maintained at constant temperatureT_0, and the heat flow through the $X\mathrm{Y}$ and $X\mathrm{Z}$ boundaries is neglected, then effective conductivity of sample can be calculated as:

$$k_{eff} = \frac{JX_0}{<T(x=0).-T_0} \quad \textbf{(18)}$$

where the $<>$ brackets indicating average over y and z in the x = 0 plane. For computing the principal components of the symmetric tensor k_{ij} (the symmetry of the tensor follows from the Onsager reciprocal relations) in other directions, similar calculations could be done in case of composites possessing anisotropy [69,70]. In most of the cases, polymer-based composites are either isotropic (only one thermal conductivity number is needed) or having a preferential filler plane orientation (two thermal conductivity numbers namely in-plane and through-plane are required).

1.3 Polyolefin-based Nanocomposites

Owing to high technology and sustainability of polymerization process, their excellent thermomechanical properties and good environmental compatibility, including easy recycling, polyolefins are considered as one of the most widely used thermoplastics. In the last few decades, much attention has been devoted worldwide to extend the applications of polyolefins by introducing novel properties through blending and mixing with different materials. Due to recent development in the field of nanotechnology, there has been growing interest in polyolefin-based nanocomposites to further expand their versatility and explore new specialty. However, fabrication of industrially viable polyolefin-based nanocomposites is extremely challenging owing to the chemical inertness of polyolefin against inorganic nanoparticles, compared to other polymers containing polar functional groups which can more or less interact with nano-fillers [71]. In most of the cases, nano-fillers do not disperse well in polyolefin resulting in formation of large and compact aggregates with significant

reduction in reinforcement and even negatively affecting ductility and transparency. Various strategies have been employed for the fabrication of polyolefin-based nanocomposites so as to improve the dispersion of nano-fillers and interfacial bonding between the matrix and the filler. The most versatile strategies to overcome the dispersion of nanoparticles include addition of a compatibilizer, typically side functionalized polyolefin such as maleic anhydride grafted polypropylene (MAPP) and to chemically modify the nanoparticles surface by short aliphatic alkyl chains, for *e.g.* silane coupling agents or ternary ammonium salts [72-74].

With their use, good dispersion could be achieved in a relatively economical way but they involve some disadvantages such as: i) formation of soft interfacial layer between the matrix and the filler, hampering the hardness of fillers and limiting the reinforcement [75]and ii) accelerated oxidative degradation of the matrix. Polymer grafting is another versatile and scalable approach due to its direct application to the conventional melt-mixing process, which aims not only at compatibilization of nano-fillers but also better interfacial interaction connection through interdiffusion and entanglement between grafted and matrix polymer chains [76-78]. Although, it provides great interfacial reinforcement but the drawback is at the elaborate synthesis of the polymer-grafted nano-fillers, which is crucial for polyolefin as the most economical plastic. Another commonly employed strategy is the *in-situ* polymerization in which olefin polymerization is conducted in the presence of nano-fillers that bear a catalytic activity [79,80]. This method facilitates good dispersion of nano-fillers without a dispersant but the performance of the catalyst (10^2-10^3 gram polymer per gram

catalyst) is unacceptably poor compared with an industrial process (10^5-10^6). Although all of these approaches have greatly refined the design of polyolefin based nanocomposites but so far none of the proposed strategies has offered a versatile solution for the cost performance problem in these nanocomposites.

1.4 Reactor Granule Technology

The process involving controlled, reproducible polymerization of olefinic monomers on an active $MgCl_2$ supported catalyst giving rise to the formation of growing, spherical polymer granule which provides a porous reaction bed within which others monomers can be introduced and polymerized to form a polyolefin alloy is termed as reactor granule technology [81,82]. The exploitation of RGT has led to the development of a class of polypropylene products ranging from supersoft alloys to superstiff, high fluidity homopolymers and stiff/impact or clear/impact heterophase copolymers.
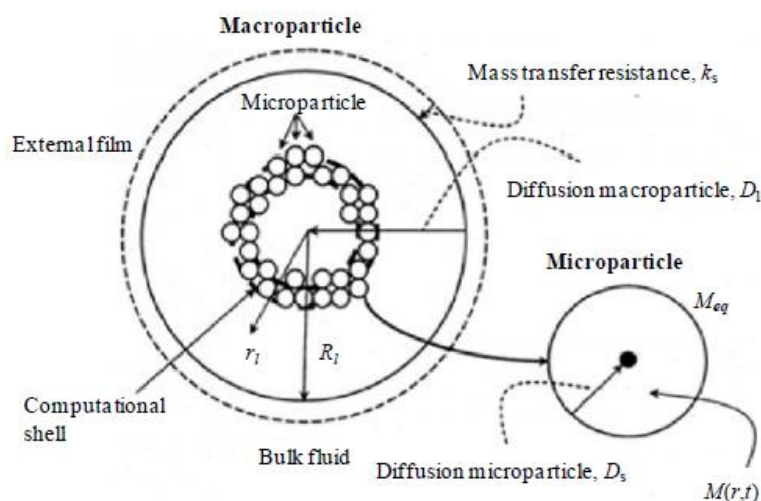

Figure 6. Schematic representation of the multigrain model [83].

In olefin polymerization, the particle growth is usually described by the "multi-grain" model [84,85]. The schematic drawing is illustrated in **Fig. 6**. According to this model, the catalysts comprises of multi grain particles (smaller fragments). As the polymerization proceeds, the initial catalyst support becomes fragmented and dispersed within the growing polymer matrix. Monomers polymerize on active centers of these catalyst fragments, forming a polymer shell and causing the catalyst grain to further expand progressively. The process of polymer formation is based on the catalyst-to-polymer replication phenomenon so that a spherical support in the size range of 10-100 μm will give spherical polymer morphology with particle size generally in the range of 100-3000 μm, dependent on the catalyst activity. The key features in the replication process are the extensive fragmentation and uniform particle growth (**Fig. 7**). These are dependent on a high surface area, a homogenous distribution of catalytically active centers throughout the particle and free access of the monomer to the innermost zones of the particle. The obtained polymer granule with a porous architecture, so called reactor granule is typically utilized for reactor blending for the production of rubber-toughened polypropylene [81,86].
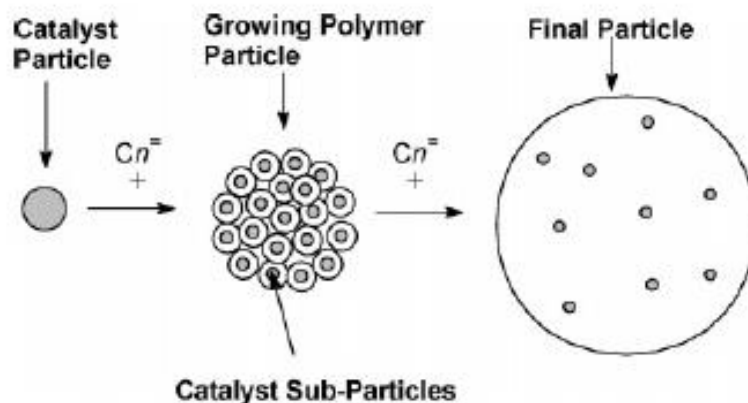
Figure 7. Polymer particle growth [86].

1.5 Purpose of the Present Research

Polymer nanocomposites have emerged as an attractive hybrid material, where the inclusion of nano-sized fillers dramatically improves the properties of base polymer at a low filler loading. Some properties such as flame retardancy, thermal conductivity, electric conductivity etc. still require a relatively high amount of filler loading to achieve industrial requirements, in which it is difficult to maintain nano-level dispersion due to the tendency of nanoparticles towards agglomeration. The most employed strategies to achieve nano-level dispersion of filler are the addition of a compatibilizer and organic modification of filler surfaces. These dispersants improve poor compatibility between hydrophilic nano-fillers and hydrophobic polymer such as polyolefins but at the same time cause problems of additional cost, limited processibility, accelerated degradation and so on. Moreover, compounding of thermoplastics generally employs melt mixing of commercially available nanofillers with

pellets, where microscopic dispersion must be achieved by mixing macroscopically separated substances (*i.e.* nano-fillers and pellets). Such a process sounds obviously inefficient for the combination of nano-fillers and polyolefins. Fabrication of highly filled polyolefin-based nanocomposite has been a key issue in polyolefin industry.

In this study, I aimed my focus on establishing a methodology which can facilitate the successful fabrication of functionally advantageous highly filled polyolefin-based nanocomposites in a simple, versatile and cost-effective manner. I have successfully disclosed a novel methodology based on pore confinement concept for the *in-situ* fabrication of polyolefin nanocomposites in a dispersant-free manner.

Reactor granule obtained by propylene polymerization was impregnated with metal alkoxide as precursor for metal hydroxide/oxide. The metal alkoxide was uniformly loaded in the porosity of the reactor granule of polypropylene (PP), which was pre-hydrolysed and chemically converted to metal hydroxide/oxide nanoparticles in melt-mixing, leading to unprecedented dispersion even at a high filler loading. The basic aim of this research is to further develop the new reactor granule technology for extensive functionalization of polyolefins and to explore the versatility of the method.

1.6. References

[1] H. F. Brinson, L. C. Brinson, Polymer Engineering Science and Viscoelasticity, Springer, U. S., 2008, pp. 55-97.

[2] C. H. Bamford, in Encyclopedia of Polymer Science & Engineering, John Wiley & Sons, New York, 1985, vol. 13, pp. 708-867.

[3] R. A. Vaia, J. F. Maguire, Polymer nanocomposites with prescribed morphology: Going beyond nanoparticle-filled polymers, Chem. Mater. 19 (2007) 2736-2751.

[4] A. D. Pomogailo, Hybrid polymer-inorganic nanocomposites, Russ. Chem. Rev. 69 (2000) 53-80.

[5] L. M. Bronstein, S. N. Sidorov, P. M. Valetsky, Nanostructured polymeric systems as nanoreactors for nanoparticle formation, Russ. Chem. Rev. 73 (2004) 501-515.

[6] A D Pomogailo, A S Rozenberg, G I Dzhardimalieva, Thermolysis of metallopolymers and their precursors as a method for the preparation of nanocomposites, Russ. Chem. Rev. 3 (2011) 257-292.

[7] J. E. Mark, Ceramic-reinforced polymers and polymer-modified ceramics, Polym. Eng. Sci. 36 (1996) 2905-2920.

[8] K Sill, S Yoo, T Emrick, Dekker Encyclopedia of Nanoscience and Nanotechnology Taylor and Francis, London, 2004, vol. 3, pp. 2999-3015.

[9] B Kocherginskaya, A. V. Romanova, I. A. Prokhorenko, D. M. Itkis, A. V. Korshun, E. A. Goodilin, Y. D. Tretyakov, Modification of quantum dots with nucleic acids, Russ. Chem. Rev. 80 (2011) 1209-1221.

[10] V. Yu. Dolmatov, Detonation synthesis ultradispersed diamonds: properties and applications, Russ. Chem. Rev. 70 (2011) 607-626.

[11] V. Yu. Dolmatov, Detonation-synthesis nanodiamonds: synthesis, structure, properties and applications, Russ. Chem. Rev. 76 (2007) 339-360.

[12] S. Sinha Ray, M. Bousmina, Biodegradable polymers and their layered silicate nanocomposites: In greening the 21st century materials world, Prog. Mater. Sci. 50 (2005) 962-1079.

[13] D. R. Paul, L. M. Robeson, Polymer nanotechnology: Nanocomposites, Polymer 49 (2008) 3187-3204.

[14] A. K. Geim, K. S. Novoselov, The rise of graphene, Nat. Mater. 6 (2007) 183-191.

[15] N Tomczak, D Jan'czewski, M. Han, C. J. Vancso, Designer polymer-quantum dot architectures, Prog. Polym. Sci. 34 (2009) 393-430.

[16] H. Oikawa, T. Onodera, A. Masuhara, H. Kasai, H. Nakanishi, New class materials of organic–inorganic hybridized nanocrystals/nanoparticles, and their assembled micro- and nano-Structure toward photonics, Adv. Polym. Sci. 231 (2009) 147-190.

[17] D. H. Park, M. S. Kim, J. Joo, Hybrid nanostructures using π-conjugated polymers and nanoscale metals: synthesis, characteristics, and optoelectronic applications, Chem. Soc. Rev. 39 (2010) 2439-2452.

[18] P. Alexandridis, Gold nanoparticle synthesis, morphology control, and stabilization facilitated by functional polymers, Chem. Eng. Technol. 34 (2011) 15-28.

[19] K. Yamamoto, Y. Sakata, Y. Nohara, Y. Takahashi, T. Tatsumi, Organic-inorganic hybrid zeolites containing organic frameworks, Science 300 (2003) 470-472.

[20] P.H.T. Vollenberg, D. Heikens, Particle size dependence of the Young's modulus of filled polymers: 1. Preliminary experiments, Polymer 30 (1989) 1656-1662.

[21] Z. S. Petrović, I. Javni, A. Waddon, and G. Bánhegyi, Structure and properties of polyurethane-silica nanocomposites, J. Appl. Polym. Sci. 76 (2000) 133-151.

[22] C.M. Chan,; J. Wu,; J.X. Li, Y.K. Cheung, Polypropylene/calcium carbonate nanocomposites, Polymer 43 (2002) 2981-2992.

[23] M.Z. Rong, M.Q. Zhang, Y.X. Zheng, H.M. Zeng, R. Walter, K. Friedrich, Structure–property relationships of irradiation grafted nano-inorganic particle filled polypropylene composites, Polymer 42 (2001) 167-183.

[24] F. Yang, Y. Ou, Z. Yu, Polyamide 6 silica nanocomposites prepared by in situ polymerization, J. Appl. Polym. Sci. 69 (1998) 355-361.

[25] Y. Ou, F. Yang, Z.Z. Yu, A new conception on the toughness of nylon 6/silica nanocomposite prepared via in situ polymerization, J. Polym. Sci. B: Polym. Phys. 36 (1998) 789-795.

[26] E. Reynaud, T. Jouen, C. Gautheir, G. Vigier, Nano fillers in polymeric matrix: a study on silica reinforced PA6, Polymer 42 (2001) 8759-8768.

[27] C. Zhang, L.J. Lee, Poly(methyl methacrylate) and polystyrene/clay nanocomposites prepared by in-situ polymerization, Macromolecules 34 (2001) 4098-4103.

[28] Y. Li, J. Yu, Z.X. Guo, The influence of silane treatment on nylon 6/nano-SiO$_2$ in situ polymerization, J. Appl. Polym. Sci. 84 (2002) 827-834.

[29] B.J. Ash, L.S. Schadler, R.W. Siegel, Glass transition temperature of alumina/polymethylmethacrylate nanocomposites, Mater. Lett. 55 (2002) 83-87.

[30] R.W. Siegel, S.K. Chang, B.J. Ash, J. Stone, P.M. Ajayan, R.W. Doremus, L.S. Schadler, Scr. Mater. 44 (2001) 2061-2064.

[31] S. Jain, H. Goossens, M. van Duin, P. Lemstra, Effect of in situ prepared silica nano-particles on non-isothermal crystallization of polypropylene, Polymer 46 (2005) 8805-8818.

[32] A. Bansal, H. Yang, C. Li, K. Cho, B.C. Benicewicz, S.K. Kumar, L.S. Schadler, Quantitative equivalence between polymer nanocomposites and thin polymer films, Nat. Mater. 9 (2005) 693-698.

[33] A. Bansal, H. Yang, C. Li, B.C. Benicewicz, S.K. Kumar, L.S. Schadler, Controlling the thermomechanical properties of polymer nanocomposites by tailoring the polymer–particle interface, J. Polym. Sci. B: Polym. Phys. 44 (2006) 2944-2950.

[34] C.I. Park, O.O. Park, J.G. Lim, H.J. Kim, The fabrication of syndiotactic polystyrene/organophilic clay nanocomposites and their properties, Polymer 42 (2001)7465-7475.

[35] M.Z. Rong, M.Q. Zhang, S.L. Pan, B. Lehmann, K. Friedrich, Analysis of the interfacial interactions in polypropylene/silica nanocomposites, Polym. Int. 53 (2004) 176-183.

[36] T. H. Zhou, W. H. Ruan, J. L. Yang, M. Z. Rong, M. Q. Zhang, Z. Zhang, A novel route for improving creep resistance of polymers using nanoparticles, Compos. Sci. Technol. 67 (2007) 2297-2302.

[37] H. Deng, T. Skipa, E. Bilotti, R.Z.D. Lellinger, L. Mezzo, Q. Fu, I. Alig , T. Peijs, Preparation of high-performance conductive polymer fibers through morphological control of networks formed by nanofillers, Adv. Func. Mater. 20 (2010) 1424-1432.

[38] J.M. Brown, D.P. Anderson, R.S. Justice, K. Lafdi, M. Belfor, K.L. Strong, D.W. Schaefer, Hierarchical morphology of carbon single-walled nanotubes during sonication in an aliphatic diamine, Polymer 46 (2005) 10854-10865.

[39] D.W. Schaefer, R.S. Justice, How Nano Are Nanocomposites?, Macromolecules 40 (2007) 8501-8517.

[40] M.E. Mackay, A. Tuteja, P.M. Duxbury, C.J. Hawker, B.V Horn, Z. Guan, G. Chen, R.S. Krishnan, General strategies for nanoparticle dispersion, Science 311 (2006) 1740-1743.

[41] A.I. Nakatani, W. Chen, R.G. Schmidt, G.V. Gordon, C.C Han, Chain dimensions in polysilicate-filled poly(dimethyl siloxane), Polymer 42 (2001) 3713-3722.

[42] A.I. Nakatani, W. Chen, R.G. Schmidt, G.V. Gordon, C.C Han, Chain Dimensions in Polysilicate-Filled Poly(Dimethyl Siloxane), Int. J. Thermophys. 23 (2002) 199-209.

[43] S. Sen, Y.P. Xie, S.K. Kumar, H.C. Yang, A. Bansal, D.L. Ho, L. Hall, J.B. Hooper, K.S. Schweizer, Chain conformations and bound-layer correlations in polymer nanocomposites, Phys. Rev. Lett. 98 (2007) 128302 1-4.

[44] J.S. Shaffer, A.K. Chakraborty, Dynamics of poly(methyl methacrylate) chains adsorbed on aluminum surfaces, Macromolecules 26 (1993) 1120-1136.

[45] J. Kalfus, J. Jancar, Relaxation processes in PVAc HA Nanocomposites, J. Polym. Sci. B: Polym. Phys. 45 (2007) 1380-1388.

[46] X. Zheng, B.B Sauer, J.G.V. Alsten, S.A. Schwarz, M.H. Rafailovich, J. Sokolov, M. Rubinstein, Reptation dynamics of a polymer melt near an attractive solid interface, Phys. Rev. Lett. 74 (1995) 407- 410.

[47] C.V.D. Linden, R.V. Leemput, Adsorption studies of polystyrene on silica I. monodisperse adsorbate, J. Colloid. Inter. Sci. 67 (1978) 48-62.

[48] R.K. Iler, Relation of particle size of colloidal silica to the amount of a cationic polymer required for flocculation and surface coverage, J. Colloid. Inter. Sci. 37 (1971) 364-373.

[49] M.A. Stuart, H. Tamai, Dynamics of adsorbed polymers. 2. Thickness relaxation of poly (ethylene oxide) on glass as a function of segmental binding energy, Langmuir 4 (1988) 1184-1188.

[50] H.E. Johnson, J.F. Douglas, S. Granick, Topological influences on polymer adsorption and desorption dynamics, Phys. Rev. Lett. 70 (1993) 3267-3270.

[51] J.C. Dijt, M.A Stuart, G.J. Fleer, Competitive adsorption-kinetics of polymers differing in length only, Macromolecules 27 (1994) 3219-3228.

[52] J.C. Dijt, M.A. Stuart, G.J. Fleer, Surface exchange kinetics of chemically different polymers, Macromolecules 27 (1994) 3229-3237.

[53] Z. Fu, M.M. Santore, Kinetics of competitive adsorption of PEO chains with different molecular weights, Macromolecules 31 (1998) 7014-7022.

[54] A. Bunde and S. Havlin (eds.), Fractals and Disordered Systems 2nd ed. Springer Verlag, Heidelberg, 1996.

[55] M. Sahimi, Application of Percolation Theory Taylor & Francis, London, 1994.

[56] D. Stauffer and A. Aharony, Introduction to Percolation Theory Taylor & Francis, London, 1992.

[57] A. Bunde, W. Dieterich, Percolation in composites, J. Electroceram. 5 (2000) 81-92.

[58] S. Kirkpatrick, Percolation and conduction, Rev. Mod. Phys. 45 (1973) 574-588.

[59] V. K. S. Shante, S. Kirkpatrick, Percolation in composites, Adv. Phys. 20 (1971) 325-328.

[60] A. Malliaris, D.T. Turner, Influence of particle size on the electrical resistivity of compacted mixtures of polymeric and metallic powders, J Appl. Phys. 42 (1971) 614-618.

[61] J. C. Halpin, J. L. Kardos, Moduli of crystalline polymers employing composite theory, J. Appl. Phys. 43 (1972) 2235-2241.

[62] J. C. Halpin, Some critical issues in advanced polymer science, Polym. Eng. Sci. 15 (1975) 132-136.

[63] A. P. Mouritz, A. G. Gibson, Fire properties of polymer composite materials, Springer, Netherlands, 2006, pp. 169-170.

[64] H. Chen, V.V. Ginzburg, J. Yang, Y.Yang, W. Liu, Y. Huang, L. Du, B. Chen, Thermal conductivity of polymer-based composites: Fundamentals and applications, Prog. Polym. Sci. 59 (2016) 41-85.

[65] D. M. Bigg, Thermal conductivity of heterophase polymer compositions. Adv. Polym. Sci. 119 (1995) 1-30.

[66] J. C. M. Garnett, Colours in metal glasses and in metallic films. Proc R Soc Lond Ser A 73 (1904) 443-445.

[67] D.A.G. Bruggeman, Berechnung verschiedener physikalischer kon-stanten von heterogenen substanzen, I. dielektrizitatskonstantenund leitfahigkeiten der mischkorper aus isotropen substanzen, Annal. Phys. Leipz . 24 (1935) 636-679.

[68] P. E. Gharagozloo, K. E. Goodson, Aggregate fractal dimensions and thermal conduction in nanofluids, J. Appl. Phys. 108 (2010) 074309/1-74309.

[69] L. Onsager Reciprocal relations in irreversible processes. I. Phys Rev. 37 (1931) 405-426.

[70] L. Onsager Reciprocal relations in irreversible processes. II. Phys Rev. 1931 (1931) 2265-2279.

[71] M.T.T. That, F.P. Sarazin, K.C. Cole, M.N. Bureau, J. Denault, Polyolefin nanocomposites: formulation and development, Polym. Eng. Sci. 44 (2004) 1212-1219.

[72] O.H. Lin, H.M. Akil, Z.A.M. Ishak, Surface-activated nanosilica treated with silane coupling agents/polypropylene composites: mechanical, morphological, and thermal studies, Polym. Compos. 32 (2011) 1568-1583.

[73] E. Pavlidou, D. Bikiaris, A. Vassiliou, M. Chiotelli and G. Karayannidis, Mechanical properties and morphological examination of isotactic Polypropylene/SiO$_2$ nanocomposite, J. Phys. 10 (2005) 190-193.

[74] M. Kawasumi, N. Hasegawa, M. Kato, A. Usuki, A. Okada, Preparation and mechanical properties of polypropylene-clay hybrids, Macromolecules 30 (1997) 6333-6338.

[75] Z.M. Wang, H. Hong, T.C. Chung, Synthesis of maleic anhydride grafted polypropylene with high molecular weight using borane/O$_2$ radical initiators and commercial PP polymers, Macromolecules 38 (2005) 8966-8970.

[76] H.J. Zhou, M.Z. Rrong, M.Q. Zhang, W.H. Ruan, K. Friedrich, Role of reactive compatibilization in preparation of nanosilica/polypropylene composites, Polym. Eng. Sci. 47 (2007) 499-509.

[77] T. Taniike, T. Toyonaga, M. Terano, Polypropylene-grafted nanoparticles as promising strategy for boosting physical properties of polypropylene-based nanocomposites, Polymer 55 (2014) 1012-1019.

[78] M. Toyonaga, P. Chammingkwan, M. Terano, T. Taniike, Well-defined polypropylene/polypropylene-grafted silica nanocomposites: roles of number and

molecular weight of grafted chains on mechanistic reinforcement, Polymers 8 (2016) 300-313.

[79] K. Scharlach, W. Kaminsky, New polyolefin-nanocomposites by in situ polymerization with metallocene catalysts, Macromol. Symp. 26 (2008) 10-17.

[80] N. Guo, S.A. DiBenedetto, D.K. Kwon, L. Wang, M.T. Russell, M.T. Lanagan, A. Facchetti, T.J. Marks, Supported metallocene catalysis for in situ synthesis of high energy density metal oxide nanocomposites, J. Am. Chem. Soc. 129 (2007) 766-767.

[81] P. Galli, J.C. Haylock, Makromol. Chem., Advances in Ziegler-Natta polymerization - unique polyolefin copolymers, alloys and blends made directly in the reactor, Macromol. Symp. 63 (1992) 19-54.

[82] G. Cecchin, G. Morini, A. Pelliconi, Polypropylene product innovation by reactor granule technology, Macromol. Symp. 173 (2001) 195-209.

[83] R. A. Hutchinson, C. M. Chen, W. H. Ray, Polymerization of olefins through heterogeneous catalysis X: Modeling of particle growth and morphology, J. Appl. Polym. Sci. 44(1992) 1389-1414.

[84] C. W. Hock, How $TiCl_3$ catalysts control the texture of as-polymerized polypropylene, J. Polym . Sci. A1 4 (1966) 3055-3064.

[85] E. Albizzati, U. Giannini, G. Collina, L. Noristi, L. Resconi, Propylene Handbook, E. P. Moore, Ed., Hanser, New York, 1996, pp. 86-89.

[86] Y. Chen, W. Chen, D. Yang, Morphology of high impact polypropylene particles, Polymer 47 (2006) 6808-6813.

Chapter 2

New Reactor Granule Technology for Highly Filled Nanocomposites: Effective Flame Retardation of Polypropylene/Magnesium Hydroxide Nanocomposites

Abstract

A novel additive-free reactor granule technology is reported for the fabrication of polyolefin-based nanocomposites, which involves *in-situ* generation of nanoparticles with unprecedented dispersion even at high filler loadings. Polypropylene reactor powder obtained by catalyzed propylene polymerization is first impregnated with magnesium ethoxide ($Mg(OEt)_2$) solution. After the solvent drying and hydration, the powder is melt mixed to convert $Mg(OEt)_2$ hydrate into magnesium hydroxide ($Mg(OH)_2$). Thus prepared $PP/Mg(OH)_2$ composites exhibit uniform dispersion of the *in-situ* formed $Mg(OH)_2$ nanoparticles even at a high filler loading (*e.g.* 20 wt%) without the use of dispersants, which is unexpected for the combination of hydrophilic filler and hydrophobic matrices. The obtained nanocomposites significantly improve the flame retardancy at filler loading much lower than those for conventional composites.

2.1. Introduction

"Polymer nanocomposites" are a relatively new class of materials, in which the inclusion of a small amount of nano-sized filler dramatically improves properties of base polymer [1]. Such dramatic improvements arise mainly from enhanced interaction between polymer and nano-sized filler embedded in polymer matrices. Enhanced interaction necessarily indicates a strong propensity of nanoparticles toward self-agglomeration, which has been a bottleneck for polymer nanocomposites, especially for hydrophobic polymer (*i.e.* the most widely used thermoplastics). A variety of strategies have been proposed to attain the nano-level dispersion of filler, in most of which both/either of compatibilizers and/or surface modifiers are employed. These dispersants alleviate poor compatibility between the two substances [2,3], but at the same time cause problems such as cost penalty, unfavorable impacts on polymer properties [4,5], accelerated degradation [6,7] and so on. Moreover, a great challenge exists when a relatively high loading of nano-sized filler is required, especially in improving dielectric properties and flame retardancy of polymer matrices, where a few tens to several tens percents of filler are usually added [8-10].

Evidently, the best approach is to achieve the nano-level dispersion without any dispersants, which in turn reduces the required loading. To realize uniform dispersion at a high filler loading, a lot of emphasis is focused on finding an additive-free route to prepare

highly filled nanocomposites with improved dispersion. In this chapter of thesis, I report a novel strategy to prepare highly filled nanocomposites having an extremely nice dispersion in a dispersant-free manner. The strategy involves solvent-aided impregnation of metal alkoxides into the porosity of polymer granule and subsequent chemical conversion of the metal alkoxides into inorganic nanoparticles during melt processing (**Fig. 2.1**), leading to unprecedented dispersion even at a high filler loading.

The proposed strategy was successfully applied to prepare flame-retardant polypropylene (PP)/magnesium hydroxide ($Mg(OH)_2$) nanocomposites: The former as the most important but the most challenging plastic due to its chemical inertness, and the latter as the most widely employed non-halogenated flame retardant. PP reactor powder directly obtained from catalyzed polymerization was first impregnated with magnesium ethoxide ($Mg(OEt)_2$) dissolved in solvent. Followed by a hydration process, the resultant powder was melt mixed for the *in-situ* conversion of $Mg(OEt)_2$ hydrate into $Mg(OH)_2$ nanoparticles. Thus prepared nanocomposites exhibited not only complete chemical conversion but also uniform dispersion of *in-situ* generated $Mg(OH)_2$ nanoparticles in a wide range of loadings (0-20 wt%). A dramatic enhancement in the flame retardancy was achieved at 20 wt%, while the addition of pre-formed nanoparticles hardly improved it at the same loading.
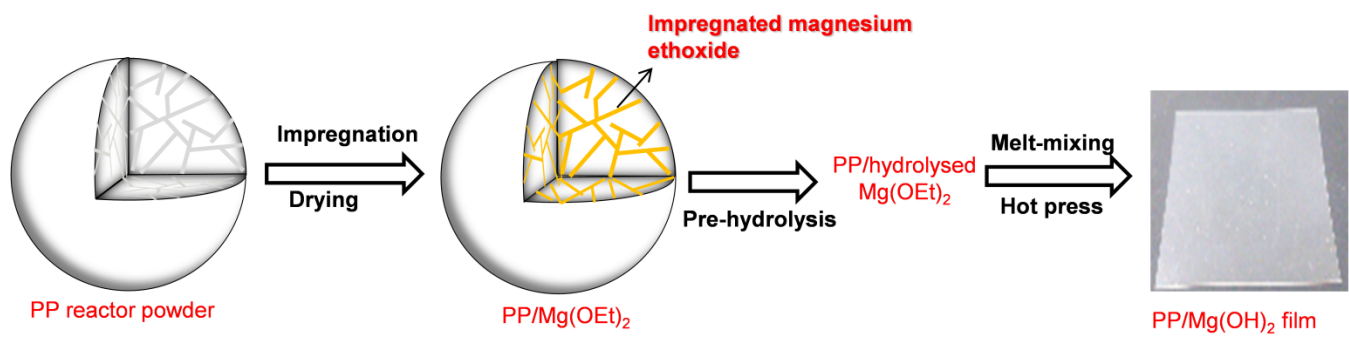
Figure 2.1. New reactor granule technology for additive-free nanocomposites.

2.2. Experimental

2.2.1. *Materials*

Reactor powder of PP (M_w= 2.6 x 105, M_w/M_n = 5.69 and *mmmm* = 98 mol%) was obtained by propylene polymerization using a $MgCl_2$-supported Ziegler-Natta catalyst. Anhydrous $Mg(OEt)_2$ used as a precursor was purchased from Sigma-Aldrich. *n*-Octdecyl-3-(3',5'-di-*t*-butyl-4'-hydroxyphenyl)-propionate (AO-50) as a stabilizer was donated by ADEKA Corporation. $Mg(OH)_2$ nanoparticles with the particle size < 100 nm were purchased from Sigma-Aldrich as a reference.

2.2.2. *Preparation of PP/Mg(OH)₂ nanocomposites*

PP/$Mg(OH)_2$ nanocomposites were prepared as follows: 40 g of the PP reactor powder was impregnated with a specific amount of $Mg(OEt)_2$ dissolved in methanol/toluene solution (1/5 v/v) at 50 °C under N_2 for 12 h. The amount of $Mg(OEt)_2$ was determined in order to satisfy 1.0, 3.0, 5.0, 10, 20 and 30 wt% of $Mg(OH)_2$ on the assumption of the full conversion of $Mg(OEt)_2$ into $Mg(OH)_2$. Followed by the impregnation and solvent removal in vacuo, the PP powder was either directly melt mixed or melt mixed after a hydration process that could be accomplished by sufficient exposure of the powder to the atmosphere. The melt mixing was implemented in the presence of 1.0 wt% of AO-50 using an internal mixer (Toyo Seiki, LaboPlastomill) at 180 °C and 100 rpm for 20 min.

For comparison, 1.0-20 wt% of the pre-formed $Mg(OH)_2$ nanoparticles was also melt mixed with the PP powder at the same conditions, and these reference samples are termed as "PP/$Mg(OH)_2$-NP" in contrast to "*in-situ* PP/$Mg(OH)_2$" prepared based on the proposed strategy. For subsequent characterization, the nanocomposites were hot pressed into 100 μm-thick films at 230 °C and 10 MPa, and then quenched at 100 °C for 5 min under N_2.

2.2.3. *Characterization*

Transmission IR spectra of the sample films were acquired on FT/IR-6100 (JASCO) with a resolution of 4 cm^{-1} and 24 scans. The dispersion of nanoparticles in the matrix was observed by transmission electron microscopy (TEM, Hitachi H-7100). TEM specimens with the thickness of 100 nm were prepared by an ultramicrotome (ULTRACUTS FCS, Leica) equipped with a diamond knife (Diatome). The crystallinity and isothermal crystallization of the prepared nanocomposites was examined by differential scanning calorimeter (DSC, METTLER TOLEDO, DSC-822) in N_2 with a flow rate of 75 mL/min and at a scanning rate of 10°C/min in the temperature range of 35-200°C. The crystallinity of the samples was calculated from the following equation:

$$X_c = (\Delta H_m m_c/m_p)/\Delta H_0$$

where, H_m is the melting enthalpy measured in the heating experiments, H_0 is the theoretical value of enthalpy of 100 % crystalline PP (H_0= 207.1 J/g) [34], m_c is the mass of the sample and m_p is the mass of PP in the sample.

The isothermal crystallization was investigated at 128 ºC. The sample was kept at 230 ºC for 10 min to erase the thermal history, and then cooled down to 128 ºC at the cooling rate of 20 ºC/min. Tensile properties of nanocomposites were acquired using a tensile tester (Abecks Inc., Abe Dat-100) at a crosshead speed of 1.0 mm/min. Sample films were die-cut into dumbbell-shaped specimens with the overall length of 23 mm and the gage length of 5 mm. Tensile properties such as tensile strength and Young's modulus were determined as an average value of 10 measurements. Dielectric properties of nanocomposites were measured using a LCR meter (Agilent, Precision LCR meter E 4980A) in the frequency range of 10^2-10^7 Hz at room temperature. A disc-shaped specimen with a diameter of 2.5 cm was coated with gold to create thin conductive layers for a parallel plate capacitor. The thermal stability of the prepared nanocomposites was measured by thermal gravimetric analysis (TGA, Seiko, and TGA/DTA-6200). The samples were heated in air with a flow rate of 200 mL/min and at a scanning rate of 10 ºC/min in the temperature range of 35-600 ºC. The flammability of the sample films ($160 \times 60 \times 0.1$ mm^3) was evaluated by limiting oxygen index (LOI) tests according to ISO 4589-2 using a flammability tester (ON-2M, Suga Test Instruments Co., Ltd.).

2.3. Results and Discussion

2.3.1. *Kinetics of pre-hydrolysis*

After impregnation of $Mg(OEt)_2$ (whose amount corresponded to 10 wt% of $Mg(OH)_2$), the PP powder was kept at room temperature under relative humidity (RH) of 25 or 75%. The kinetics of the reaction between $Mg(OEt)_2$ and moisture was tracked by observing the weight increase/loss of the powder. As can be seen in **Fig. 2.2**, the PP/$Mg(OEt)_2$ powder underwent gradual weight loss, whose kinetics depended on RH. The weight loss converged into *ca.* 67.3 wt% after 70 h, while into 66.6 wt% after 30 h. Thus, more humid circumstance accelerates the kinetics. Similar weight-loss kinetics was observed for pristine $Mg(OEt)_2$ powder. The weight loss clearly indicated that the exposure to the atmosphere made partial hydrolysis to liberate ethanol. The apparent chemical composition corresponded to roughly $Mg(OEt)_{1.2}(OH)_{0.8}$
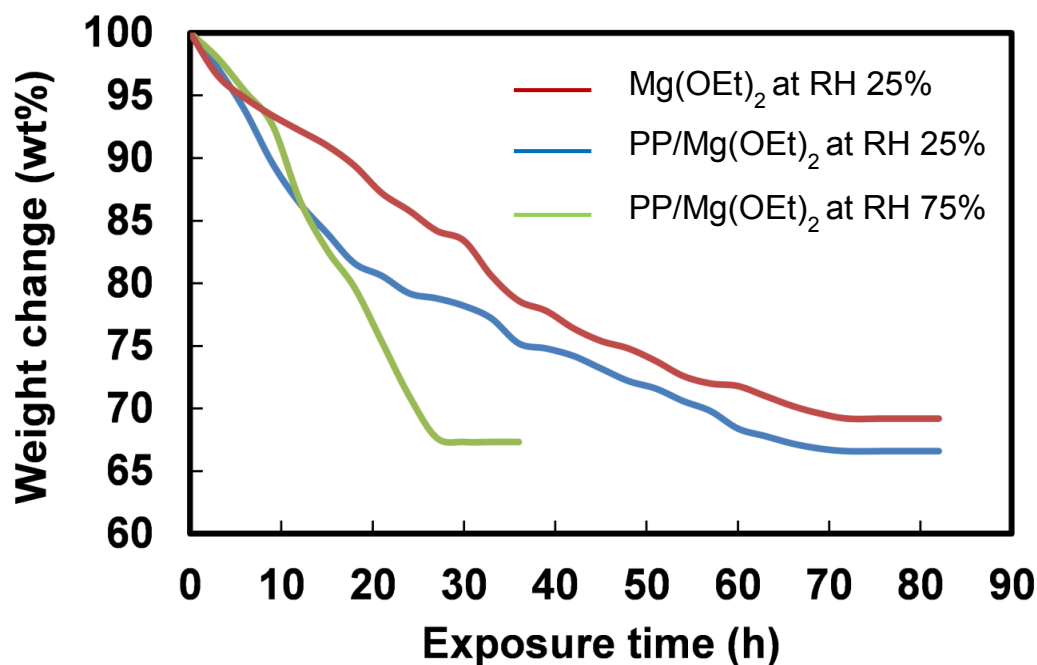
.

Figure 2.2. Kinetics of the reaction between Mg(OEt)$_2$ and moisture.

2.3.2. *Chemical conversion*

   PP/Mg(OH)$_2$ nanocomposites with different Mg(OH)$_2$ loadings were prepared based on the proposed strategy. The chemical conversion of Mg(OEt)$_2$ into Mg(OH)$_2$ was investigated by IR, and the results were compared with those for neat PP and PP/Mg(OH)$_2$-NP (**Fig. 2.3**). As can be seen in **Fig. 2.3a and 2.3d**, the inclusion of Mg(OH)$_2$ nanoparticles in PP resulted in absorption bands specific to Mg(OH)$_2$: A broad band at 450-550 cm^{-1} for the Mg-O

stretching vibration, and a sharp band at 3690 cm^{-1} for the O-H stretching vibration [11,12].

When the Mg(OEt)$_2$-impregnated reactor powder was melt mixed without the pre-treatment process, the said two bands for Mg(OH)$_2$ hardly appeared (**Fig. 2.3b**). Instead, two bands specific to Mg(OEt)$_2$ were observed at around 500-600 cm^{-1} and 1080 cm^{-1}, respectively corresponding to the Mg-O (ethoxide group) and C-O stretching vibration [13,14].

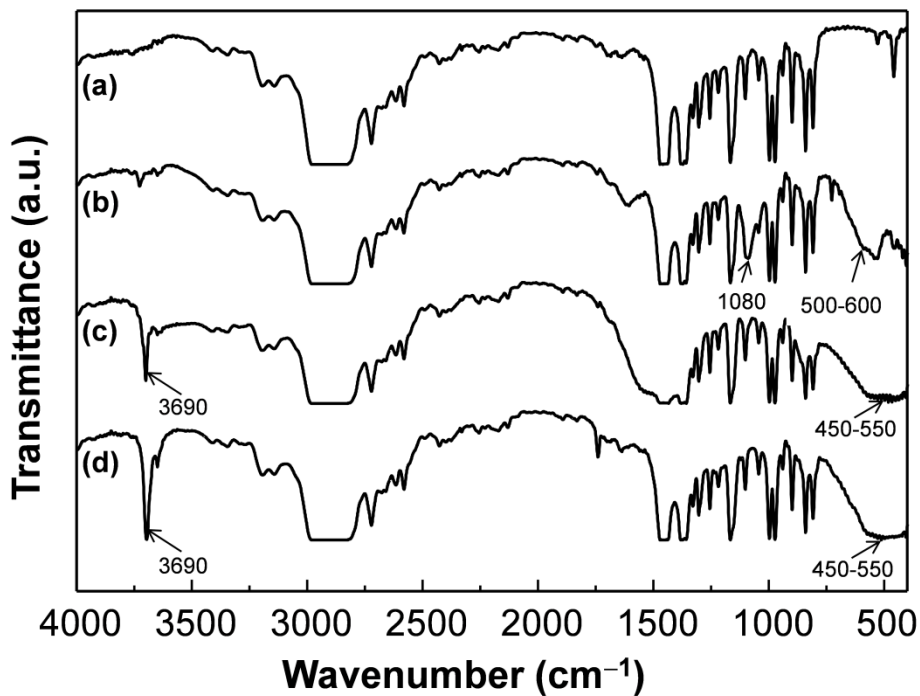**Figure 2.3.** FT-IR spectra: a) Neat PP, b) *in-situ* PP/Mg(OH)$_2$ without hydration, c) *in-situ* PP/Mg(OH)$_2$ with hydration and d) PP/Mg(OH)$_2$-NP. The Mg(OH)$_2$ loading for the nanocomposite samples was 5.0 wt%.

This fact clearly indicated that $Mg(OEt)_2$ immobilized in the porosity of the reactor powder remained un-reacted during the melt mixing. The exposure of the impregnated reactor powder to the atmosphere prior to the melt mixing dramatically improved the chemical conversion of $Mg(OEt)_2$ into $Mg(OH)_2$.

In **Fig. 2.3c**, it was found that the two peaks for $Mg(OEt)_2$ were totally displaced by those for $Mg(OH)_2$. Thus, *in-situ* fabrication of $Mg(OH)_2$ was successfully accomplished when the powder was hydrated prior to the melt mixing. $Mg(OEt)_2$ is known to facilely absorb water to form hydrate [15]. It is plausible that the absorbed water was utilized to fully hydrolyse Mg-OEt bonds into Mg-OH. Hereafter, all the $PP/Mg(OH)_2$ samples were prepared after the hydration process.

2.3.3. Inorganic content

For verifying the actual inorganic content in the prepared nanocomposites, the weight fraction of the formed oxides was evaluated using TGA. At 600 °C under air, all organic contents present in the nanocomposites are burned out and the remaining ash is considered to represent the inorganic content. **Table 2.1** summarizes the inorganic content for all the prepared *in-situ* $PP/Mg(OH)_2$ nanocomposites. It was found the actual inorganic content obtained from TGA was similar to the value expected from the theoretical content at the filler loading of 1.0 and 3.0 wt%. On the other hand, the actual inorganic content was found to be lower than the theoretical content at 5.0 wt%. When the pre-treatment process was employed, the inorganic content became much closer to the corresponding theoretical content.

This fact along with the IR results suggested that the pre-treatment process is essential at high filler loading for obtaining the desired amount of $Mg(OH)_2$.

Table 2.1. TGA results for *in-situ* nanocomposites

Sample	Theoretical content[a] (wt%)	Actual content[b] (wt%)
PP/Mg(OH)$_2$ (no pre-treatment)	1.0	0.9
	3.0	2.8
	5.0	3.7
PP/Mg(OH)$_2$ (pre-treatment)	5.0	4.8
	10	9.4
	20	18.9

[a] Theoretical contents were estimated based on the assumption of the full conversion to oxides.
[b] Measured by TGA.

2.3.4. *Spatial distribution of nanoparticles*

Fig. 2.4 summarizes TEM images for the two types of PP/Mg(OH)$_2$ nanocomposites at 5.0 and 20 wt%. As is frequent, the melt mixing of pre-formed Mg(OH)$_2$ nanoparticles resulted in the formation of micro-sized aggregates, which became more serious at the higher loading (**Fig. 2.4a and 2.4b**). Critical differences were observed when Mg(OH)$_2$ was *in-situ* generated from Mg(OEt)$_2$ in PP (**Fig. 2.4c and 2.4d**). The formed particles were basically

nano-sized with the dimensions of 50-100 and 250-300 nm for 5.0 and 20 wt%, respectively. Moreover, the dispersion of nanoparticles was quite uniform irrespective of the filler loading. Such uniform dispersion of hydrophilic nanoparticles in hydrophobic matrices was never seen and quite unexpected especially at a high filler loading like 20 wt%. Notably, it was achieved for PP, as the most important but most challenging thermoplastic, without using any dispersants. To rationalize the obtained results, the following mechanism was proposed: First, dissolved $Mg(OEt)_2$ molecules diffuse in the porosity of the reactor powder in impregnation, and gradually precipitate as a crystalline material during drying, where the crystalline growth and/or secondary agglomeration of $Mg(OEt)_2$ was confined in the porosity. Second, the $Mg(OEt)_2$ particles present in the porosity absorb water molecules during pre-treatment to become hydrolysed, whose size is also restricted by the porosity. In the melt-processing, the hydrolyzed $Mg(OEt)_2$ is fully converted into $Mg(OH)_2$. The size and dispersion of formed $Mg(OH)_2$ particles retain those of $Mg(OEt)_2$ uniformly impregnated in the porosity, where not only facile conversion but also the viscosity of molten polymer are believed to prevent the growth and agglomeration of the nanoparticles.
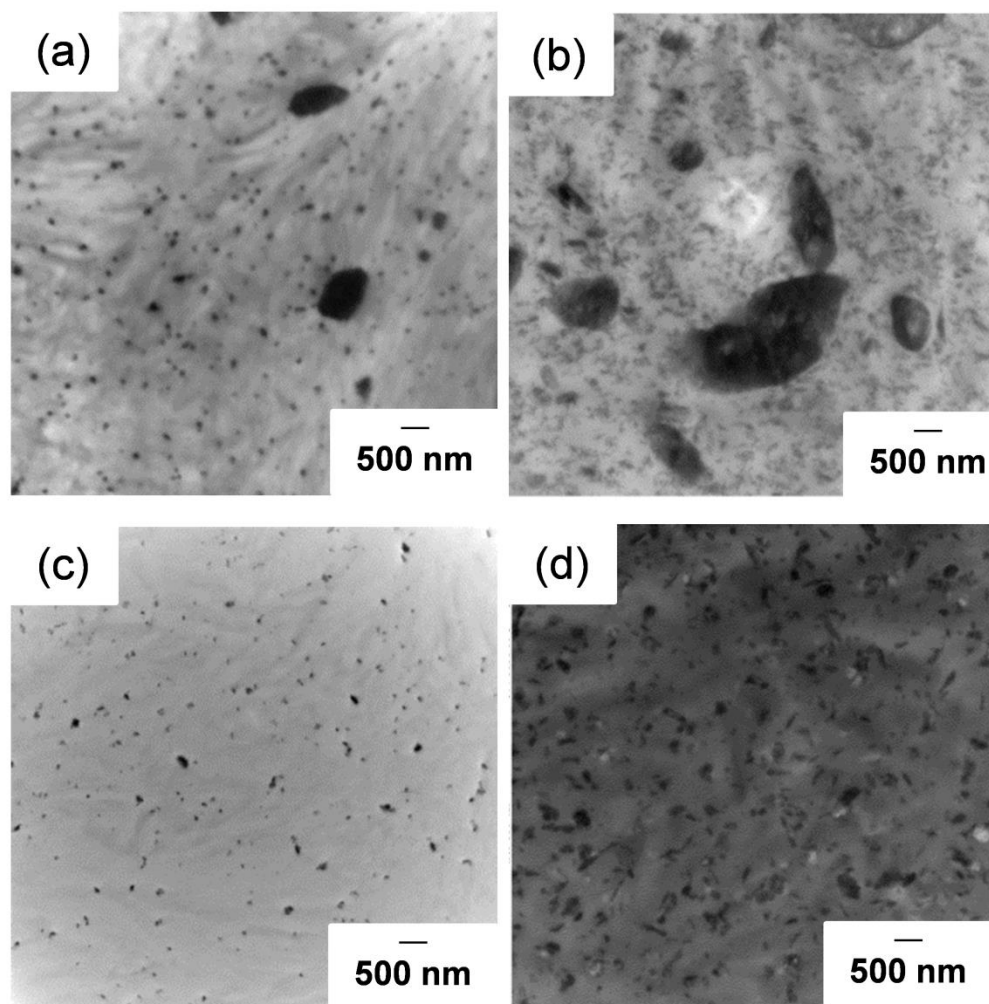
Figure 2.4. TEM micrographs: a,b) PP/Mg(OH)$_2$-NP and c,d) *in-situ* PP/Mg(OH)$_2$ nanocomposites at 5.0 and 20 wt%, respectively.

2.3.5. <u>Crystallization behavior</u>

DSC results for neat PP, *in-situ* PP/Mg(OH)$_2$ and PP/Mg(OH)$_2$-NP nanocomposites are shown in **Fig. 2.5**. The crystallinity of PP was enhanced at 1.0 and 3.0 wt% for both of the *in-situ* PP/Mg(OH)$_2$ and PP/Mg(OH)$_2$-NP nanocomposites. But as the amount of filler increased the two types of nanocomposites showed the opposite trends. In the case of *in-situ* PP/Mg(OH)$_2$ nanocomposites, the crystallinity increased monotonically along the filler content. This may be attributed to heterogeneous nucleation effect of Mg(OH)$_2$ [38]. But in the case of PP/Mg(OH)$_2$-NP nanocomposites, the crystallinity rather decreased above 3 wt%. The larger aggregates might weaken the nucleation effect of Mg(OH)$_2$ [39].
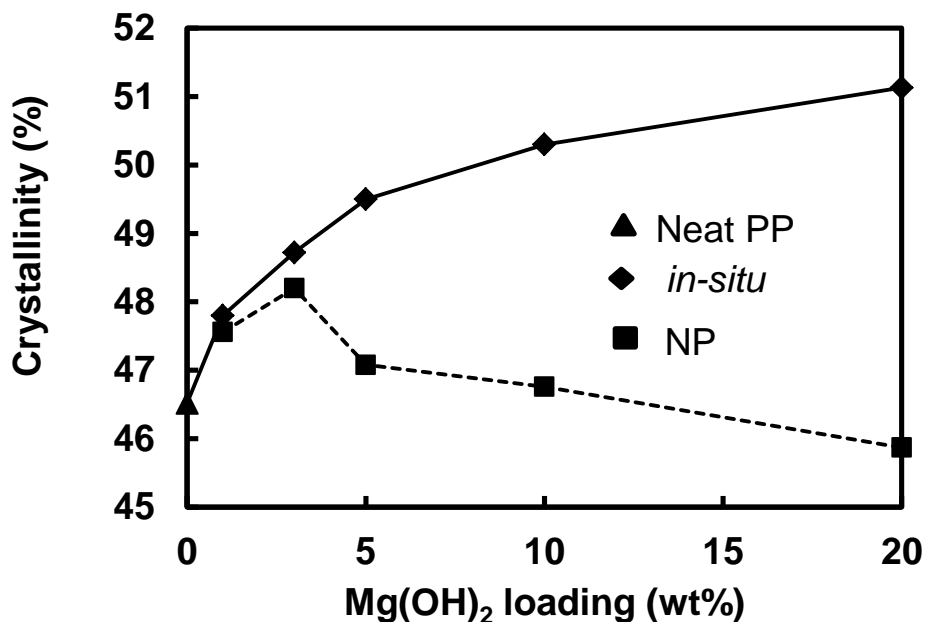

Figure 2.5. Crystallinity for (▲) neat PP, (◆) *in-situ* PP/Mg(OH)$_2$ and (■) PP/Mg(OH)$_2$-NP nanocomposites.

The results of half-time of crystallization ($t_{1/2}^{-1}$) at different filler loadings is shown in **Fig. 2.6**. The isothermal crystallization showed a significantly faster rate of crystallization for PP/Mg(OH)$_2$ composites as compared to neat PP. For instance, the crystallization increased by ca. five folds at the filler loading of 5 wt%. But as the concentration increased from 5 wt%, the change in $t_{1/2}^{-1}$ is not so significant, suggesting that at 5 wt%, the composite is saturated with enough nucleation sites.
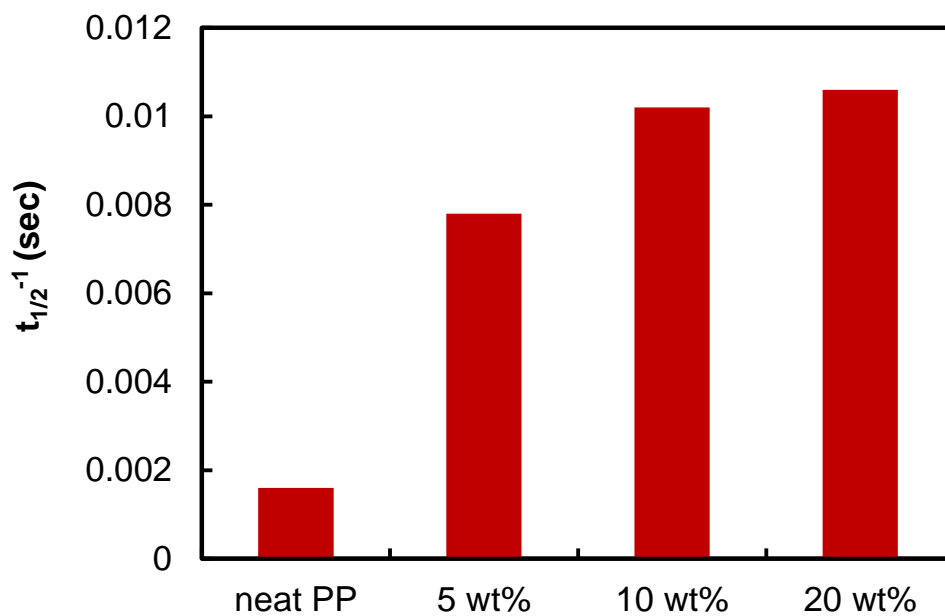

Figure 2.6. Isothermal crystallization kinetics for neat PP and PP/Mg(OH)$_2$ nanocomposites at different filler loading

2.3.6. Mechanical Properties

   A uniaxial test was performed to evaluate the mechanical properties of the prepared

$Mg(OH)_2$ nanocomposites. The tensile strength and young's modulus are plotted against the

filler loading in **Fig. 2.7 and Fig. 2.8**. It is well known that the mechanical properties of the

nanocomposites are mainly influenced by the stiffness, the dispersion of nanoparticles and

the adhesion between the matrix and the nanoparticles. It can be seen that the *in-situ* samples

exhibited better mechanical properties than those of the samples prepared by direct melt-

mixing of pre-formed nanoparticles. Both the tensile strength and young's modulus followed
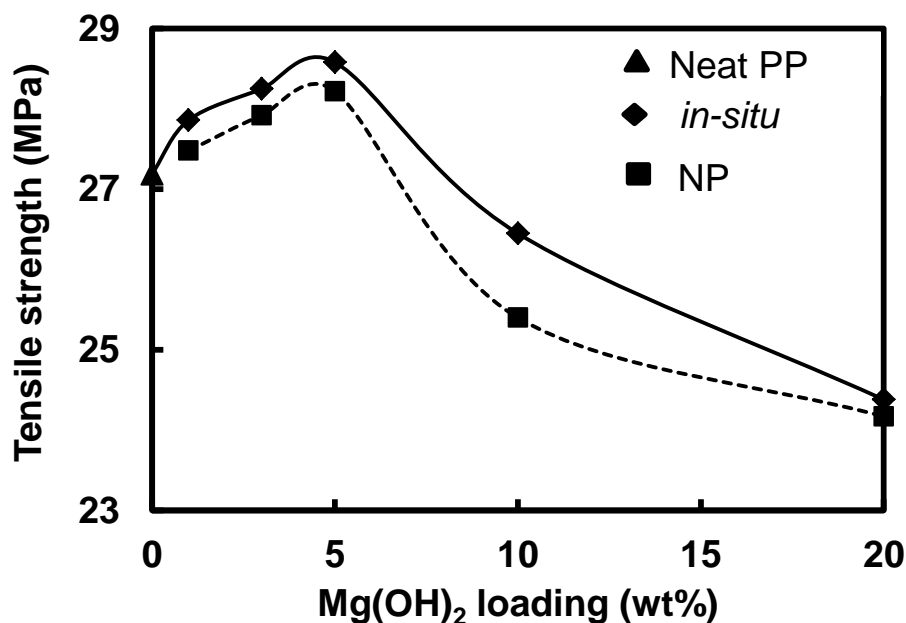
the similar trend.

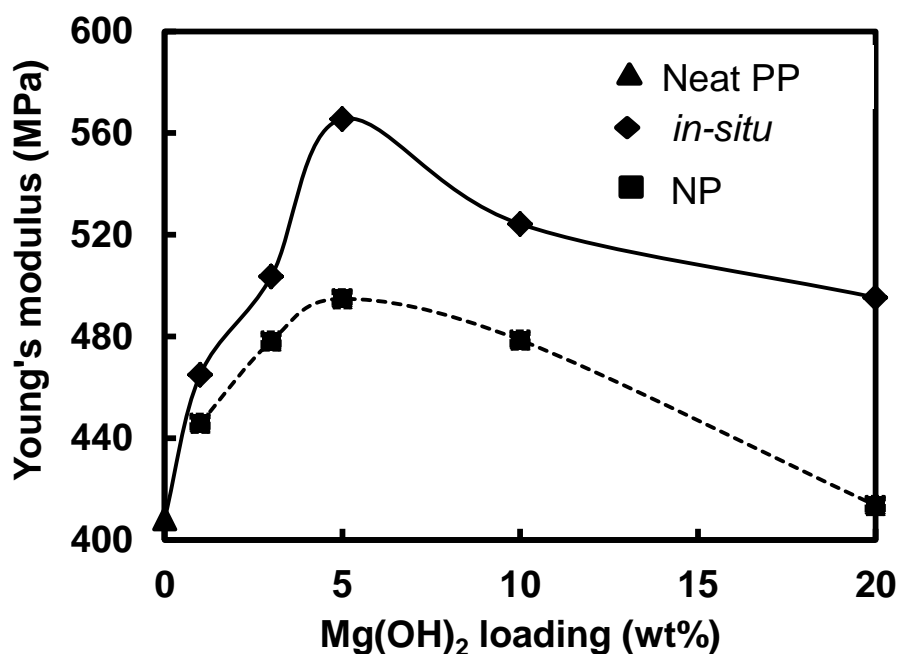**Figure 2.7.** Tensile strength for neat PP and PP/$Mg(OH)_2$ nanocomposites.

Figure 2.8. Young's modulus for neat PP and PP/Mg(OH)$_2$ nanocomposites.

2.3.7. *Dielectric Characeristics*

Fig. 2.9 represents the variation of the dielectric constant along the frequency for neat PP and *in-situ* PP/Mg(OH)$_2$ nanocomposites at different filler loadings. Neat PP exhibited the dielectric constant of 2.3 and the value of dielectric constant remained constant in the whole frequency range. This is attributed to the non-polar nature of PP, as a result of which there is almost no dielectric relaxation.
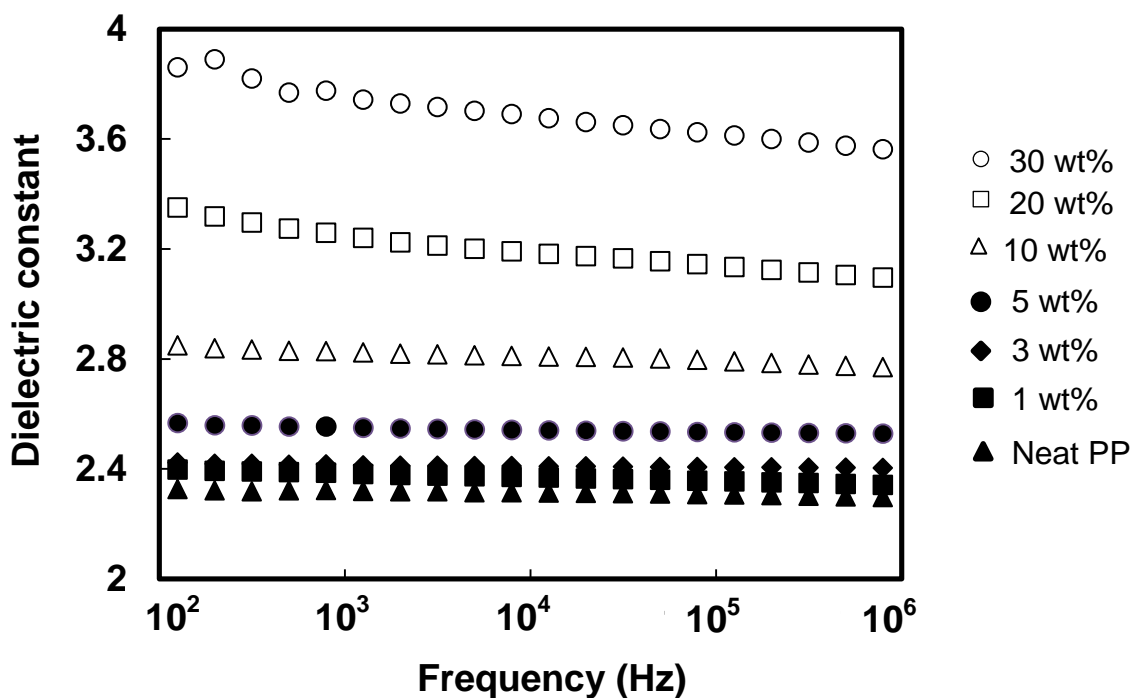
Figure 2.9. Frequency dependence of the dielectric constant for neat PP and *in-situ* PP/Mg(OH)$_2$ nanocomposites.

In case of nanocomposites, since Mg(OH)$_2$ possesses a relatively high dielectric permittivity, its inclusion in PP resulted in an increment of the dielectric constant of the resultant PP/Mg(OH)$_2$ nanocomposites along the filler loading. Moreover, a frequency dependent behavior was observed in the nanocomposites due to the existence of interfacial polarization [29]. At high frequencies, dipolar groups are not capable of following the field variation, thus decreasing the dielectric constant [30].
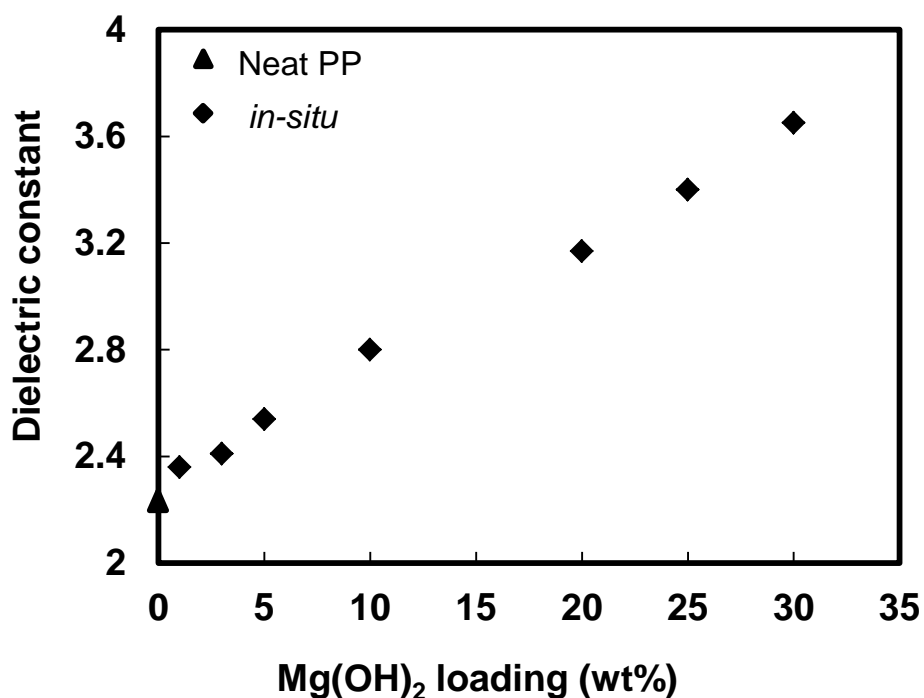
Figure 2.10. Dielectric constant (at 10^5 Hz) of Neat PP and *in-situ* PP/Mg(OH)$_2$ nanocomposites plotted against the filler loading.

2.3.8. *Thermoanalytical investigations*

In order to study the thermal oxidation behaviour of the prepared PP/Mg(OH)$_2$ nanocomposites, TGA was performed under air. As can be seen in **Fig. 2.11**, *in-situ* PP/Mg(OH)$_2$ increased the thermal oxidation resistance in a more efficient manner compared with PP/Mg(OH)$_2$-NP. Representatively, T$_{50\%}$ (temperature at which 50 % weight loss

occurred) was 404°C for *in-situ* PP/Mg(OH)$_2$ compared with 393°C for PP/Mg(OH)$_2$-NP at 30 wt%. This revealed that the thermal stability of *in-situ* PP/Mg(OH)$_2$ was higher than that of PP/Mg(OH)$_2$-NP, indicating that *in-situ* generation of Mg(OH)$_2$ nanoparticles is more effective in increasing the thermal stabiliy of PP.
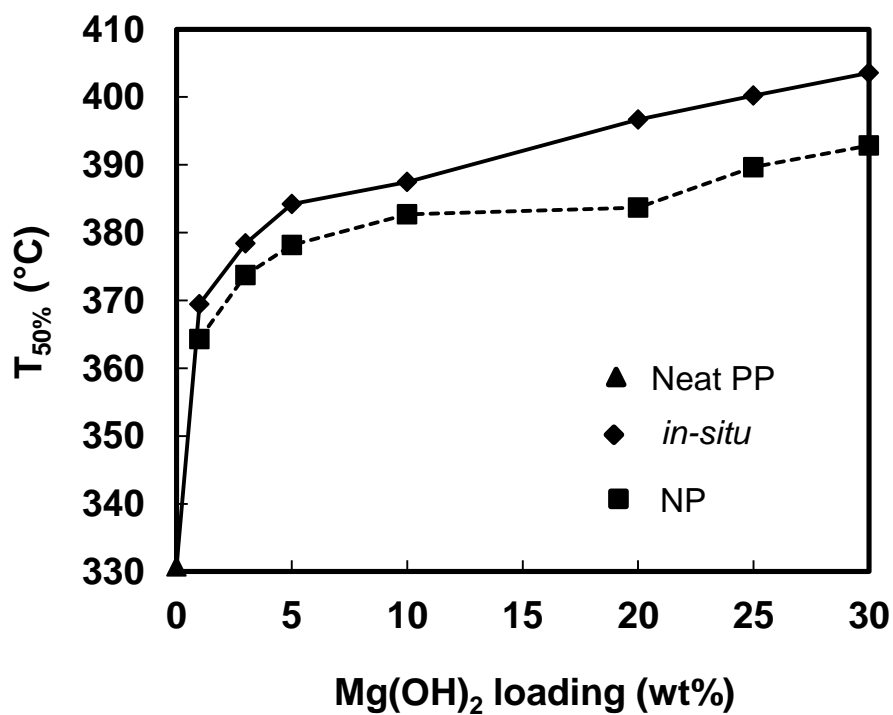

Figure 2.11. T$_{50\%}$ for (▲) neat PP, (◆) *in-situ* PP/Mg(OH)$_2$ and (■) PP/Mg(OH)$_2$-NP nanocomposites.

2.3.9. *Flame retardant behavior*

$Mg(OH)_2$ is the most widely used non-halogenated flame retardant. Flammability of the nanocomposites was examined by the LOI tests. The results are plotted in **Fig. 2.12** along the filler loading for *in-situ* $PP/Mg(OH)_2$ and $PP/Mg(OH)_2$-NP. The flame retardation of polyolefin usually requires the $Mg(OH)_2$ loading as high as 60 wt% [16-18]. The LOI value of $PP/Mg(OH)_2$-NP samples was hardly improved even when 20 wt% of pre-formed $Mg(OH)_2$ nanoparticles was added (only 18.5 compared with 18.0 for neat PP). However, the *in-situ* $PP/Mg(OH)_2$ samples exhibited a totally different behaviour: The LOI value increased almost linearly even at low loadings, and reached to 26.5 at 30 wt%. The dispersion of nanoparticles in the polymer matrices has a significant effect on their flammability properties [19]. Such superior flame retardancy for *in-situ* $PP/Mg(OH)_2$ was attributed to extremely nice dispersion of the *in-situ* generated nanoparticles. Well-dispersed $Mg(OH)_2$ nanoparticles exert barrier effects and help in the formation of more compact and cohesive charred layer during combustion. This protective layer insulates the matrix from heat flux and prevents the combustion.
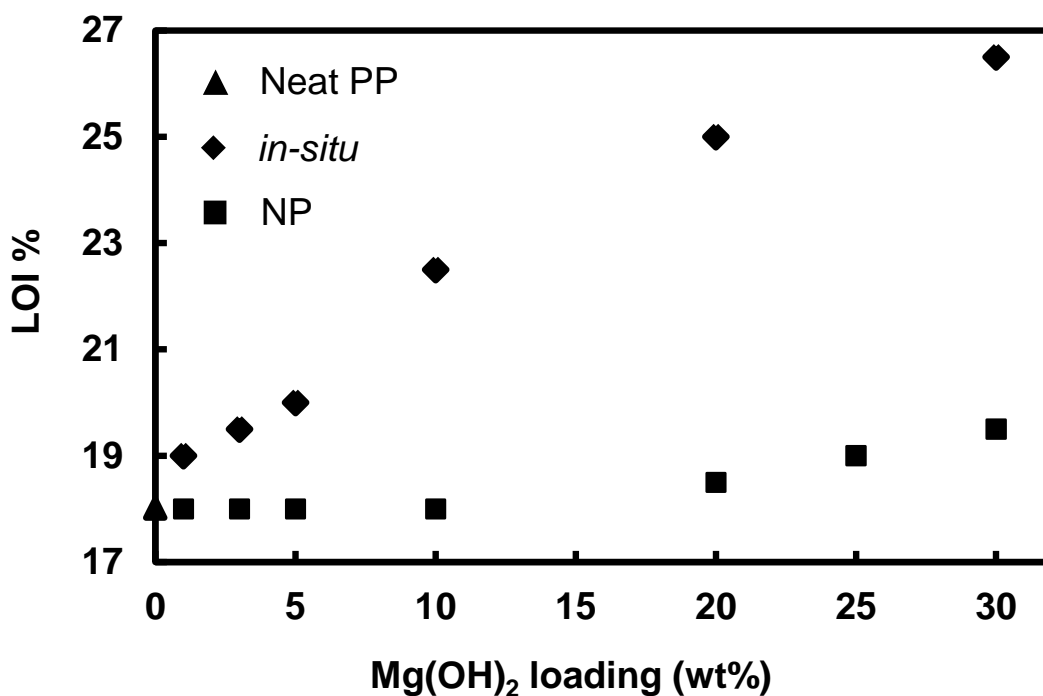
Figure 2.12. LOI of (▲) neat PP, (◆) *in-situ* PP/Mg(OH)$_2$ and (■) PP/Mg(OH)$_2$-NP nanocomposites.

2.4. Conclusions

A novel reactor granule strategy has been presented for the fabrication of highly filled nanocomposites without the use of any dispersants. It involved impregnation of metal alkoxides in the porosity of polymer reactor powder and subsequent conversion into well-dispersed nanoparticles in melt processing. A successful demonstration was given for PP/Mg(OH)$_2$ nanocomposites with extremely nice dispersion of Mg(OH)$_2$ at a high filler loading and superior flame retardancy, thereby. So far, poor dispersion and negative

influences of additives have severely hampered the development of polyolefin-based nanocomposites. This is one of rare examples that successfully exploits a great potential of polyolefin-based nanocomposites in the simplest and versatile process, which could be easily extended to similar nanocomposite materials.

2.5 References

[1] L. Peponi, D. Puglia, L. Torre, L. Valentini, J. M. Kenny, Processing of nanostructured polymers and advanced polymeric based nanocomposites, Mater. Sci. Eng. R 85 (2014) 1-46.

[2] N. Hasegawa, H. Okamoto, M. Kato, A. Usuki, Preparation and mechanical properties of polypropylene-clay hybrids based on modified polypropylene and organophilic clay, J. Appl. Polym. Sci. 78 (2000) 1918-1922.

[3] E. Pavlidou, D. Bikiaris, A. Vassiliou, M. Chiotelli, G. Karayannidis, Mechanical properties and morphological examination of isotactic Polypropylene/SiO$_2$ nanocomposites containing PP-g-MA as compatibilizer, J. Phys. Conf. Ser. 10 (2005) 190-193.

[4] J. W. Lim, A. Hassan, A. R. Rahmat, M. U. Wahit, Morphology, thermal and mechanical behavior of polypropylene nanocomposites toughened with poly(ethylene-co-octene) Polym. Int.55 (2006) 204-215.

[5] Y. Wang, F. B. Chen, K. C. Wu, Effect of the molecular weight of maleated polypropylenes on the melt compounding of polypropylene/organoclay nanocomposites, J. Appl. Polym. Sci.97 (2005) 1667-1680.

[6] S. Morlat, B. Mailhot, D. Gonzalez, J. L. Gardette, Photo-oxidation of polypropylene/montmorillonite nanocomposites. 1. Influence of nanoclay and compatibilizing agent, Chem. Mater. 16 (2004) 377-383.

[7] B. Mailhot, S. Morlat, J. L. Gardette, S. Boucardb, J. Duchet, J. F. Gerard, photodegradation of polypropylene nanocomposites, Polym. Deg. Stab.82 (2003) 163-167.

[8] G. I. Titelman, Y. Gonen, Y. Keidar, S. Bron, Discolouration of polypropylene-based compounds containing magnesium hydroxide, Polym. Deg. Stab.77 (2002) 345-352.

[9] X. Huang, L. Xie, K.Yang, C.Wu, P. Jiang, S. Li, S. Wu, K. Tatsumi, The future of nanodielectrics in the electrical power industry, T. Tanaka, *IEEE Trans. Dielectr. Electr. Insul.* 11 (2004) 797-80.

[10] Z. Lin, Y. Qiu, K. Mai, Crystallization and melt behavior of magnesium hydroxide/polypropylene composites modified by functionalized polypropylene, J. Appl. Sci 91(2004) 3899-3908.

[11] L. Shen, Y. Chen, P. Li, Synergistic catalysis effects of lanthanum oxide in polypropylene/magnesium hydroxide flame retarded system, Composites: Part A. 43(2012) 1177-1186.

[12] X. Chen, J. Yu, S. Guo, S. Lu, Z. Luo, M. He, Surface modification of magnesium hydroxide and its application in flame retardant polypropylene composites, J. Mater. Sci. 44 (2009) 1324-1332.

[13] L. L. Mguni, M. Mukenga, E. Muzenda, K. Jalama, R. Meijboom, Expanding the synthesis of Stöber spheres: towards the synthesis of nano-magnesium oxide and nano-zinc oxide, J. Sol-Gel Sci. Technol. 66 (2013) 91-99.

[14] H. S. Jung, J. K. Lee, J. Y. Kim, K. S. Hong, Crystallization behaviors of nanosized MgO particles from Mg alkoxides, J. Colloid Interface Sci. 259 (2003) 127-132.

[15] S. Utamapanya, K. J. Klabunde, J. R. Schlup, Nanoscale metal oxide particles/clusters as chemical reagents, Synthesis and properties of ultrahigh surface area magnesium hydroxide and magnesium oxide, Chem. Mater. 3 (1991)175-181.

[16] C. M. Tai, R. K. Y. Li, Mechanical properties of flame retardant filled polypropylene composites, J. Appl. Polym. Sci.80 (2001) 2718-2728.

[17] R. N. Rothon, P. R. Hornsby, Flame retardant effects of magnesium hydroxide, Polym. Deg. Stab. 54 (1996) 383-385.

[18] H. Lu, Y. Hu, L. Yang, Z. Wang, Z. Chen, W. Fan, Study of the fire performance of magnesium hydroxide sulfate hydrate whisker flame retardant polyethylene, Macromol. Mater. Eng. 289 (2004) 984-989.

[19] S. P. Liu, J. R. Ying, X. P. Zhou, X. L. Xie, Y. W. Mai, Dispersion, thermal and mechanical properties of polypropylene/magnesium hydroxide nanocomposites compatibilized by SEBS-*g*-MA, Compos. Sci. Technol. 69 (2009) 1873-1879.

Chapter 3

Reactor Granule Technology for Fabrication of Functionally Advantageous Polypropylene Nanocomposites with Oxide Nanoparticles

Abstract

Polypropylene (PP)/TiO$_2$ and PP/Al$_2$O$_3$ nanocomposites were fabricated based on a new technology that involves the impregnation of metal alkoxide precursors in the porosity of PP reactor granule and subsequent conversion of the precursors into oxides during melt mixing. The so-called reactor granule technology enabled *in-situ* generation of highly dispersed oxide nanoparticles over a wide range of the loading extending up to 20 wt% without the use of dispersants. The confinement of metal alkoxide precursors in the porosity of the PP reactor granule and their facile chemical conversion into oxides were found to be crucial for the dispersion of the nanoparticles. The excellent dispersion of Al$_2$O$_3$ nanoparticles led to significant improvements in tensile properties, dielectric constants, and thermal conductivity as compared to conventional nanocomposites using a compatibilizer. It was concluded that the reactor granule technology is a simple and versatile way for the fabrication of polyolefin-based nanocomposites with superior functionalities.

3.1. Introduction

Since the discovery of a nylon-6/clay system, polymer nanocomposites have been regarded as a promising approach to modify properties of base polymer [1]. Numerous efforts in these decades covered almost all the combinations of polymer matrices and nano-sized fillers, among which polyolefin nanocomposites have maintained continuous attention due to its industrial significance. The history of polyolefin nanocomposites has evolved to overcome poor interaction of inert polyolefin with nanofillers [2]. Various strategies have been proposed for this system so as to improve the dispersion of fillers and interfacial bonding between the matrix and fillers. The most widely employed strategy is the addition of maleic anhydride-grafted polyolefin as a compatibilizer often combined with organic modification of filler surfaces [3-5]. Their use offers good dispersion in a relatively economical way, but concomitant drawbacks make the resultant nanocomposites less attractive: The compatibilizer and surface modifier form a soft interfacial layer between the matrix and fillers [6], which hampers the hardness of the fillers and limits the reinforcement. It is also known that maleic anhydride-grafted polyolefin accelerates oxidative degradation of the matrix [7]. An alternative strategy is to graft polymer chains onto filler surfaces [8]. Grafted chains not only work as a compatibilizer but also strengthen the interfacial bonding through entanglement, inter-diffusion and co-crystallization mechanisms [9,10]. The biggest drawback of this strategy is at elaborate synthesis of polymer-grafted nanofillers, which is crucial for polyolefin as the most economical plastic. The last but not least is an *in-situ* strategy, in which olefin polymerization is conducted in the presence of nanofillers that bear

a catalytic ability [11,12]. The growth of polymer chains mechanically forces the separation and exfoliation of fillers, leading to good dispersion even without a dispersant. Recently, Yoon and coworkers have reported *in-situ* fabrication of polyethylene-based nanocomposites using flake-like MoS_2 or granulated graphene bearing with Ziegler-Natta catalytic components [13,14]. They reported a great reinforcement of polyethylene owing to the successfully dispersed two-dimensional fillers. However, the correspondence between the polymerization yield and the filler loading in the *in-situ* formed matrix necessitates the operation of a catalyst at a yield level of 10^2-10^3 gram polymer per gram catalyst, which is unacceptably poor compared with an industrial level (10^5-10^6). So far, none of the proposed strategies have offered versatile solution for the cost performance problem in polyolefin nanocomposites.

Recently, a concept of pore confinement has been explored in the field of nanocatalysts, where catalyst nanoparticles are synthesized inside nano-sized pores of support materials such as metal-organic frameworks [15,16]. The spatial confinement of the formed nanoparticles in the porous scaffolds restricts their excessive growth, and prevents their sintering in catalysis even without capping agents. A similar concept would be also appealing for the preparation of polyolefin nanocomposites. State-of-the-art solid catalysts for olefin polymerization such as Ziegler-Natta, Phillips, and supported metallocene catalysts comprise of multi-grained particles, which are crucial for kinetic and morphological control of polymerization. Through fragmentation and replication mechanisms, each multi-grained

particle of a catalyst is converted into a polymer granule with a porous architecture, so-called reactor granule [17]. The reactor granule is immediately melt-processed into pellets for shipping, and thus the porous architecture is not normally utilized except in reactor blending for the production of rubber-toughened polypropylene (PP) [18,19].

Our research group has successfully applied the pore confinement concept for the *in-situ* fabrication of polyolefin nanocomposites. A molecular precursor of fillers is impregnated in the porosity of reactor granule and subsequently converted into dispersed nanoparticles in melt processing. The new reactor granule technology was firstly exemplified for the preparation of PP nanocomposites with titanium dioxide (TiO_2) [20]. The *in-situ* fabrication of TiO_2 nanoparticles from impregnated titanium alkoxide and their extremely nice dispersion (at 3 wt%) proved the advantage of the new technology. The prepared PP/TiO_2 nanocomposite films exhibited UV shielding properties without sacrificing visible-light transparency, in contrast to the usual turbidity caused by imperfect dispersion of nanoparticles. Following this success, the reactor granule technology was applied to prepare flame retardant PP/magnesium hydroxide ($Mg(OH)_2$) nanocomposites in the last chapter [21]. We found that hydrolysis of impregnated magnesium alkoxide prior to melt mixing enables good dispersion of $Mg(OH)_2$ nanoparticles even at a high filler loading over 10 wt%. The prepared nanocomposites achieved a self-extinguishing level in flame retardation at 20-30 wt%, in comparison to 60 wt% for conventional PP/$Mg(OH)_2$ composites. These results revealed that the reactor granule technology not only offers uniform dispersion of

nanoparticles in a dispersant-free manner, but also allows an access for the fabrication of highly filled nanocomposites suitable for some specific applications such as dielectric properties and thermal conductivity [22-24].

My next aim is to generalize the reactor granule technology to various kinds of highly filled PP nanocomposites. Specifically, highly filled PP/TiO$_2$ and PP/alumina (Al$_2$O$_3$) nanocomposites were studied in this chapter of the thesis. TiO$_2$ and Al$_2$O$_3$ were chosen because they are one of the most widely used and cost-effective fillers. Synthetic aspects of highly filled PP/TiO$_2$ and PP/Al$_2$O$_3$ nanocomposites were studied with the aid of various characterization methods. Then, application-oriented properties such as tensile properties, dielectric properties and thermal conductivity were further investigated for PP/Al$_2$O$_3$ nanocomposites.

3.2. Experimental

3.2.1. *Materials*

PP reactor granule (M_w = 2.6 x 10^5, M_w/M_n = 5.69 and *mmmm* = 98 mol%) was synthesized by propylene polymerization using a Mg(OEt)$_2$-based Ziegler-Natta catalyst. The median size (D$_{50}$) and pore volume of the granule were determined as 480 μm and 0.56 mL/g based on laser scattering in ethanol (HORIBA partica, LA-950V2) and mercury porosimetry (Shimazu, Autopore IV 9505), respectively. Titanium isopropoxide (Ti(O*i*Pr)$_4$) and aluminium isopropoxide (Al(O*i*Pr)$_3$) were supplied by Sigma-Aldrich and used as precursors. Preformed nanoparticles of TiO$_2$ (NT-500B, Tayca, diameter = 35 nm) and Al$_2$O$_3$ (Alu C, Nippon Aerosil, diameter = 15 nm) were used to prepare reference nanocomposites. PP grafted with maleic anhydride (PP-*g*-MA, MFI = 10.1 g/min, MA content = 1 wt%) was purchased from Chemtura as a compatibilizer. *n*-Octdecyl-3-(3',5'-di-*t*-butyl-4'-hydroxyphenyl)-propionate (AO-50) and bis(1,2,2,6,6-pentamethyl-4-piperidyl) sebacate (LA-77) were donated by ADEKA. They were used as an anti-oxidant stabilizer and catalyst for the sol-gel reaction, respectively.

3.2.2. *Fabrication of Polymer Nanocomposites*

PP/TiO$_2$ and PP/Al$_2$O$_3$ nanocomposites were prepared as follows: 40 g of the PP reactor granule was impregnated with a specific amount of Ti(O*i*Pr)$_4$ dissolved in 60 mL of heptane or Al(O*i*Pr)$_3$ dissolved in 80 mL of toluene at 50 °C under N$_2$ for 12 h. The amount of the

precursors was determined so as to obtain 3.0, 5.0, 10 and 20 wt% loading of oxides in resultant nanocomposites under the assumption of full conversion of metal alkoxides to oxides.

After the impregnation and solvent removal in vacuo, the granule was either directly melt-mixed or melt-mixed after a pre-treatment process to expose the impregnated granule to water vapor at 80 °C and 100% RH for 24 h in an oven. In some of experiments, HCl or NH_3 aqueous vapor was employed instead of water vapor for the pre-treatment. The melt mixing was carried out using an internal mixer (Toyo Seiki, LaboPlastomill) at 180 °C and 100 rpm for 20 min. Thus, prepared samples were termed as "*in-situ* PP/TiO_2 or PP/Al_2O_3" nanocomposites.

Reference samples were also prepared by mixing preformed nanoparticles with the reactor granule in the absence or presence of 5.0 wt% of PP-*g*-MA. They were termed as "PP/Al_2O_3-NP" and "PP/PP-*g*-MA/Al_2O_3-NP" nanocomposites in the case of Al_2O_3, and vice versa.

Nanocomposite samples were hot-pressed into films with a thickness of 200 μm. The hot pressing was performed at 230 °C and 10 MPa for 10 min, followed by quenching at 100 °C for 5 min and subsequently at 0 °C for 5 min.

3.2.3. *Characterization*

   To investigate the role of the porosity of PP reactor granule in the impregnation of metal alkoxides, the cross-sectional morphology of the granule was observed using scanning electron microscopy (SEM, Hitachi S-4100) at an accelerating voltage of 20 kV. The reactor granule was cut into two halves using a razor blade. The impregnated granule was pre-treated by water vapor prior to the SEM measurements. The pre-treatment aimed at the solidification of metal alkoxides and the suppression of their vaporization loss in the SEM vacuum chamber. The cut granule was coated with Pt before the measurements. The immobilization of the precursors in the porosity was also confirmed by an electron probe micro analyzer (EPMA, JEOL JXA-8900 L) equipped with a wavelength dispersive X-ray spectrometer. The *in-situ* formation of oxides was confirmed by transmission IR spectra (JASCO, FT/IR 6100) for sample films. The spectra were acquired over the range of 400-4000 cm^{-1} with a resolution of 4 cm^{-1} and 24 scans. The loading of *in-situ* formed oxides was determined based on thermogravimetric analysis (TGA, Seiko, TGA/DTA-6200). Sample films were heated in air up to 600 ℃ at 10 ℃/min and the loading was regarded as the residual inorganic content at 600 ℃. The dispersion of nanoparticles in the PP matrix was evaluated by transmission electron microscopy (TEM, Hitachi H-7100) with an accelerating voltage of 100 kV. The TEM specimens with a thickness of 100 nm were prepared by an ultramicrotome (ULTRACUT FCS, Leica) equipped with a diamond knife. Tensile properties of nanocomposites were acquired using a tensile tester (Abecks Inc., Abe Dat-100) at a crosshead speed of 1.0 mm/min. Sample films were die-cut into dumbbell-

shaped specimens with the overall length of 23 mm and the gage length of 5 mm. Tensile properties such as tensile strength and Young's modulus were determined as an average value of 10 measurements. The crystalline structure of the nanocomposites was evaluated by wide-angle X-ray diffraction (WAXD, Rigaku, Smartlab). The measurements were performed at room temperature using CuKα radiation (40 kV, 30 mA) at the step of 0.01° in the 2Θ range of 10° to 30° and the scanning speed of 0.5 °/min. Dielectric properties of nanocomposites were measured using a LCR meter (Agilent, Precision LCR meter E 4980A) in the frequency range of 10^2-10^7 Hz at room temperature. A disc-shaped specimen with a diameter of 2.5 cm was coated with gold to create thin conductive layers for a parallel plate capacitor. The thermal diffusivity (α) of nanocomposites was measured using a temperature wave analyzer (ai-Phase mobile 1u/2, Hitachi High-Tech Science) equipped with a sensor of 0.5 x 0.2 mm in size. The sample was sandwiched between the heater and the sensor plates, and the distance between the two plates was adjusted to create a firm contact with both surfaces of the sample. The applied voltage was set to 1.4 V and the delay in phase of the temperature wave was measured at eight frequency points within a range of 0.2-2 Hz. The thermal conductivity (λ) was derived from

$$\lambda = \alpha \, C_p \rho$$

where C_p is the specific heat capacity and ρ is the density of a sample. The specific heat capacity at room temperature was determined by differential scanning calorimeter (DSC, Mettler Toledo DSC-822). The temperature was swept in the range of 0-50 ℃ at 20 ℃/min under nitrogen flow of 200 mL/min.

3.3. Results and Discussion

3.3.1. SEM and EPMA analysis

In our previous study, it was proposed that the step of pore filling is one of the key factor for the *in-situ* fabrication of highly dispersed nanoparticles without the use of any dispersants. Since the above developed pre-hydrolytic treatment enables to solidify the metal alkoxide in the porosity, it has become possible to directly observe this pore filling by electron microscopy. **Fig. 3.1** summarizes cross-sectional SEM images for PP reactor granule before and after the impregnation of titanium and aluminum alkoxides. In heterogeneous olefin polymerization, the pore structure of reactor granule generally reflects the inner structure of catalyst particles. When the reactor granule is generated from a $Mg(OEt)_2$-based Ziegler-Natta catalyst, macropores tend to concentrate in an outer shell near the outermost surfaces [25]. In **Fig. 3.1a and 3.1b**, the majority of macropores were found within 100 μm from the outermost surface. The impregnation of titanium and aluminum alkoxides (at 10 wt% loading for each oxide) and their treatment with water vapor immobilized the alkoxides in the porosity. **Figs. 3.1c, 3.1d, 3.1e and 3.1f** clearly represent that the macropores were filled by inorganic components (distinguished as brighter areas).
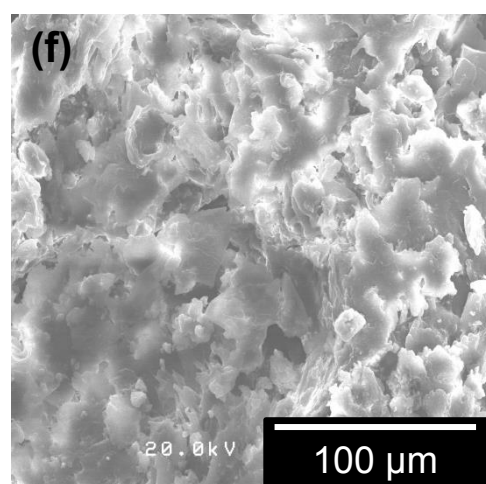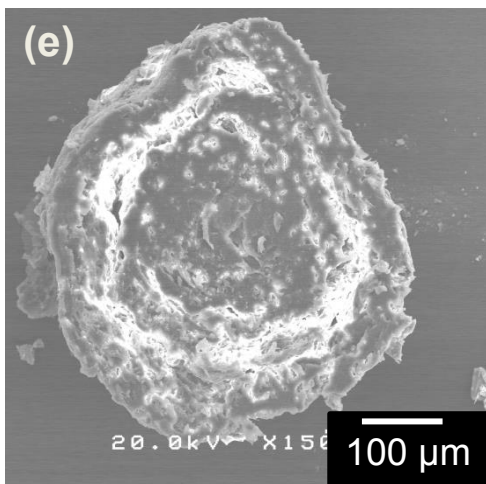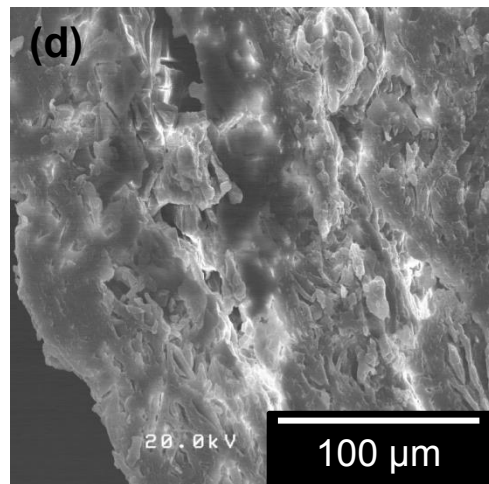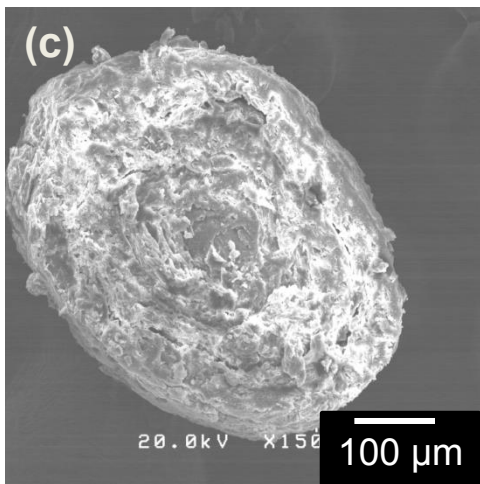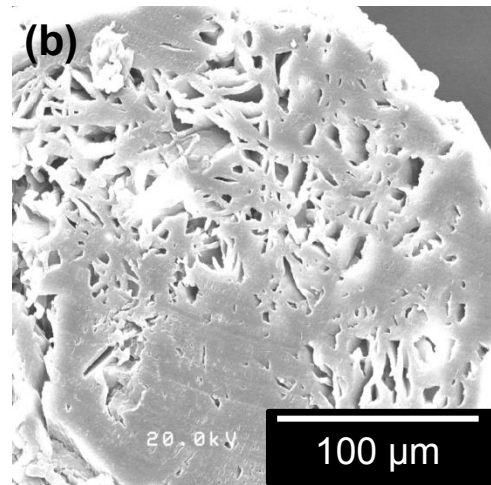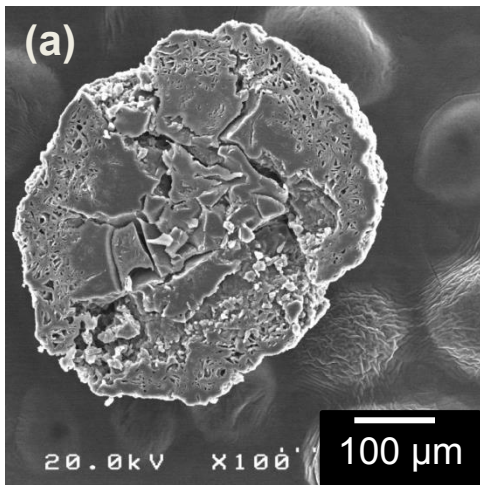
Figure 3.1. Cross-sectional SEM images of PP reactor granule: (a,b) Neat, and impregnated with (c,d) Ti(OiPr)$_4$ and (e,f) Al(OiPr)$_3$. The amount of the alkoxides was adjusted to satisfy 10 wt% of the corresponding oxides. All the samples were hydrolytically pre-treated before the measurements.

Further, EPMA technique was additionally employed to examine the pore filling. **Fig. 3.2** summarizes the results of EPMA for two different particles of reactor granule that was impregnated with Ti(OiPr)$_4$ at the filler loading of 10 wt% and thereafter pre-treated with water vapor at 80 °C and 100% RH for 24 h. **Figs. 3.2a and 3.2b** show the distribution of back scattered electrons, which represent the morphology of the sample while the characteristic X-ray maps specify the spatial distribution of each element (**Figs. 3.2c, 3.2d, 3.2e and 3.2f**). From the Ti distribution, it was clarified that the titanium alkoxide was mainly located in the macropores near the outermost surfaces with less concentration at the core of the granule. The distribution was not completely uniform but was considered sufficient for the dispersion of *in-situ* formed nanoparticles.
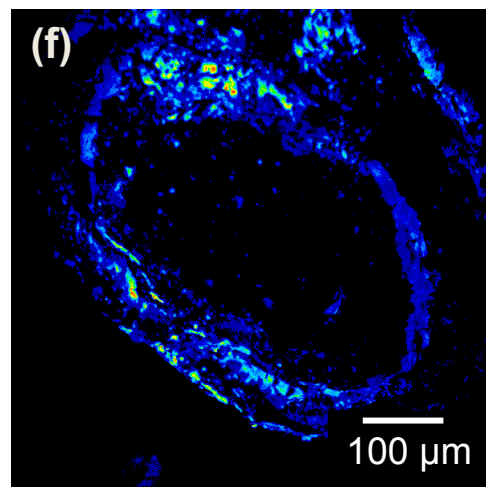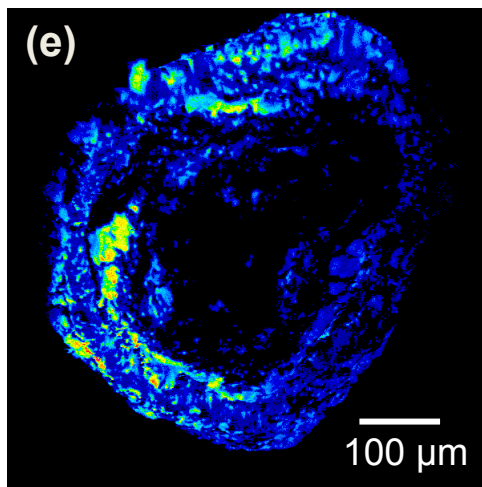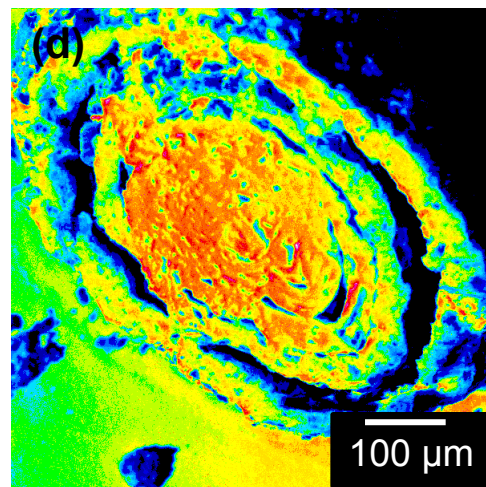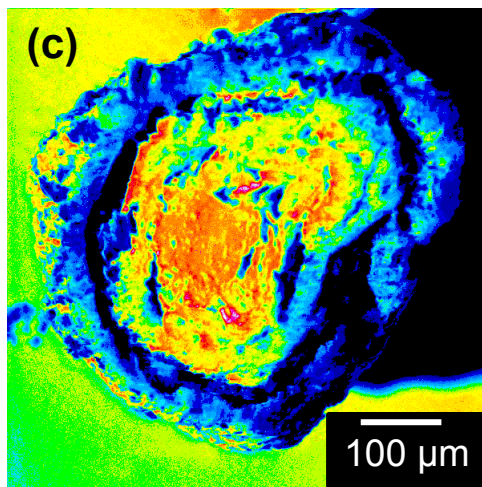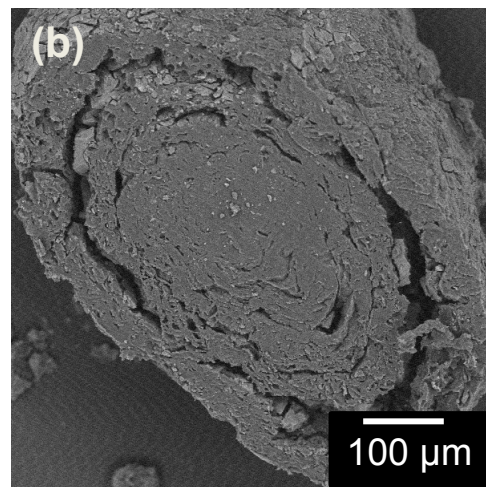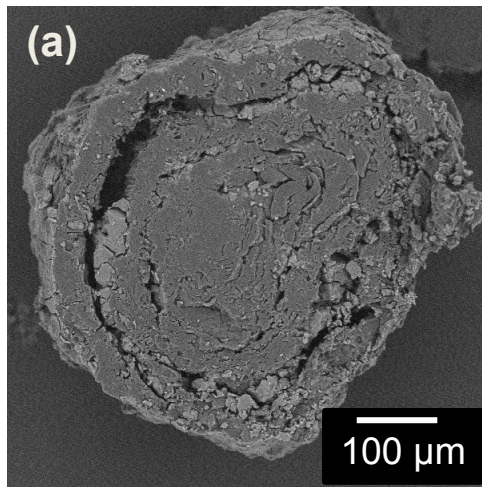
Figure 3.2. EPMA images for two different cross-sectioned reactor granule: (a,b) back-scattered electron images and (c,d) the distribution of carbon atoms and (e,f) titanium atoms. The amount of the alkoxides was adjusted to satisfy 10 wt% of the corresponding oxides. All the samples were hydrolytically pre-treated before the measurements.

3.3.2. *Chemical conversion*

After the preparation of nanocomposites, the chemical conversion of the precursors was investigated with transmission IR spectra for 50 µm-thick films (**Fig. 3.3**). In **Fig. 3.3b**, the IR spectrum of an *in-situ* PP/TiO_2 nanocomposite sample that was melt-mixed immediately after the impregnation shows absorption bands at around 600-700 cm^{-1} and 1000-1150 cm^{-1} in addition to the bands for PP. They were respectively assigned to Ti-O-Ti and Ti-O-C groups indicating not only the formation of TiO_2 in PP but also the incomplete consumption of Ti(OiPr)$_4$ [20,26]. In order to enhance the conversion, an additional pre-treatment process was employed, in which impregnated PP reactor granule was treated in a glass reactor with water vapor at 80 °C and 100% RH for 24 h in an oven. It was found that the band corresponding to the Ti-O-C group disappeared from the spectrum (**Fig. 3.3c**). It was clear that the pre-treatment process was essential for enhancing the conversion of Ti(OiPr)$_4$ into TiO_2. Thereafter, all the *in-situ* PP/TiO_2 samples were prepared by employing the additional pre-treatment process.
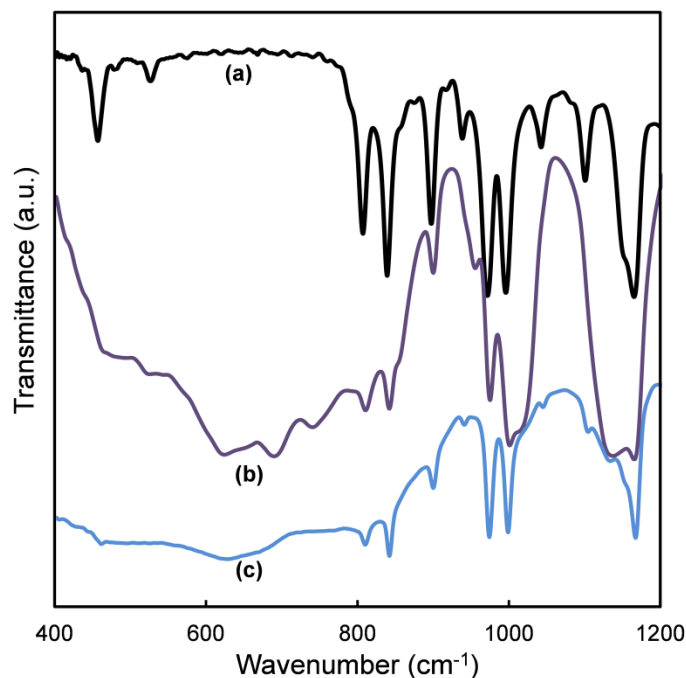
Figure 3.3. Transmission IR spectra of (a) neat PP, and *in-situ* PP/TiO$_2$ nanocomposites prepared (b) without pre-treatment, and (c) with pre-treatment under 80 °C and 100% RH for 24 h. Nanocomposites with the theoretical filler loading of 10 wt% were used.

Fig. 3.4a shows the transmission IR spectrum of an *in-situ* PP/Al$_2$O$_3$ nanocomposite sample prepared without any pre-treatment process. A new broad peak at around 600 cm^{-1} corresponding to the vibration of Al-O-Al bonds was observed to confirm the formation of Al$_2$O$_3$ [27]. However, absorption bands at 1070 cm^{-1} and 1560 cm^{-1}, which are respectively assigned to Al-O-C and Al-OH groups, were also present [28,29]. The presence of unreacted

precursors as well as $Al(OH)_3$ intermediate in the nanocomposite sample suggested incomplete hydrolysis and condensation.
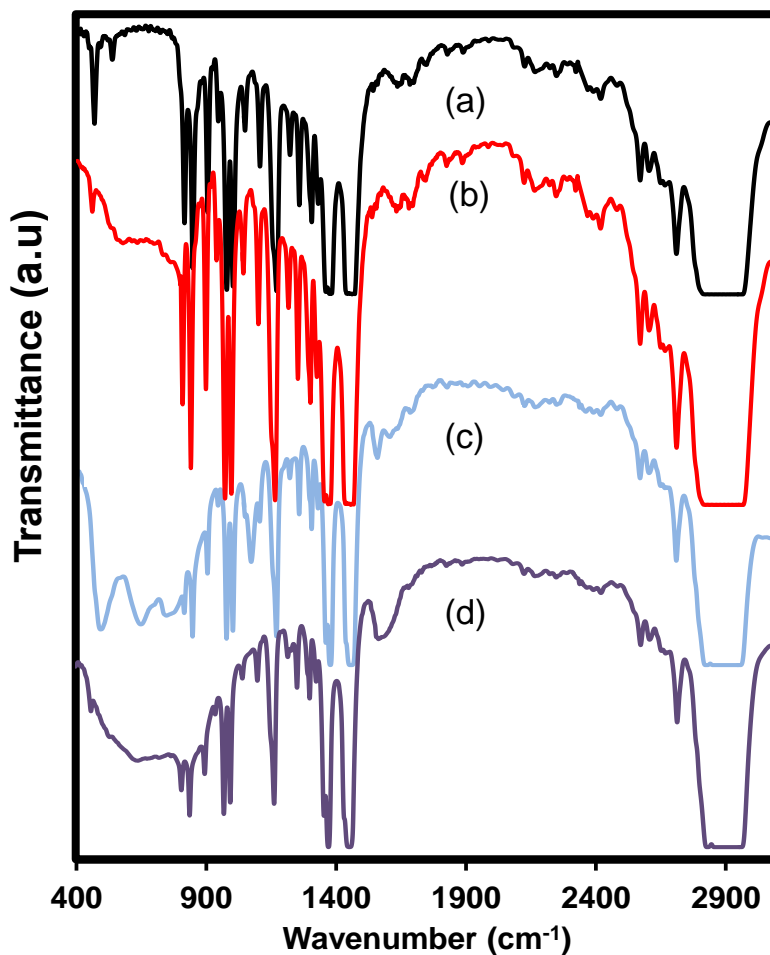
Figure 3.4. Transmission IR spectra of (a) neat PP, (b) PP/Al_2O_3-NP and *in-situ* PP/Al_2O_3 nanocomposites prepared (c) without pre-treatment, and (d) with pre-treatment under 80 °C and 100% RH for 24 h. Nanocomposites with the theoretical filler loading of 5.0 wt% were used.

When the pre-treatment process similar to the PP/TiO$_2$ nanocomposites was employed, it was found that the band corresponding to the Al-O-C group disappeared from the spectrum but the band originated from Al-OH groups still remained in the sample (**Fig. 3.5a**).
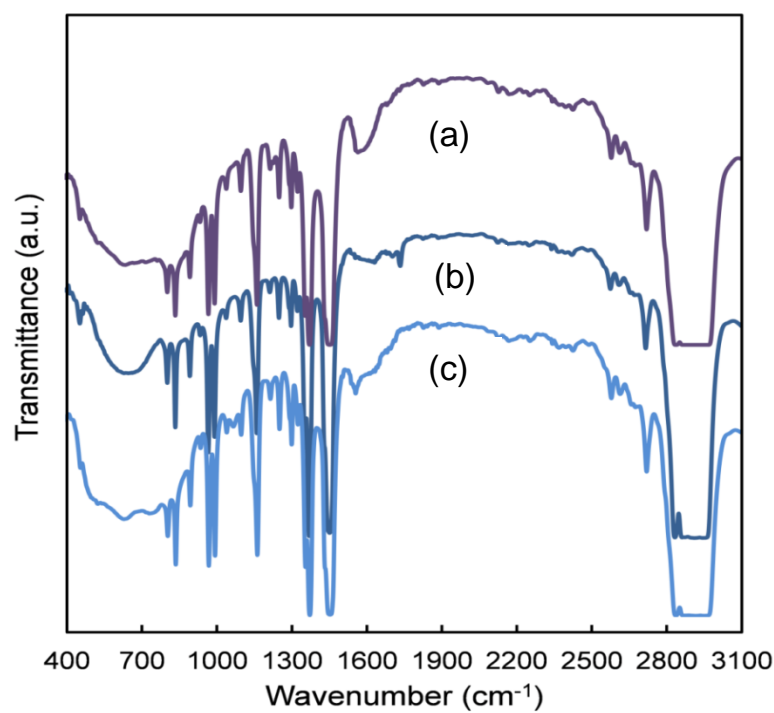
Figure 3.5. Transmission IR spectra of *in-situ* PP/Al$_2$O$_3$ nanocomposites prepared (a) with pre-treatment under 80 °C and 100% RH for 24 h. The atmosphere of the pre-treatment was replaced by (b) HCl vapor and (c) NH$_3$ vapor. Nanocomposites with the theoretical filler loading of 5.0 wt% were used.

To further enhance the conversion of Al(OH)$_3$ to Al$_2$O$_3$, two different pre-treatment processes, one involving HCl and the other involving NH$_3$ aqueous vapor instead of water vapor, were employed. Both of the pre-treatment processes resulted in the reduction of the

Al-OH peak (**Figs. 3.5b and 3.5c**), but only the pre-treatment with acid achieved almost full conversion to Al_2O_3. Since the harsh acid treatment can lead to the degradation of the matrix polymer, the nanocomposites were prepared by employing the pre-treatment process involving neutral water vapor for further analysis.

3.3.3. Inorganic content

For verifying the actual inorganic content in the prepared nanocomposites, the weight fraction of the formed oxides was evaluated using TGA. At 600 °C under air, all organic contents present in the nanocomposites are burned out and the remaining ash is considered to represent the inorganic content. **Table 3.1** summarizes the inorganic content for all the prepared *in-situ* PP/TiO_2 and PP/Al_2O_3 nanocomposites. In accordance with the previous chapter, I found the actual inorganic content obtained from TGA was similar to the value expected from the theoretical content at the filler loading of 3.0 wt%. On the other hand, the actual inorganic content was found to be lower than the theoretical content at 5.0 wt%, which was attributed to the vaporization loss of the precursors before its complete immobilization in the matrix. When the pre-treatment process was employed, the vaporization loss was suppressed and the inorganic content became much closer to the corresponding theoretical content. This fact along with the IR results suggested that the pre-treatment process is essential at high filler loading. It not only accelerates the chemical conversion of the

precursors into solid oxides (or at least hydroxides) by promoting the hydrolysis, but also aids in the retention of the precursors in the matrix.

Table 3.1. TGA results for *in-situ* nanocomposites

Sample	Theoretical content[a] (wt%)	Actual content[b] (wt%)
PP/TiO$_2$ (no pre-treatment)	3.0	2.9
	5.0	3.9
PP/TiO$_2$ (pre-treatment)	5.0	4.8
	10	9.4
	20	18.9
PP/Al$_2$O$_3$ (no pre-treatment)	3.0	2.9
	5.0	4.1
PP/Al$_2$O$_3$ (pre-treatment)	5.0	4.9
	10	9.6
	20	18.8

[a] Theoretical contents were estimated based on the assumption of the full conversion to oxides.

[b] Measured by TGA.

3.3.4. Spatial distribution of nanoparticles

Since the overall performance of the nanocomposites relies on the dispersion state of the nanoparticles inside the matrix, TEM was employed to observe the spatial distribution of the formed nanoparticles inside PP. **Figs. 3.6** and 3.**7** show representative micrographs for all kinds of nanocomposites at different filler loading. As was expected, the direct melt-mixing of pre-formed nanoparticles with PP resulted in the formation of micron-sized aggregates due to poor compatibility (**Figs. 3.6a and 3.7a**). The introduction of PP-*g*-MA as a compatibilizer improved the dispersion at the filler loading of 5.0 wt% (**Fig. 3.6b**), but with the increase of the filler loading, the dispersion began to deteriorate as can be seen from the presence of a large number of agglomerates. This indicated the inability of PP-*g*-MA to attain good dispersion at high filler loading (**Fig. 3.6c**).

A totally different situation was observed when the nanoparticles were generated *in-situ*. The *in-situ* nanocomposites that were prepared without the pre-treatment showed uniform dispersion of nanoparticles with the particle size below 10 nm, at the filler loading of 3.0 wt% (**Fig. 3.6b and Fig. 3.7d**). When the filler loading was increased to 5.0 wt%, the nanocomposites showed massive agglomeration of nanoparticles, leading to the formation of gel-like network (**Fig. 3.6c and Fig. 3.7e**). From the IR and TGA results, we hypothesized that at elevated filler loading, the extent of solidification of a precursor in the porosity is not sufficient and the remaining unsolidified precursors undergo migration and phase separation, resulting in the formation of agglomerates. It was found that when the nanocomposites were

prepared with the pre-treatment process, the gel-like network disappeared and the particles were well dispersed at least up to the filler loading of 20 wt% (**Figs. 3.6d, 3.6e and 3.6f and Figs. 3.7f, 3.7g and 3.7h**).
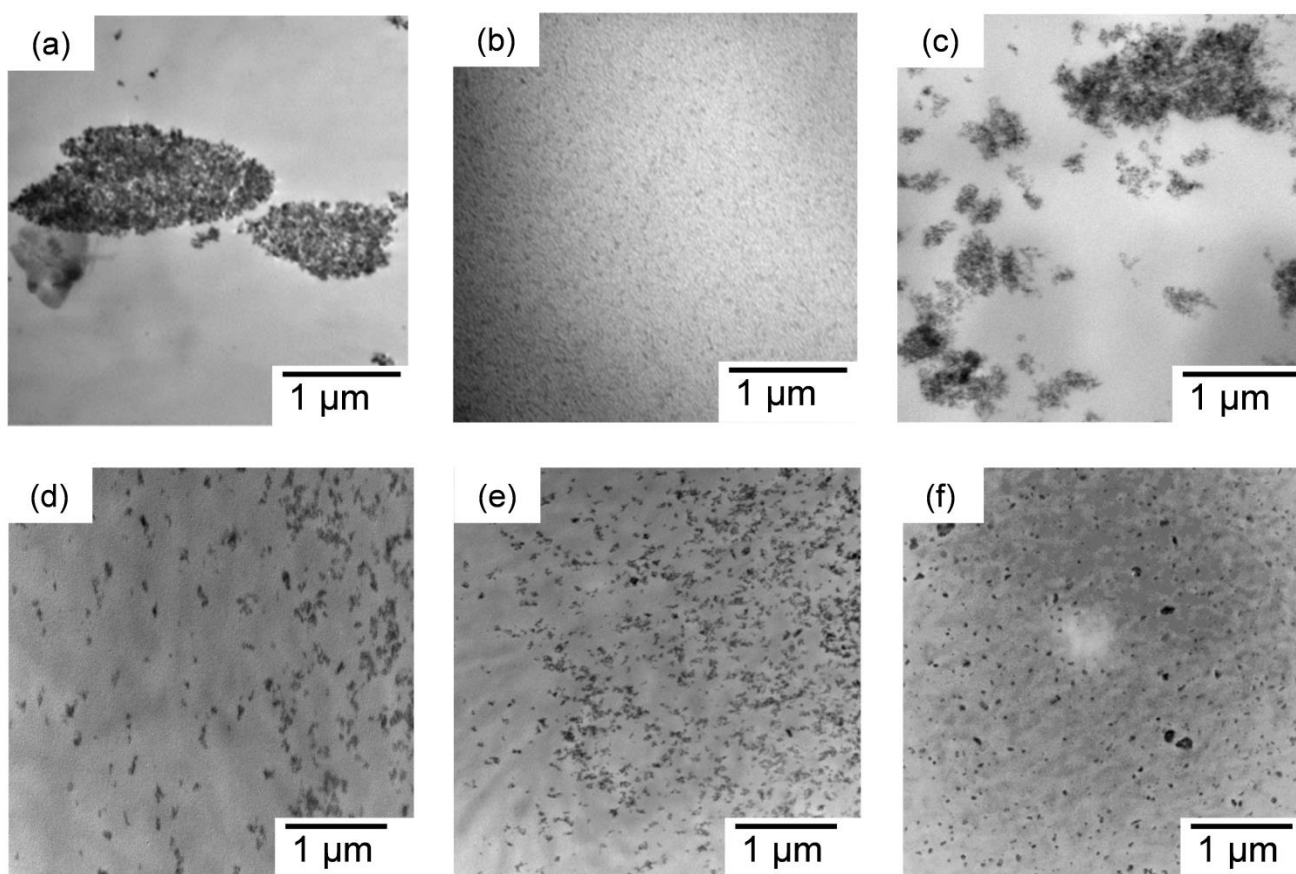
Figure 3.6. TEM micrographs of PP/TiO$_2$ nanocomposites: (a) NP (5.0 wt%), (b,c) *in-situ* without pre-treatment (3.0 and 5.0 wt%), and (d-f) *in-situ* with pre-treatment under 80 °C and 100% RH for 24 h (5.0, 10, and 20 wt%).

Figure 3.7. TEM micrographs of PP/Al$_2$O$_3$ nanocomposites: (a) NP (5.0 wt%), (b,c) PP-*g*-MA/NP (5.0 and 10 wt%), (d,e) *in-situ* without pre-treatment (3.0 and 5.0 wt%), and (f-h) *in-situ* with pre-treatment under 80 °C and 100% RH for 24 h (5.0, 10, and 20 wt%).
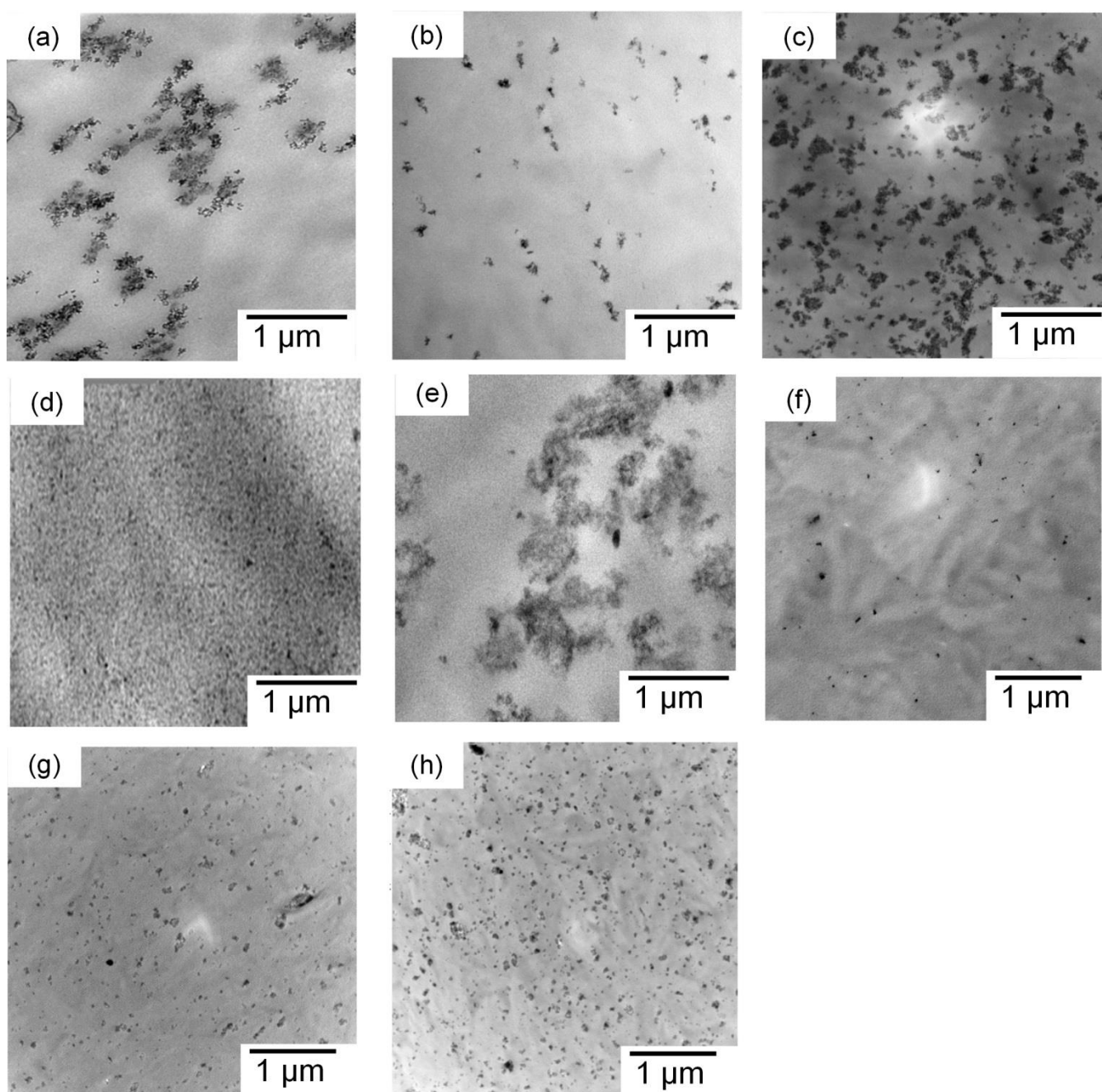
It was believed that during the pre-treatment process, the water vapor aids the hydrolysis of precursors, as a result of which the precursors get solidified and are retained in the porosity. The particle size distribution of the *in-situ* generated nanoparticles was derived from the TEM images by processing more than 200 particles with the aid of ImageJ software. Thus obtained median size (D_{50}) was found to be 53.4, 77.6 and 125.3 nm for *in-situ* PP/TiO_2 nanocomposites at the filler loading of 5.0, 10 and 20 wt%, respectively, and 48.3, 72.0 and 120.5 nm for *in-situ* PP/Al_2O_3 nanocomposites at the filler loading of 5.0, 10 and 20 wt%, respectively. Even though the increase of the filler loading and the pre-treatment process resulted in larger particle size, the formed nanoparticles were basically nano-sized and highly dispersed, which were attributed to the impregnation and confinement of the precursors in the porosity of the reactor granule.

We have demonstrated the synthetic aspects of highly filled PP/TiO_2 and PP/Al_2O_3 nanocomposites. Firstly, the examination of the impregnated reactor granule (pre-treated) using SEM and EPMA analysis proved that the porosity plays an important role in effective confinement and pre-dispersion of the molecular precursors. Secondly, a critical role of the pre-treatment was identified for the successful fabrication of highly filled nanocomposites. The pre-treatment process plays the following roles: i) Promotes hydrolysis of metal alkoxides, and ii) aids the solidification of the precursors in the matrix, thereby offering excellent dispersion of nanoparticles even at high filler loading without the use of any dispersants. Hereafter, the advantages of the reactor granule technology were examined in terms of application-oriented properties, for which PP/Al_2O_3 nanocomposites were selected.

3.3.5. *Crystalline structure*

The WAXD patterns of neat PP and *in-situ* PP/Al$_2$O$_3$ nanocomposites at different filler loading are shown in **Fig. 3.8**.
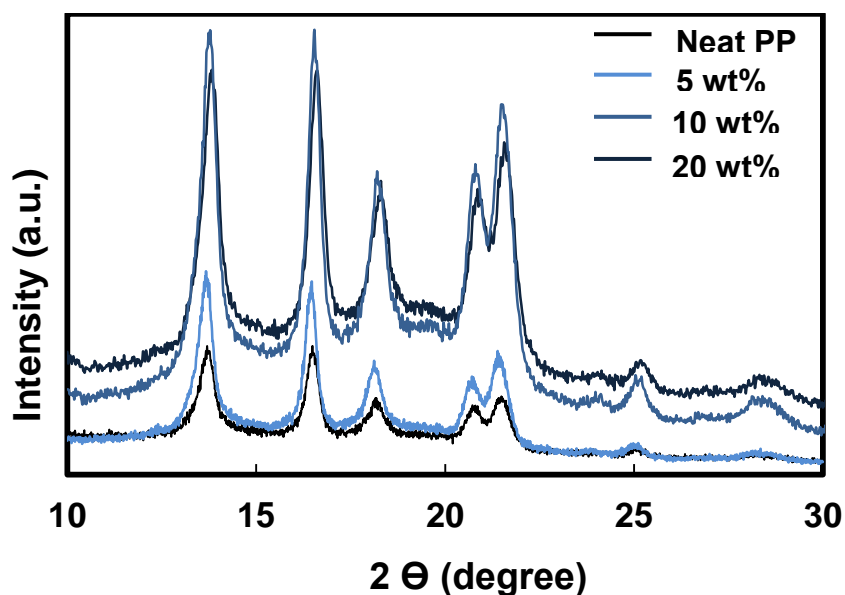
Figure 3.8. WAXD patterns of neat PP and *in-situ* PP/Al$_2$O$_3$ nanocomposites at different filler loading.

Neat PP displayed the peaks at 2Θ = 13.7, 16.3, 18.2, 20.4, 21.2, 25.0, and 27.8°, respectively corresponding to (110), (040), (130), (111), (041), (060) and (220) planes of the α-form crystal of PP [30]. The WAXD patterns of all the PP/Al$_2$O$_3$ nanocomposites exhibited the same α-form characteristics similar to neat PP with the complete absence of the β-form. The crystallinity of the nanocomposites was calculated [31] as 48.6, 52.5, and 52.2% at the filler loading of 5.0, 10, and 20 wt% in contrast to 47.0% for neat PP. Thus, the inclusion of slightly Al$_2$O$_3$ promoted the crystallization of PP.

3.3.6. *Mechanical properties*

To evaluate the mechanical properties of the prepared PP/Al$_2$O$_3$ nanocomposites, the uniaxial test was carried out. **Figs. 3.9a and 3.9b** represent stress-strain curves of the samples at 5.0 and 20 wt% of the filler loading, respectively. The plots of tensile strength and Young's modulus with the filler loading are shown in **Fig. 3.10 and Fig. 3.11**.
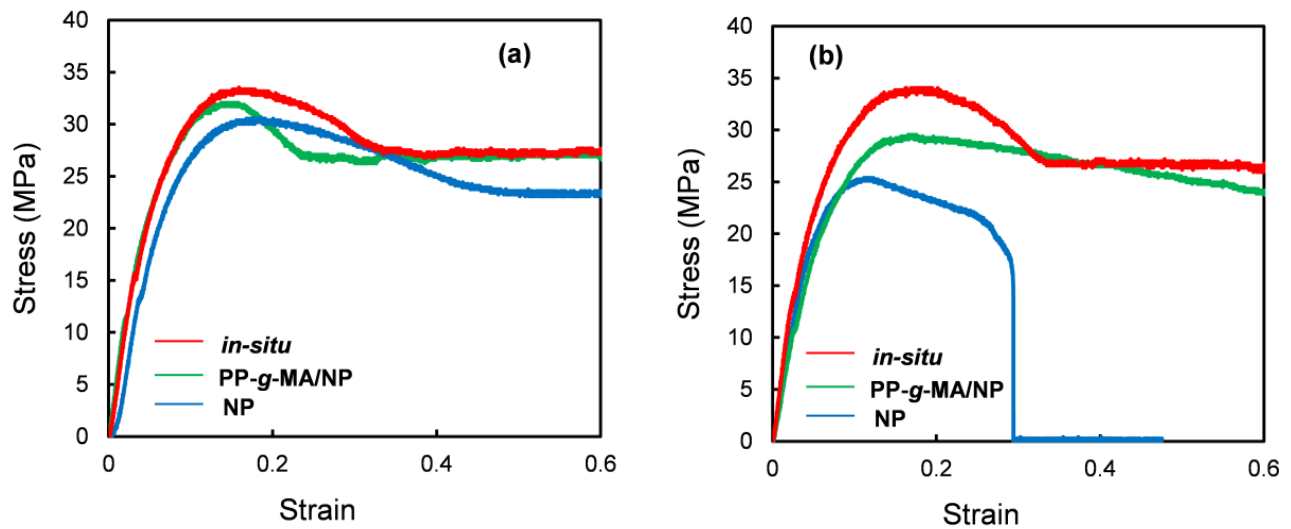
Figure 3.9. Tensile stress-strain curves for three types of PP/Al$_2$O$_3$ nanocomposites at the filler loading of (a) 5.0 and (b) 20 wt%.
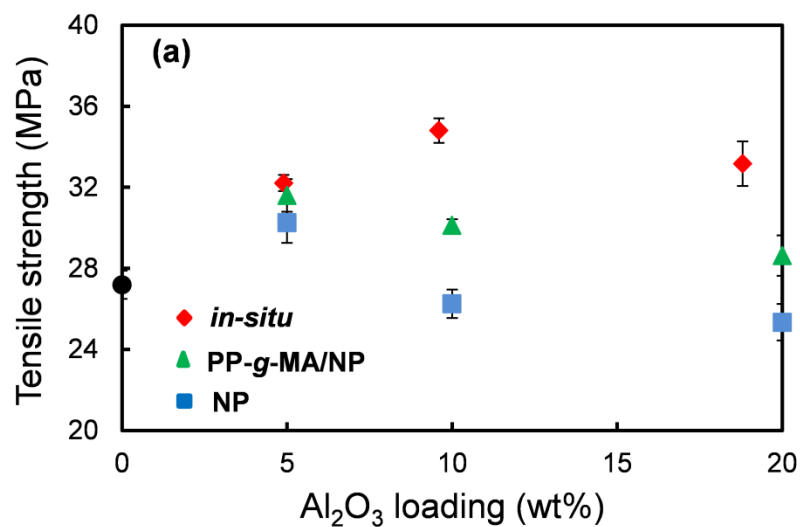
Figure 3.10. Tensile strength for three types of PP/Al$_2$O$_3$ nanocomposites.
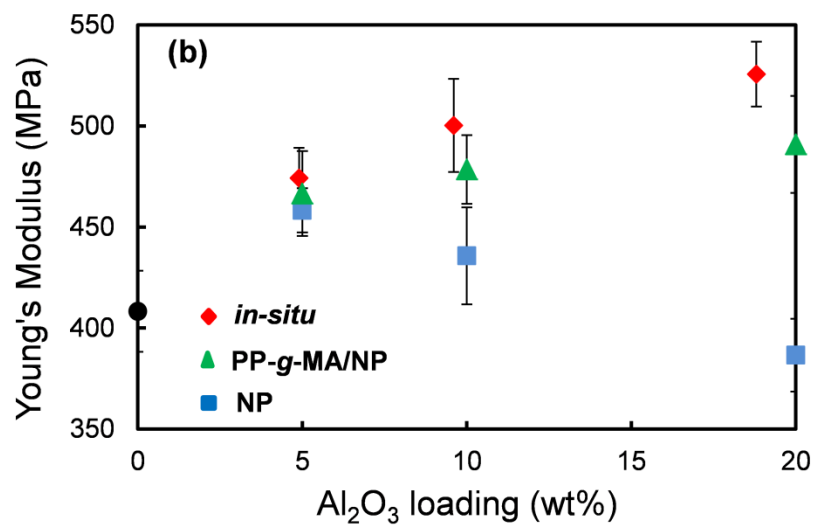
Figure 3.11. Tensile strength for three types of PP/Al$_2$O$_3$ nanocomposites.

At 5.0 wt%, all the types of nanocomposites exhibited almost a similar extent of reinforcement over neat PP. However, by increasing the filler loading, the extent of the reinforcement was largely dependent on the type of nanocomposites. It is well known that particle agglomeration tends to reduce the strength of a material, as agglomerates act as a stress concentrator [32]. PP/Al$_2$O$_3$-NP samples showed the maximum reinforcement at the filler loading of 5.0 wt% and further addition deteriorated the tensile strength, due to excessive agglomeration. The nanocomposites prepared using PP-g-MA as a compatibilizer also showed a similar tendency but the decrement in values became moderate compared with PP/Al$_2$O$_3$-NP. This could be understood by the fact that the addition of PP-g-MA improved the dispersion but not sufficiently at high filler loading. In contrast, the *in-situ* nanocomposites displayed a monotonous increment in the tensile strength owing to the similarly good dispersion for the entire filler loading. The Young's modulus followed similar tendencies, except the fact that the deterioration at higher loading was less pronounced than that for the tensile strength.

3.3.7. *Dielectric characteristics*

Fig. 3.12 represents the variation of the dielectric constant versus frequency for neat PP and *in-situ* PP/Al$_2$O$_3$ nanocomposites at different filler loading. Neat PP exhibited the dielectric constant of 2.3. The dielectric constant increased along the filler loading. PP/Al$_2$O$_3$ nanocomposites containing 18.8 wt% of Al$_2$O$_3$ attained a dielectric constant value of 3.57 at a frequency of 10^5 Hz. PP as a non-polar polymer hardly exhibited dielectric

relaxation, as a result of which the dielectric constant remained practically invariant in the examined frequency range. However, a frequency dependent behavior was observed in the nanocomposites due to the existence of interfacial polarization [33]. At high frequencies, dipolar groups are not capable of following the field variation, thus decreasing the dielectric constant [34]. The obtained experimental results were also compared with the theoretically calculated values and are reflected as a solid line in **Fig. 3.13**. The theoretical values were obtained based on the simple rule of mixture model for a two component system: $\varepsilon_c = \Phi \, \varepsilon_f +$ $(1 - \Phi) \, \varepsilon_m$, where ε and Φ are the dielectric constant and volume fraction, respectively. The suffixes c, f and m represent the composite, filler and matrix, respectively [35]. The obtained experimental values well reproduced the theoretical model.
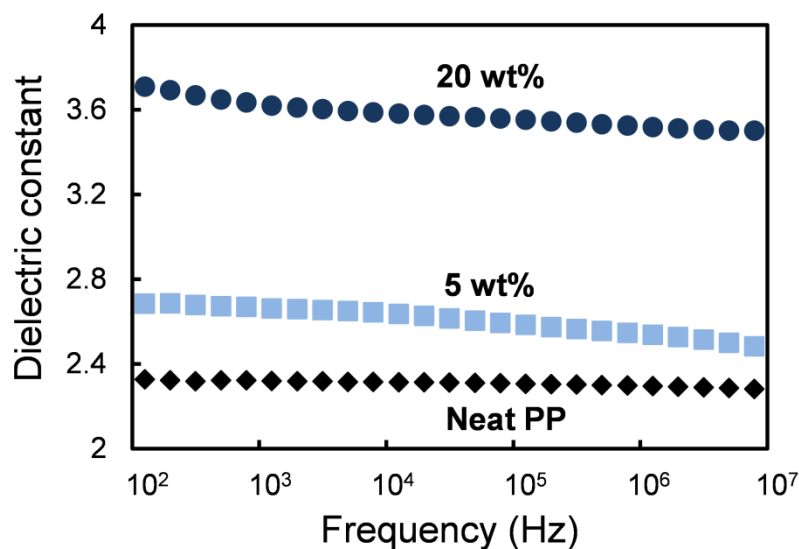
Figure 3.12. Frequency dependence of the dielectric constant for neat PP and *in-situ* PP/Al$_2$O$_3$ nanocomposites.
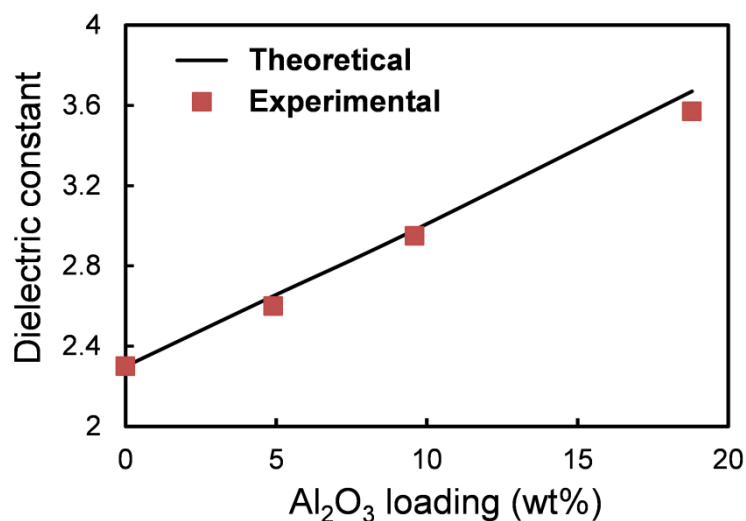
Figure 3.13. Dielectric constant (at 10^5 Hz) plotted against the filler loading. A solid line represents a theoretical estimation based on the simple rule of mixture model for a two component system.

3.3.8. Heat releasing property

Table 3.2 shows the densities, specific heat capacities and thermal diffusivities of different types of PP/Al$_2$O$_3$ nanocomposites, from which the thermal conductivities were determined. **Fig. 3.14** shows the thermal conductivities of the samples as a function of the filler loading. It can be seen that the values of the density and the specific heat capacity were almost similar for all the types of nanocomposites. So that, the main difference in the thermal conductivity was attributed to the variation in the thermal diffusivity.

Table 3.2. Physical properties of PP/Al$_2$O$_3$ nanocomposites for thermal conductivity calculation

Sample	Loading (wt%)	Density (g/cm^3)	Specific heat capacity[a] (J/g K)	Thermal diffusivity[b] (mm^2/s)
Neat PP	0	0.89 ± 0.02	1.82 ± 0.02	0.130 ± 0.007
NP	5.0	1.02 ± 0.02	1.72 ± 0.02	0.135 ± 0.002
	10	1.16 ± 0.04	1.71 ± 0.01	0.145 ± 0.004
	20	1.48 ± 0.03	1.57 ± 0.02	0.153 ± 0.005
PP-*g*-MA/NP	5.0	1.06 ± 0.02	1.72 ± 0.05	0.138 ± 0.002
	10	1.17 ± 0.03	1.70 ± 0.01	0.148 ± 0.006
	20	1.48 ± 0.02	1.58 ± 0.03	0.157 ± 0.004
in-situ	5.0	1.04 ± 0.03	1.74 ± 0.03	0.145 ± 0.002
	10	1.18 ± 0.01	1.70 ± 0.02	0.158 ± 0.005
	20	1.50 ± 0.02	1.60 ± 0.01	0.170 ± 0.006

[a] Measured by DSC.

[b] Measured by a temperature wave analyzer.

The thermal conductivity of neat PP was found to be around 0.21 W/m K. With the incorporation of Al$_2$O$_3$ in the PP matrix, the thermal conductivity of all types of nanocomposites improved nearly proportionally to the loading, as anticipated from relatively higher thermal conductivity of Al$_2$O$_3$ as compared to PP. At the filler loading of 5.0 wt%, the thermal conductivities of the three types of nanocomposites were nearly the same. Meanwhile, the difference in the values became significant upon increasing the filler loading. When compared at the filler loading of 20 wt%, *in-situ* PP/Al$_2$O$_3$ nanocomposites exhibited

the highest potential for improving the thermal conductivity of PP, reaching a value of 0.41 W/m K, which is 95 % higher than that of neat PP.

The thermal conductivity is a measure of heat transfer through a material. Specifically, in the present case of PP and its nanocomposites, the main energy carriers for heat conduction are phonons [36]. Their effective transport for achieving high thermal conductivity is believed to be dependent on the following factors: i) Particle organization – in the case of agglomerates, phonons are diffusively scattered, disrupting the heat flow in a uniform direction; ii) temperature gradient – temperature discontinuity created by locally high thermal conductivity of agglomerated particles causes non-uniform flow of heat; and iii) propagation pathway – as the phonons prefer to travel through the particle phase, the length of the polymer phase involved in phonon propagation becomes longer in the case of agglomerated particles [36,37]. These factors dictate the significance of the uniform dispersion of nanoparticles in a polymer matrix for the effective thermal conductivity of nanocomposites. In this viewpoint, the obtained trend of the thermal conductivity for all the three types of nanocomposites could be well explained on the basis of the dispersion state of the nanoparticles in the polymer matrix. The *in-situ* samples exhibited the highest thermal conductivity due to the uniform dispersion. The lower conductivity of the other two types of samples originated from poor dispersion, especially at elevated loading.

Unless prohibitively expensive fillers (such as boron nitride) are employed, high loading of filler is generally required for achieving an appropriate level of dielectric properties and thermal conductivity. But such high filler loading necessarily deteriorates the mechanical

properties of PP due to inevitable agglomeration. It must be noted that the nanocomposites fabricated by the developed technology offered the uniform dispersion of nanoparticles even at high filler loading and superior functional properties without deteriorating the mechanical properties.
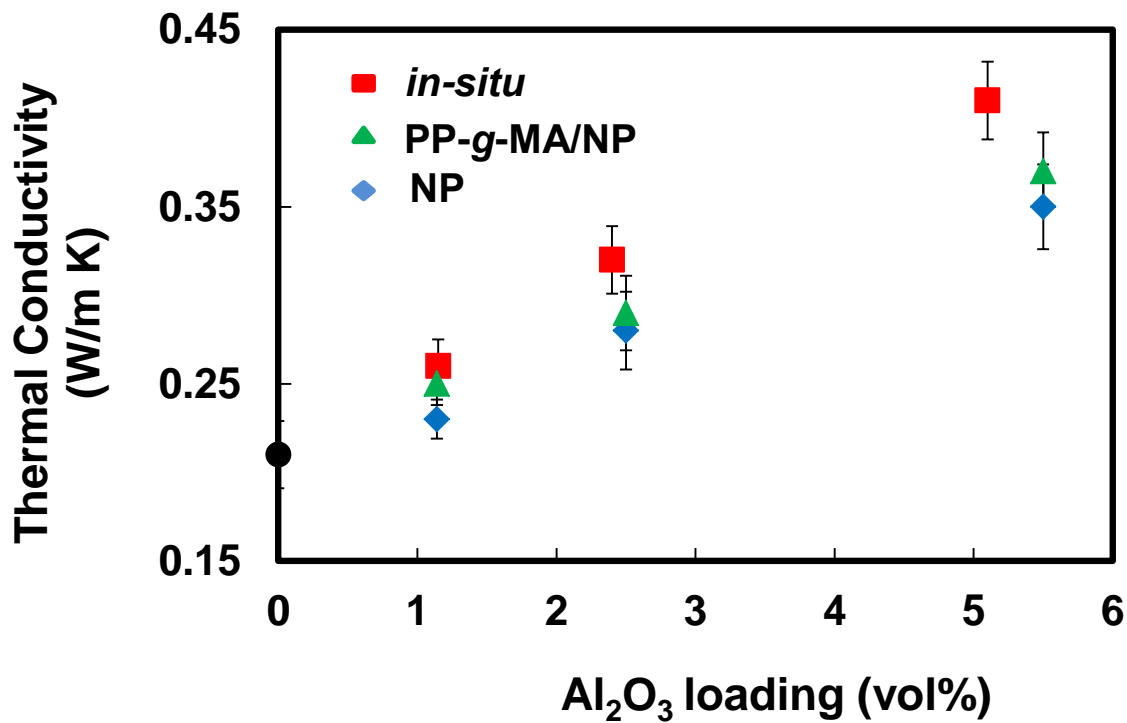
Figure 3.14. Thermal conductivity of three types of PP/Al_2O_3 nanocomposites at different filler loading.

3.4. Conclusion

In this chapter, the versatility of a new reactor granule technology for the fabrication of highly filled PP/TiO$_2$ and PP/Al$_2$O$_3$ nanocomposites was demonstrated. It was found that the confinement of metal alkoxide precursors in the porosity of PP reactor granule and their facile conversion into oxides results in the uniform dispersion of nanoparticles. Furthermore, a hydrolytic pre-treatment was a key for the solidification of precursors in the porosity and for achieving excellent dispersion of nanoparticles at high filler loading. Compared to conventional nanocomposites, the reactor granule technology never deteriorated the mechanical properties of PP at high filler loading. The dielectric constant of PP/Al$_2$O$_3$ nanocomposites reached 3.57 at 20 wt% of the filler loading. The thermal conductivity of PP/Al$_2$O$_3$ nanocomposites was mainly determined by the dispersion state and it was increased up to 0.41 W/m K at 20 wt%, *i.e.* almost double as that of neat PP. In the end, the reactor granule technology is a versatile approach for the fabrication of polyolefin-based nanocomposites, offering excellent dispersion over a wide range of filler loading and superior properties even without the use of any dispersants.

3.5. References

[1] A. Okada, A. Usuki, Twenty years of polymer nanocomposites, Macromol. Mater. Eng. 291 (2006) 1449-1476.

[2] M.T.T. That, F.P. Sarazin, K.C. Cole, M.N. Bureau, J. Denault, Polyolefin nanocomposites: formulation and development, Poly. Eng. Sci. 44 (2004) 1212-1219.

[3] O.H. Lin, H.M. Akil, Z.A.M. Ishak, Surface-activated nanosilica treated with silane coupling agents/polypropylene composites: mechanical, morphological, and thermal studies, Polym. Compos. 32 (2011) 1568-1583.

[4] E. Pavlidou, D. Bikiaris, A. Vassiliou, M. Chiotelli and G. Karayannidis, Mechanical properties and morphological examination of isotactic Polypropylene/SiO_2 nanocomposite, J. Phys. 10 (2005) 190-193.

[5] M. Kawasumi, N. Hasegawa, M. Kato, A. Usuki, A. Okada, Preparation and mechanical properties of polypropylene-clay hybrids, Macromolecules 30 (1997) 6333-6338.

[6] Z.M. Wang, H. Hong, T.C. Chung, Synthesis of maleic anhydride grafted polypropylene with high molecular weight using borane/O_2 radical initiators and commercial PP polymers, Macromolecules 38 (2005) 8966-8970.

[7] B. Mailhot, S. Morlat, J.L. Gardette, S. Boucardb, J. Duchet, J.F. Gerard, Photodegradation of polypropylene nanocomposites, Polym. Degrad. Stabil. 82 (2003) 163-167.

[8] H.J. Zhou, M.Z. Rrong, M.Q. Zhang, W.H. Ruan, K. Friedrich, Role of reactive compatibilization in preparation of nanosilica/polypropylene composites, Polym. Eng. Sci. 47 (2007) 499-509.

[9] T. Taniike, T. Toyonaga, M. Terano, Polypropylene-grafted nanoparticles as promising strategy for boosting physical properties of polypropylene-based nanocomposites, Polymer 55 (2014) 1012-1019.

[10] M. Toyonaga, P. Chammingkwan, M. Terano, T. Taniike, Well-defined polypropylene/polypropylene-grafted silica nanocomposites: roles of number and molecular weight of grafted chains on mechanistic reinforcement, Polymers 8 (2016) 300-313.

[11] K. Scharlach, W. Kaminsky, New polyolefin-nanocomposites by in situ polymerization with metallocene catalysts, Macromol. Symp. 26 (2008) 10-17.

[12] N. Guo, S.A. DiBenedetto, D.K. Kwon, L. Wang, M.T. Russell, M.T. Lanagan, A. Facchetti, T.J. Marks, Supported metallocene catalysis for in situ synthesis of high energy density metal oxide nanocomposites, J. Am. Chem. Soc. 129 (2007) 766-767.

[13] H. X. Zhang, E. B. Ko, J.H. Park, Y. K. Moon, X. Q. Zhang, K. B. Yoon, Fabrication of Polyethylene/MoS_2 nanocomposites using a novel exfoliated-MoS_2-MgCl Bi-supported Ziegler-Natta catalyst via in-situ polymerization, Compos. Sci. Technol. 137 (2016) 9-15.

[14] H. X. Zhang, E. B. Ko, J.H. Park, Y. K. Moon, X. Q. Zhang, K. B. Yoon, Fabrication of polyethylene/graphene nanocomposites through in-situ polymerization with a spherical

graphene/MgCl$_2$-supported Ziegler-Natta catalyst, Compos. Sci. Technol. 136 (2016) 61-66.

[15] H.L. Jiang, T. Akita, T. Ishida, M. Haruta, Q. Xu, Synergistic catalysis of Au@Ag core-shell nanoparticles stabilized on metal-organic framework, J. Am. Chem. Soc. 133 (2011) 1304-1306.

[16] C. Zlotea, R. Campesi, F. Cuevas, E. Leroy, P. Dibandjo, C. Volkringer, T. Loiseau, G. Ferey, M. Latroche, Pd nanoparticles embedded into a metal-organic framework: synthesis, structural characteristics, and hydrogen sorption properties, J. Am. Chem. Soc. 132 (2010) 2991-2997.

[17] E. Albizzati, U. Giannini, G. Collina, L. Noristi, L. Resconi, Propylene Handbook, E. P. Moore, Ed., Hanser, New York, 1996, pp. 86-89.

[18] P. Galli, The reactor granule technology: the ultimate expansion of polypropylene properties?, J. Macromol. Sci. A 36 (1999) 1561-1586.

[19] Y. Chen, W. Chen, D. Yang, Morphology of high impact polypropylene particles, Polymer 47 (2006) 6808-6813.

[20] K. Kaneko, N. Yadav, K. Takeuchi, B. Maira, M. Terano, T. Taniike, Versatile strategy for fabrication of polypropylene nanocomposites with inorganic network structures based on catalyzed *in-situ* sol-gel reaction during melt-mixing, Compos. Sci. Technol. 102 (2014) 120-125.

[21] B. Maira, P. Chammingkwan, M. Terano, T. Taniike, New reactor granule technology for highly filled nanocomposites: effective flame retardation of

polypropylene/magnesium hydroxide nanocomposites, Macromol. Mater. Eng. 300 (2015) 679-683.

[22] Z. Lin, Y. Qiu, K. Mai, Crystallization and melt behavior of magnesium hydroxide/polypropylene composites modified by functionalized polypropylene, J. Appl. Sci., 91(2004) 3899-3908.

[23] L. Fang, C. Wu, R. Qian, L. Xie, K. Yang, P. Jiang, Nano-micro structure of functionalized boron nitride and aluminium oxide for epoxy composites with enhanced thermal conductivity and breakdown strength, RSC Adv. 4 (2014) 21010-21017.

[24] X. Huang, P. Jiang, L. Xie, Ferroelectric polymer/silver nanocomposites with high dielectric constant and high thermal conductivity, Appl. Phys. Lett. 95 (2009) 242901-242903.

[25] T. Taniike, V.Q. Thang, N.T. Binh, Y. Hiraoka, T. Uozumi, M. Terano, Initial particle morphology development in Ziegler-Natta propylene polymerization tracked with stopped-flow technique, Macromol. Chem. Phys. 212 (2011) 723-729.

[26] R. Parra, M.S. Góes, M.S. Castro, E. Longo, P. R. Bueno, J.A. Varela, Reaction pathway to the synthesis of anatase via the chemical modification of titanium isopropoxide with acetic acid, Chem. Mater. 20 (2008) 143–150.

[27] K. Yoshida, H. Hyuga, N. Kondo, H. Kita, Synthesis of precursor for fibrous mullite powder by alkoxide hydrolysis method, Mater. Sci. Eng. B 173 (2010) 66-71.

[28] A. Vázquez, T. López, R. Gómez, Bokhimi, A. Morales, O. Novarot, X-ray diffraction, FTIR and NMR characterization of sol-gel alumina doped with lanthanum and cerium, J Solid State Chem. 128 (1997) 161-168.

[29] S.Y.R. López, R.S. Acuña, R.L. Juárez, J.S. Rodríguez, Analysis of the phase transformation of aluminum formate $Al(O_2CH)_3$ to α-alumina by Raman and infrared spectroscopy, J. Ceram. Process. Res. 14 (2013) 627-631.

[30] P. Chammingkwan, K. Matsushita, T. Taniike, M. Terano, Enhancement in mechanical and electrical properties of polypropylene using graphene oxide grafted with end-functionalized polypropylene, Materials 9 (2016) 540-554.

[31] Z. Mo, H. Zhang, The degree of crystallinity in polymers by wide-angle X-Ray diffraction (Waxd), J. Macromol. Sci. Part C 35 (1995) 555-580.

[32] M. Garc, G.V. Vliet, S. Jain, B.A.G. Schrauwen, A. Sarkissov, W.E.V. Zyl, B. Boukamp, Polypropylene/SiO_2 nanocomposites with improved mechanical properties, Rev. Adv. Mater. Sci. 6 (2004) 169-175.

[33] N. K. Subramani, S. K. Nagaraj, S. Shivanna, H. Siddaramaiah, Highly flexible and visibly transparent poly(vinyl alcohol)/calcium zincate nanocomposite films for UVA shielding applications as assessed by novel ultraviolet photon induced fluorescence quenching, Macromolecules 49 (2016) 2791-2801.

[34] Z.M. Dang, L. Wang, Y. Yin, Giant dielectric permittivites in functionalized carbon-nanotube/electroactive-polymer nanocomposites, J. Adv. Mater. 19 (2007) 852-857.

[35] M. Dinulovi, B. Rašuo, Dielectric properties modeling of composite materials, FME Transactions 37 (2009) 117-122.

[36] A. Tessema, D. Zhao, J. Moll, S. Xu, R. Yang, C. Li, S.K. Kumar, A. Kidane, Effect of filler loading, geometry, dispersion and temperature on thermal conductivity of polymer nanocomposites, Polym. Test. 57 (2017) 101-106.

[37] S. Agarwal, N.S. Saxena, V. Kumar, Study on effective thermal conductivity of zinc sulphide/poly(methyl methacrylate) nanocomposites, Appl. Nanosci. 5 (2015) 697-702.

Chapter 4

Development of Heat Releasing Polyolefin Nanocomposites based on Reactor Granule Technology

Chapter 4

Abstract

Development of thermally conductive polyolefin nanocomposites based on utilization of a novel technology that involves impregnation of metal alkoxide precursors in the porosity of PP reactor granule and subsequent conversion of the precursors into oxides during melt mixing was focused. The so called reactor granule technology along with three additional strategies was applied for the fabrication of PP/Al_2O_3 nanocomposites. The potency of the strategies was evaluated on the basis of thermal diffusivity and conductivity. The first strategy aimed at the formation of filler-rich and polymer-rich domains by mixing highly filled reactor granule with neat PP in order to cause localization of Al_2O_3 nanoparticles. The resultant nanocomposites exhibited promising value of thermal conductivity. Moreover, the impregnated reactor granule showed positive influence as a dispersant for pre-formed nanoparticles (second strategy). These results suggest that impregnated reactor granule serve as suitable masterbatch for the fabrication of functionalized polyolefin grade. The third strategy which involved utilization of silane coupling agent as interfacial modifier for *in-situ* generated Al_2O_3 nanoparticles gave the highest increment in thermal conductivity. Thus, reactor granule technology has emerged as a potential methodology for the fabrication of heat releasing polyolefin based nanocomposites.

Keywords: thermal conductivity, alumina, localization, interfacial modification, reactor granule technology

4.1. Introduction

Due to rapid escalation of power densities in electronic devices along with the trend to reduce device dimensions, the issue of thermal management has become essential. The possession of high thermal conductivity is crucial for the dissipation of heat to ensure the efficient operational performance of these devices [1-3]. Previously, metals were used as major materials for effective dissipation of heat. But, their deficiencies including high density, limited design flexibilities and propensity for corrosion have posed limitation in their usage. Polymers having low density as well as superior processibilty and design flexibility offer a potential alternative [4], while low thermal conductivity of these commonly used polymers constitutes a bottle neck in their widespread use [5]. An approach to improve the heat transfer through the polymers is the use of thermally conductive fillers [6]. Thus, polymer composites with improved thermal conductivity portend as an effective heat dissipative materials to fill in the gap [7].

One way is to introduce electrically conductive inclusions (*e.g.* graphene, carbon nanotube, etc.) with high intrinsic thermal conductivity into the polymer matrix [8-10]. Though these fillers can notably increase the thermal conductivity but sharply reduce the breakdown strength, leading the target composites to be electrically conductive [11]. A balance is required that maximizes the heat dissipation ability of the electrically insulating material while achieving superior device performance. The other is the addition of electrically insulating ceramic fillers (*e.g.* BN, AlN, Al_2O_3) [12-15]. Ceramic fillers have

become attractive alternative because they offer high thermal conductivity while maintaining the desired level of electrical insulation.

For effective designing of thermally conductive polymer nanocomposites, not only the use of appropriately selected polymers and fillers is sufficient, but a holistic approach to satisfy all the application requirements is needed. The filler type, loading level, filler shapes as well as size have a strong influence on the thermal conductivity of the polymer nanocomposites. Moreover, the spatial arrangement of fillers (dispersed individual particles, aggregates, fractal clusters, percolated network etc.), their orientation and interaction between polymers and fillers are also important to the thermal conductivity [16]. For instance, hexagonal boron nitride, an anisotropic filler enables to achieve high thermal conductivity at relatively low loading level as compared to other ceramic fillers owing to large aspect ratio [17]. Many researchers have utilized ceramics as the thermal dissipative filler for the preparation of composite materials. Goh *et al.* prepared the Al_2O_3 and ZnO reinforced silicone rubber and found about 70 % enhancement of thermal conductivity at 10 vol% of the filler loading [18]. Kou *et al.* investigated the effect of particle size of alumina on the thermal conductivity of silicone rubber. Thermal conductivity of the prepared nanocomposites improved with small diameter of Al_2O_3 nanoparticles at the same volume fraction [19].

The inclusion of these aforementioned fillers improves the thermal conductivity of polymer matrices. The elaborate synthesis and exorbitant price of BN makes it less preferred for large scale production of nanocomposites. On the other hand, high filler loadings greater than 30 vol% is required to achieve the necessary level of thermal conductivity, unless some prohibitory expensive fillers (such as boron nitride) are employed [20,21]. Such high filler loadings adversely affect the dispersion of fillers in the polymer matrices and deteriorate the physical properties of the resultant nanocomposites. Moreover, fabrication of industrially significant polyolefin based nanocomposites with good dispersion as well as improved physical properties is a serious challenge due to the chemical inertness of polyolefins.

In the previous chapter, the fabrication of highly filled PP/Al_2O_3 nanocomposites based on established reactor granule technology has been reported [22]. Among various fillers, Al_2O_3 has been chosen due to its combination of moderate thermal conductivity, low coefficient of thermal expansion, non-toxicity and low cost [23]. The methodology is based on the pore confinement concept for the *in-situ* fabrication of nanocomposites [22]. A molecular precursor of filler is impregnated in the porosity of PP reactor granule and is subsequently converted to highly dispersed nanoparticles during melt-processing. It is believed that the spatial confinement offered by the porosity of reactor granule prevents the agglomeration of the formed nanoparticles even without the use of any capping agents. The prepared nanocomposites not only revealed extremely nice dispersion of nanoparticles up to filler loading of 20 wt% with improved physical properties but also exhibited promising values of thermal conductivity.

Based on these findings, herein this chapter, the aim was focused on maximizing the potential of the reactor granule technology for further improving the thermal conductivity by utilizing Al_2O_3 based PP nanocomposites. To realize this, three strategies were additionally applied. The first one is aimed at achieving localization of Al_2O_3 nanoparticles by forming Al_2O_3-rich and Al_2O_3-poor domains in the resultant PP/Al_2O_3 nanocomposites.by dilution of highly filled reactor granule with neat PP. The second strategy is based on exploiting the dispersing ability of impregnated reactor granule as dispersant for pre-formed nanoparticles at elevated filler loadings. The last one utilizes the fact that interface plays a critical role in determining the effective thermal conductivity of the resultant nanocomposites [24-27]. The improved interfacial interaction between the matrix and the filler results in higher values of thermal conductivity. Therefore, PP/Al_2O_3 nanocomposites were fabricated by additionally employing silane coupling agent during the impregnation as interfacial modifier for the *in-situ* generated Al_2O_3 nanoparticles. The advantage of the prepared nanocomposites lies at the fact that not only they will serve as promising candidates with high heat releasing capacity but will also provide a platform to fairly compare the effect of different strategies on the same polymer/filler system.

4.2. Experimental

4.2.1. Materials

PP reactor granule (M_w = 2.6 x 10^5, M_w/M_n = 5.69 and *mmmm* = 98 mol%) was synthesized by propylene polymerization using a $Mg(OEt)_2$-based Ziegler-Natta catalyst. The median size (D_{50}) and pore volume of the granule were determined as 480 μm and 0.56 mL/g based on laser scattering in ethanol (HORIBA partica, LA-950V2) and mercury porosimetry (Shimazu, Autopore IV 9505), respectively. Aluminium isopropoxide ($Al(OiPr)_3$) was supplied by Sigma-Aldrich and used as precursor. Preformed nanoparticles of Al_2O_3 (Alu C, Nippon Aerosil, diameter = 15 nm) were used to prepare nanocomposites. PP grafted with maleic anhydride (PP-*g*-MA, MFI = 10.1 g/min, MA content = 1 wt%) was purchased from Chemtura as a compatibilizer. Dodecyl trimethoxy silane (DTMS) was supplied by TCI and used as interfacial modifier for *in-situ* generated nanoparticles. *n*-Octdecyl-3-(3',5'-di-*t*-butyl-4'-hydroxyphenyl)-propionate (AO-50) and bis(1,2,2,6,6-pentamethyl-4-piperidyl) sebacate (LA-77) were donated by ADEKA. They were used as an anti-oxidant stabilizer and catalyst for the sol-gel reaction, respectively.

4.2.2. *Fabrication of Polymer Nanocomposites*

PP/Al$_2$O$_3$ samples were prepared according to the procedure described in our recent work [18]. Briefly, PP reactor granule was impregnated with specific amount of Al(OiPr)$_3$ dissolved in toluene so as to obtain 5.0, 10, 20, 30 and 40 wt% loading of Al$_2$O$_3$ in the resultant nanocomposites, under the assumption of full conversion of metal alkoxides to oxides. After impregnation and solvent removal in vacuo, the granule was pre-hydrolysed with subsequent melt-mixing. The conditions of the impregnation and pre-hydrolysis were same with those as mentioned in our recent work [18]. The prepared samples were termed as "*in-situ*" PP/Al$_2$O$_3$ nanocomposites. Reference samples were also prepared by melt-mixing preformed nanoparticles with the reactor granule in the absence or presence of 5.0 wt% of PP-g-MA. They were termed as "PP/Al$_2$O$_3$-NP" and "PP/PP-g-MA/Al$_2$O$_3$-NP" nanocomposites respectively. The melt-mixing was carried out using an internal mixer (Toyo Seiki, LaboPlastomill) at 180 °C and 100 rpm for 20 min. All the nanocomposite samples were hot-pressed into films with a thickness of 200 μm. The hot pressing was performed at 230°C and 10 MPa for 10 min, followed by quenching at 100 °C for 5 min and subsequently at 0 °C for 5 min.

Other kinds of Al_2O_3 based PP nanocomposites based on three different strategies were also prepared.

i) Dilution of impregnated reactor granule – The reactor granule preliminary impregnated to obtain 20 and 40 wt% of Al_2O_3 loading and pre-hydrolyzed was melt-mixed with neat PP to prepare nanocomposites with the final filler loading of 3.0; 5.0; 10 and 10; 20; 30 wt% respectively. The prepared samples were termed as "*in-situ* + PP" nanocomposites. The list of the prepared nanocomposites is summarized in **Table 4. 1**.

ii) Concentration of impregnated reactor granule – the reactor granule preliminary impregnated to obtain 10 wt% of Al_2O_3 loading and pre-hydrolyzed was melt-mixed with preformed Al_2O_3 nanoparticles to prepare nanocomposites with the final filler loading of 20, 30 and 40 wt%. The prepared samples were termed as "*in-situ* + NP" nanocomposites. The list of the prepared nanocomposites is summarized in **Table 4.1**.

iii) Using DTMS as interfacial modifier – The similar procedure as that for *in-situ* samples was carried out to prepare nanocomposites with the Al_2O_3 loading of 20 wt% with the further addition of different amounts of DTMS corresponding to Si/Al ratio as 0.006, 0.03 and 0.06 mol/mol during the impregnation step. The prepared samples were termed as "*in-situ* + DTMS" nanocomposites.

Table 4.1. Sample list of nanocomposites prepared based on utilization of highly filled reactor granule.

Code	Masterbatch	Addition	Theoretical loading (wt%)
in-situ + PP	PP/Al$_2$O$_3$ (*in-situ*) 20 wt%	Neat PP	10
			5.0
			3.0
in-situ + PP	PP/Al$_2$O$_3$ (*in-situ*) 40 wt%	Neat PP	30
			20
			10
in-situ + NP	PP/Al$_2$O$_3$ (*in-situ*) 10 wt%	Al$_2$O$_3$ NPs	20
			30
			40

4.2.3. Characterization

Fourier transform infrared image mapping analysis of PP/Al$_2$O$_3$ nanocomposites prepared based on masterbatch method was performed using Spotlight 200 FTIR microscope (Perkin Elmer). The IR mapping data was acquired in transmission mode between 1500 and 500 cm$^-$^{1} with a spectral resolution of 8 cm^{-1}. For each sample an area of 500 X 500 µm was selected for imaging. The dispersion of nanoparticles in the PP matrix was evaluated by

transmission electron microscopy (TEM, Hitachi H-7100) with an accelerating voltage of 100 kV. The TEM specimens with a thickness of 100 nm were prepared by an ultramicrotome (ULTRACUT FCS, Leica) equipped with a diamond knife. The thermal diffusivity (α) of nanocomposites was measured using a temperature wave analyzer (ai-Phase mobile 1u/2, Hitachi High-Tech Science) equipped with a sensor of 0.5 x 0.2 mm in size. The sample was sandwiched between the heater and the sensor plates, and the distance between the two plates was adjusted to create a firm contact with both surfaces of the sample. The applied voltage was set to 1.4 V and the delay in phase of the temperature wave was measured at eight frequency points within a range of 0.2-2 Hz. The thermal conductivity (λ) was derived from

$$\lambda = \alpha\, C_p \rho$$

where C_p is the specific heat capacity and ρ is the density of a sample. The specific heat capacity at room temperature was determined by differential scanning calorimeter (DSC, Mettler Toledo DSC-822). The temperature was swept in the range of 0-50 ºC at 20 ºC/min under nitrogen flow of 200 mL/min.

4.3. Results and Discussion

The results of *in-situ* and reference PP/Al$_2$O$_3$ nanocomposites have been embodied from the work of previous chapter to have an overview and comparison of all the strategies. TEM images of representative PP/Al$_2$O$_3$ nanocomposites are summarized in **Fig. 4.1**. As usual, the direct melt-mixing of pre-formed nanoparticles with PP resulted in the formation of huge PP aggregates in PP (**Fig. 4.1a**). The addition of PP-*g*-MA as compatibilizer partially improved the dispersion but at the high filler loading, the extent of improvement was not satisfactory as can be seen from the presence of large number of aggregates (**Figs. 4.1b and 4.1c**). A totally different state of dispersion was observed when the nanoparticles were *in-situ* generated (**Figs. 4.1d, 4.1e and 4.1f**). It was found that uniform dispersion of nanoparticles was achieved irrespective of the filler loading. Even though the increase of the filler loading and the pre-treatment process resulted in larger particle sizes, the formed nanoparticles were basically nano-sized and highly dispersed, which were attributed to the impregnation and confinement of the precursors in the porosity of the reactor granule. It can be concluded that reactor granule technology is the most practical way in dispersing nano-sized Al$_2$O$_3$ at all filler loading.
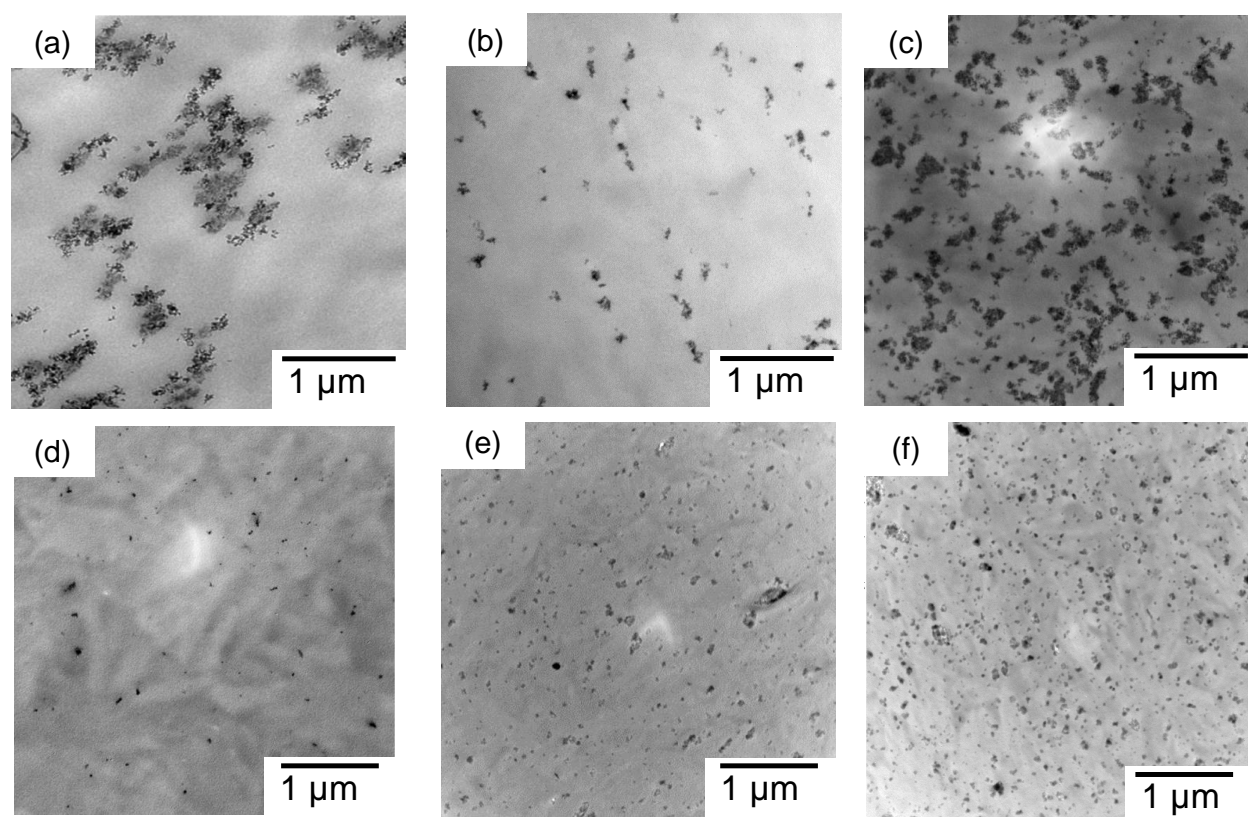
Figure 4.1. TEM micrographs of PP/Al$_2$O$_3$ nanocomposites: (a) NP (5.0 wt%), (b,c) PP-*g*-MA/NP (5.0 and 10 wt%) and (d-f) *in-situ* with pre-treatment under 80 °C and 100% RH for 24 h (5.0, 10, and 20 wt%).

In order to realize heat releasing plastics, one of the most effective ways is the addition of Al$_2$O$_3$ to polyolefin, in which the utilization of nanoparticles is expected to lower the filler loading, as long as the dispersion is controlled. As mentioned above, the reactor granule technology has its advantage in dispersing nano-sized Al$_2$O$_3$ irrespective of the filler loading. Therefore, the thermal conductivity of all the prepared PP/Al$_2$O$_3$ nanocomposites was

extensively examined. **Table 4.2** summarizes the value of different parameters which were

used to determine the thermal conductivity of *in-situ* and reference PP/Al$_2$O$_3$ nanocomposites.

Table 4.2. Physical properties of *in-situ* and reference PP/Al$_2$O$_3$ nanocomposites for thermal
conductivity calculation.

Sample	Loading (wt%)	ρ (g/cm^3)	C_p (J/g K)	α (mm^2/s)
Neat PP	0	0.89 ± 0.02	1.82 ± 0.02	0.130 ± 0.007
NP	5.0	1.02 ± 0.02	1.72 ± 0.02	0.135 ± 0.002
	10	1.16 ± 0.04	1.71 ± 0.01	0.145 ± 0.004
	20	1.48 ± 0.03	1.57 ± 0.02	0.153 ± 0.005
PP-*g*-MA/NP	5.0	1.06 ± 0.02	1.72 ± 0.05	0.138 ± 0.002
	10	1.17 ± 0.03	1.70 ± 0.01	0.148 ± 0.006
	20	1.48 ± 0.02	1.58 ± 0.03	0.157 ± 0.004
in-situ	5.0	1.04 ± 0.03	1.74 ± 0.03	0.145 ± 0.002
	10	1.18 ± 0.01	1.70 ± 0.02	0.158 ± 0.005
	20	1.50 ± 0.02	1.60 ± 0.01	0.170 ± 0.006
	30	1.80 ± 0.03	1.52 ± 0.02	0.224 ± 0.005

As can be seen, the value of specific heat capacity (C_p) and density (ρ) of nanocomposites

hardly changed among the different nanocomposites, but varied with the amount of filler

loading. However, at the same filler loading, the value of thermal conductivity was not same

for different type of samples as can be seen in **Fig. 4.2**. This change originated from the

variation in the value of thermal diffusivity (α), which is a measure of the transient thermal

response of a material to a change in temperature. When compared, it was found that the thermal diffusivity followed the order of PP/Al$_2$O$_3$ (*in-situ*) > PP/PP-*g*-MA/Al$_2$O$_3$ (NP) > PP/Al$_2$O$_3$ (NP) at all the filler loadings *i.e.* the same order with that of dispersion. Also, the thermal diffusivity increased with the filler loading. Considering both these facts, it was inferred that the thermal diffusivity was improved by shortening the organic pathway and maximizing the inorganic pathway during heat transfer which is possible due to the uniform dispersion of nanoparticles. Based on these results, we further aimed at exploiting Al$_2$O$_3$ based PP nanocomposites to further maximize the potential of reactor granule technology for the development of heat releasing polyolefin-based nanocomposites.
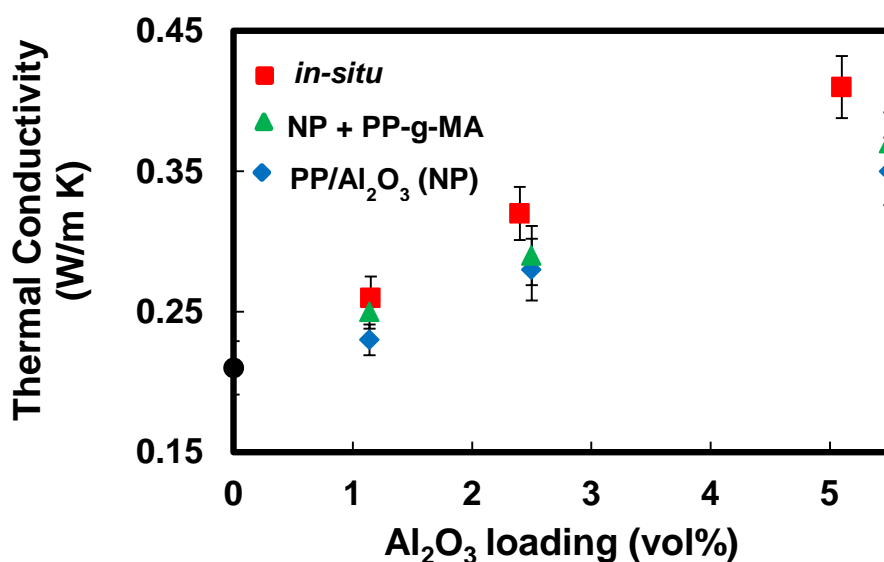

Figure 4.2. Thermal conductivity of *in-situ* and reference PP/Al$_2$O$_3$ nanocomposites at different filler loading.

Next, PP/Al$_2$O$_3$ nanocomposites prepared by dilution of highly filled reactor granule with neat PP were studied. Transmission FT-IR images of *in-situ* + PP nanocomposites are shown in **Fig. 4.3**.
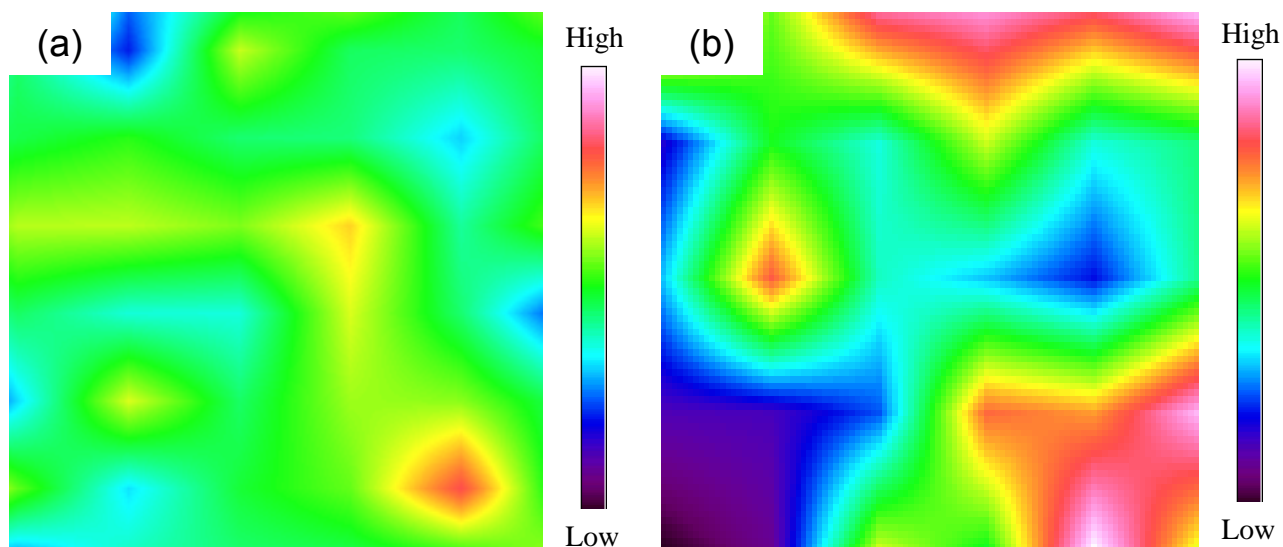

Figure 4.3. FTIR image mapping of (a) *in-situ* and (b) *in-situ* + PP nanocomposites (40 → 20 wt%).

The intensity scale associated with each image is such that blue and red extremes respectively correspond to low and high absorption values as given by spectral integration. The relative intensity of FT-IR band is proportional to the relative concentration of the components in a sample. Local concentration of Al$_2$O$_3$ was evaluated by the absorbance intensity of band related to alumina (500-650 cm^{-1}) normalized using the absorbance intensity of the C-H band of PP at around 960 cm^{-1}. FT-IR maps analysis of Al-O-Al band shows the distribution of Al$_2$O$_3$ in the nanocomposite sample, as blue and red colors indicate low and high Al$_2$O$_3$ contents in the sample, respectively. In the obtained IR maps, the concentration gradient was observed as expected due to the formation of Al$_2$O$_3$-rich and

Al_2O_3-poor domain in the nanocomposite on dilution of impregnated reactor granule with neat PP. On dilution, the overall (bulk) filler concentration does not change but the polymer-rich and filler rich domains are formed in which the respective concentration are significantly higher than the bulk concentration of polymer and filler respectively.

A seen above, the preparation protocol largely affected the thermal properties of the resultant nanocomposites. The effect of dilution of impregnated reactor granule with neat PP was assessed based on the thermal conductivity. The parameters for determination of thermal conductivity for the *in-situ* + PP nanocomposites are summarized in **Table 4.3** and the thermal conductivity values are shown in **Fig. 4.4**.

Table 4.3. Physical properties of *in-situ* + PP nanocomposites for thermal conductivity calculation.

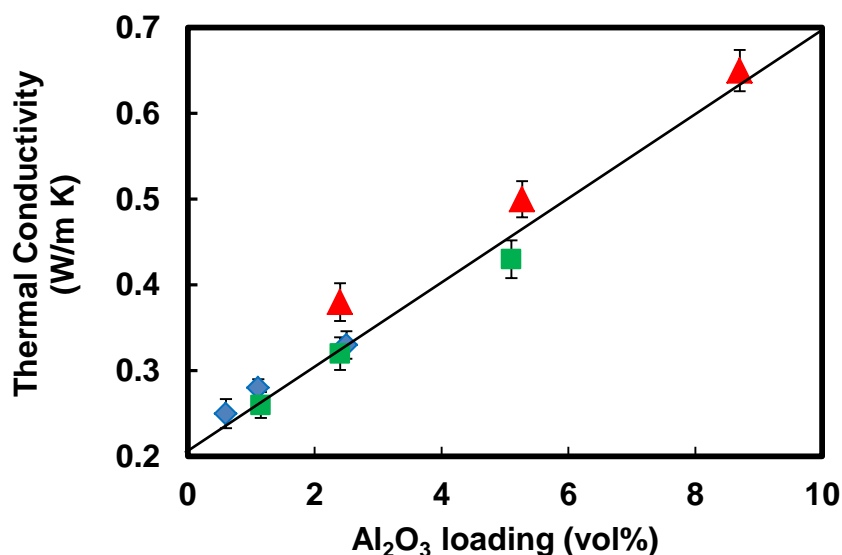| Sample	Loading (wt%)	ρ (g/cm^3)	C_p (J/g K)	α (mm^2/s)
in-situ + PP	40 →30	1.82 ± 0.01	1.51 ± 0.04	0.236 ± 0.01
	20	1.51 ± 0.03	1.59 ± 0.02	0.208 ± 0.02
	10	1.20 ± 0.03	1.68 ± 0.03	0.187 ± 0.03
in-situ + PP	20 → 10	1.18 ± 0.02	1.70 ± 0.03	0.163 ± 0.002
	5	1.05 ± 0.02	1.75 ± 0.02	0.152 ± 0.001
	3	0.98 ± 0.03	1.76 ± 0.03	0.148 ± 0.003

Figure 4.4. Thermal conductivity of PP/Al$_2$O$_3$ nanocomposites prepared by dilution of impregnated reactor granule with neat PP.

The positive trend in the values was obtained. When compared, at the filler loading of 20 wt%, the thermal conductivity for the "*in-situ* + PP" obtained was 0.50 vs 0.41 for the "*in-situ*" sample. The positive consequence of dilution was attributed to the fact that the addition of neat PP to impregnated reactor granule leads to the formation of filler-rich domains having a higher than bulk (average) filler concentration and polymer-rich domains having lower than bulk (average) filler concentration. The overall (bulk) concentration of the filler doesn't change, only the filler particles and the organic component are distributed into respective regions of higher concentrations. The areas of higher than average filler concentration can form semi-continuous or continuous pathways of conductive filler material extending

throughout the nanocomposite. These pathways provide a low resistance route through which thermal phonons can travel, resulting in enhanced values of thermal conductivity. The ability of the impregnated reactor granule as dispersant was evaluated by means of thermal conductivity. The required parameters are summarized in **Table 4.4** and the thermal conductivity is depicted in **Fig. 4.5.** When the pre-formed nanoparticles were added to the reactor granule containing Al(O*i*Pr)$_3$ at 10 wt%, the thermal diffusivity obtained was 0.40. It was found that the value of "*in-situ* + NP" is higher than that of "PP/PP-*g*-MA/Al$_2$O$_3$-NP". This originated due to the fact that the dispersion of nanoparticles was much more improved upon the addition of impregnated granule as compared when the nanoparticles are directly melt-mixed in the presence of a compatibilizer. Thus, the impregnated reactor granule has a better dispersing ability for the pre-formed nanoparticles.

Table 4.4. Physical properties of *in-situ* + NP nanocomposites for thermal conductivity calculation.

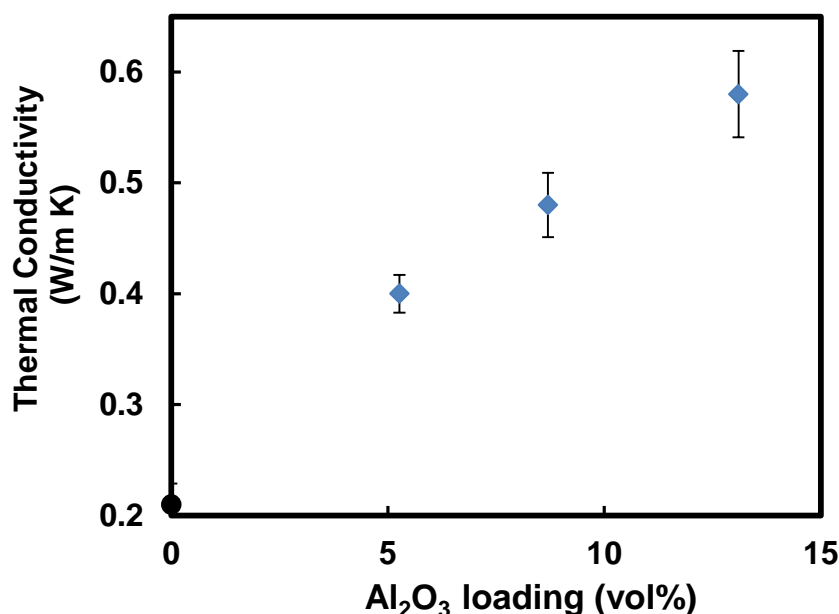| Sample	Loading (wt%)	ρ (g/cm^3)	C_p (J/g K)	α (mm^2/s)
	20	1.52 ± 0.03	1.60 ± 0.02	0.165 ± 0.002
in-situ + NP	30	1.81 ± 0.02	1.50 ± 0.03	0.178 ± 0.005
	40	2.10 ± 0.02	1.42 ± 0.03	0.195 ± 0.003

Figure 4.5. Thermal conductivity of PP/Al₂O₃ nanocomposites prepared by the addition of impregnated granule to preformed nanoparticle.

The effectiveness of DTMS as interfacial modifier was evaluated in terms of thermal diffusivity and conductivity. The parameters required for the evaluation of thermal conductivity of the samples prepared by the addition of DTMS as interfacial modifier are summarized in **Table 4.5** and the thermal conductivity values are shown in **Fig. 4.6**. Different amounts of DTMS corresponding to Si/Al ratio as 0.006, 0.03 and 0.06 mol/mol were added and their effect on thermal conductivity was assessed. It was found that on increasing the amount of DTMS from 0.006 to 0.03 mmol, the thermal conductivity increased but there was no significant change in the values on increasing the DTMS content from 0.03 and 0.06 mmol, indicating that 0.03 mmol of DTMS was sufficient. The increase in values of thermal conductivity is attributed to the improved interfacial interaction between the PP and *in-situ* generated Al₂O₃ nanoparticles.

Table 4.5. Physical properties of *in-situ* + DTMS nanocomposites for thermal conductivity calculation.

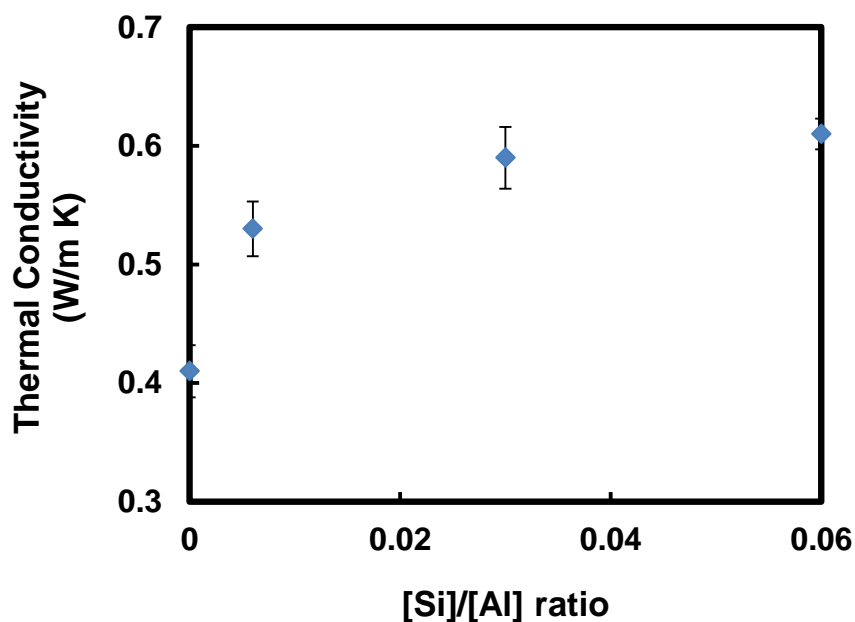| Sample	Amount of DTMS (mmol)	ρ (g/cm^3)	C_p (J/g K)	α (mm^2/s)
	0.0	1.50 ± 0.02	1.60 ± 0.01	0.170 ± 0.06
	0.006	1.52 ± 0.03	1.62 ± 0.02	0.214 ± 0.02
in-situ + DTMS	0.03	1.53 ± 0.02	1.62 ± 0.03	0.240 ± 0.03
	0.06	1.55 ± 0.01	1.63 ± 0.01	0.242 ± 0.02

Figure 4.6. Thermal conductivity of PP/Al$_2$O$_3$ nanocomposites prepared using DTMS as interfacial modifier.

4.4. Conclusion

In this study, we aimed at maximizing the potential of reactor granule technology for the development of thermally conductive polyolefin-based nanocomposites. To achieve this, three different strategies were applied. The first one was based on the formation of filler-rich and polymer-rich domains by the dilution of impregnated granule with neat PP. FT-IR image mapping confirmed the presence of filler-rich and polymer-rich domains in the resultant PP/Al$_2$O$_3$ nanocomposites. The second strategy aimed at evaluating the dispersing ability of impregnated reactor granule for the preformed Al$_2$O$_3$ nanoparticles. The last one employed silane coupling agent as interfacial modifier for the *in-situ* generated Al$_2$O$_3$ nanoparticles. From the results of *in-situ* and reference PP/Al$_2$O$_3$ nanocomposites, it was found that the preparation protocol largely affected the thermal properties of the resultant nanocomposites. The effectiveness of the employed strategies was studied in terms of thermal diffusivity and conductivity. The results indicated that the formation of Al$_2$O$_3$-rich and Al$_2$O$_3$-poor domain resulted in the improvement of thermal conductivity. Among the three strategies employed, the interfacial modification of *in-situ* generated Al$_2$O$_3$ nanoparticles was most effective in improving the thermal conductivity.

4.5. References

[1] J. Miranda, R. Yang, Effect of a metallic coating on the thermal conductivity of carbon nanofiber-dielectric matrix composites, Compos Sci Technol. 109 (2015) 18-24.

[2] K.T. Regner, J. Freedman, J. Malen, Advances in studying phonon mean free path dependent contributions to thermal conducitivity, Nanosc Microsc Therm, 19 (2016) 183-205.

[3] J. D. Renteria, D. L. Nika, A. A. Balandin, Graphene thermal properties: applications in thermal management and energy storage, Appl. Sci 4 (2014) 525-547.

[4] I. Ngo, C. Byon, A generalized correlation for predicting the thermal conductivity of composites with heterogeneous nanofillers, Int. J. Heat Mass Transfer 90 (2015) 894-899.

[5] R. Paresher, Thermal interface materials: Historical perspective, status, and future directions, Proc. IEEE 94(2006) 1571.

[6] H. Liem, H. Choy, Superior thermal conductivity of polymer nanocomposites by using graphene and boron nitride as fillers, Solid State Commun 163 (2013) 41-45.

[7] N. Burger, A. Laachachi, B. Mortazavi, M. Ferriol, M. Lutz, D. Ruch, Alignment and network of graphite fillers to improve thermal conductivity of epoxy-based nanocomposites, Int. J. Heat Mass Transfer 89 (2015) 505-513.

[8] R. Qian, J. Yu, C. Wu, Alumina-coated graphene sheet hybrids for electrically insulating polymer composites with high thermal conductivity, RSC Adv.3 (2013) 17373-17379.

[9] Z. Han, A. Fina, Thermal conductivity of carbon nanotubes and their polymer nanocomposites: A review, Prog. Polym. Sci. 36 (2011) 914-944.

[10] C. Min, D. Yu, J. Cao, A graphite nanoplatelet/epoxy composite with high dielectric constant and high thermal conductivity, Carbon, 55 (2013) 116-125.

[11] X. Huang, X. Qi, F. Boey, Graphene-based composite, Chem. Soc. Rev. 41 (2012) 666-686.

[12] T. Li, S. L. Hsu, Enhanced Thermal Conductivity of Polyimide Films via a Hybrid of Micro- and Nano-Sized Boron Nitride, J. Phys. Chem. B,114 (2010) 6825-6829.

[13] M. Harada, N. Hamaura, M. Ochi, Thermal conductivity of liquid crystalline epoxy/BN filler composites having ordered network structure, Composites Part B 55(2013) 306.

[14] W. Peng, X. Huang and J. Yu, Electrical and thermophysical properties of epoxy/aluminum nitride nanocomposites: Effect of nanoparticle surface modification Composites, Part A 41(2010) 1201-1209.

[15] S. Gupta, P. C. Ramamurthy and G. Madras, Synthesis and characterization of flexible epoxy nanocomposites reinforced with amine functionalized alumina nanoparticles: a potential encapsulant for organic devices, Polym. Chem. 2 (2011) 221-228.

[16] H. Chen, V. V. Ginzburg, J. Yang, Y. Yuang, W. Liu, Y. Hang, L. Du, B. Chen, Thermal conductivity of polymer-based composites: Fundamentals and applications, Prog. Polym. Sci. 59 (2016) 41-85.

[17] C. Yuan, B. duan, L. Li, B. Xie, M. Huang, X. Luo, Thermal conductivity of polymer-based composites with magnetic aligned hexagonal boron nitride paltelets, ACS Appl. Mater. Interfaces, 7 (2015) 13000-13006.

[18] L.C. Sim, S.R. Ramanan, H. Ismail, K.N. Seetharamu, T.J. Goh, Thermal characterization of Al_2O_3 and ZnO reinforced silicone rubber as thermal pads for heat dissipation purposes, Thermochim. Acta. 430 (2005) 155-165.

[19] W. Zhou, C. Wang, J. Kou, Effect of the particle size of Al_2O_3 on the properties of filled heat-conductive silicone rubber, J Appl Polym Sci. 104 (2007) 1312-18.

[20] C. I. Idumah, A. Hassan, Recently emerging trends in thermal conductivity of polymer nanocomposites, Rev. Chem. Eng. 32 (2016) 413-457.

[21] X. Huang, P. Jiang, L. Xie, Ferroelectric polymer/silver nanocomposites with high dielectric constant and high thermal conductivity, Appl. Phys. Lett. 95 (2009) 242901-242903.

[22] B. Maira, P. Chammingkwan, M. Terano, T. Taniike, New reactor granule technology for highly filled nanocomposites: effective flame retardation of polypropylene/magnesium hydroxide nanocomposites, Macromol. Mater. Eng. 300 (2015) 679-683.

[23] Y. Yao, X. Zeng, K. Guo, J. Xu, The effect of interfacial state on the thermal conductivity of functionalized Al_2O_3 filled glass fibers reinforced polymer composites, Compos Part A Appl. Sci. Manuf. 100 (2015) 37-44.

[24] M. Wong, M. Paramsothy, X.J. Xu, Y. Ren, S. Li, K. Liao, Physical interactions at carbon nanotube-polymer interface, , Polymer 44 (2003) 7757-7764.

[25] J. Yu, X. Huang, Chao Wu, X. Wu, G. Wang, P. Jiang, Interfacial modification of boron nitride nanoplatelets for epoxy composites with improved thermal properties, Polymer 53 (2012) 471-480.

[26] Y. Lei, Z. Tang, L Guo, L. Zhu, D. Jia, Functional thiol ionic liquids as novel interfacial modifiers in SBR/HNTs composites, Polymer 52 (2011) 1337-1344.

[27] M. Bhattacharya, A. K. Bhowmick, Polymer–filler interaction in nanocomposites: New interface area function to investigate swelling behavior and Young's modulus, Polymer 49 (2008) 4808-4818.

Chapter 5

General Summary and Conclusions

Chapter 5

In this thesis, in ***Chapter 2***, a novel reactor granule technology based on pore confinement concept for the *in-situ* fabrication of polyolefin-based nanocomposites in a dispersant-free manner has been disclosed. A molecular precursor of fillers is impregnated in the porosity of reactor granule and subsequently converted into dispersed nanoparticles in melt-processing. The successful application of the methodology for the fabrication of $PP/Mg(OH)_2$ nanocomposites has been demonstrated. It was found that the hydrolysis of impregnated magnesium alkoxide prior to melt mixing enables good dispersion of $Mg(OH)_2$ nanoparticles even at a high filler loading over 10 wt%. The prepared nanocomposites achieved a self-extinguishing level in flame retardation at 20-30 wt%, in comparison to 60 wt% for conventional $PP/Mg(OH)_2$ composites. The results revealed that the methodology not only offers uniform dispersion of nanoparticles in a dispersant-free manner, but also allows an access for the fabrication of highly filled nanocomposites. I believe that the study presented in ***Chapter 2*** is one of the rare examples that successfully exploit the great potential of polyolefin-based nanocomposites in a simple and versatile process and can be easily extended to similar nanocomposite materials.

To generalize the reactor granule technology to various kinds of highly filled nanocomposites, in ***Chapter 3***, the reactor granule technology was applied for fabrication of functionally advantageous PP nanocomposites with oxide nanoparticles, namely PP/TiO_2 and PP/Al_2O_3 nanocomposites. Firstly, the synthetic aspects of highly filled PP/TiO_2 and PP/Al_2O_3 nanocomposites were demonstrated. From SEM and EPMA analysis, it was

proved that the porosity plays an important role in effective confinement and pre-dispersion of the molecular precursors. Furthermore, a hydrolytic pre-treatment was found to be crucial for the solidification of precursors in the porosity of PP reactor granule and for achieving excellent dispersion of nanoparticles at higher filler loading. Next, the advantages of reactor granule technology with focus on PP/Al_2O_3 nanocomposites were examined in terms of application-oriented properties. The excellent dispersion of Al_2O_3 nanoparticles led to significant improvement of mechanical properties of PP when compared to conventional composites. It was found that the dispersion state mainly affected the thermal conductivity of the resultant nanocomposites. At 20 wt% of filler loading, the thermal conductivity of nanocomposites was almost double to that of neat PP. From the study presented in **Chapter 3**, it can be concluded that the reactor granule technology is a versatile approach for the fabrication of polyolefin-based nanocomposites, offering excellent dispersion over a wide range of filler loading and superior properties even without the use of any dispersants.

In **chapter 4**, the development of heat releasing polyolefin nanocomposites based on reactor granule technology is presented. Three different strategies were applied: i) the first one is based on the idea of forming filler-rich and polymer-rich domains in the resultant nanocomposites by diluting highly filled reactor granule with neat PP; ii) examining the dispersing ability of impregnated reactor granule as dispersant for pre-formed nanoparticles at elevated filler loadings; and iii) employing silane coupling agent as interfacial modifier for

the *in-situ* generated Al_2O_3 nanoparticles. The effectiveness of the three employed strategies was studied based on the thermal diffusivity and conductivity of the resultant nanocomposites. Form the study presented in *Chapter 4*, it was concluded that impregnated reactor granule serve as suitable masterbatch for the preparation of functionalized polyolefin grades. The usage of silane coupling agent improved the thermal conductivity of resultant PP/Al_2O_3 nanocomposites and is attributed to the improved interfacial interaction between Al_2O_3 nanoparticles and PP matrix. Among the employed strategies, use of silane coupling agents proved to be most effective in the formulation of high thermally conductive polyolefin-based nanocomposites.

I believe that the research work carried out in this thesis has established a novel and promising route for the fabrication of functionally advantageous nanostructured polymer nanocomposites in a simple and efficient manner. Furthermore, I have solved a few of the major challenges in the field of general polymer composites and hybrids such as a) use of dispersants to achieve nano-level dispersion, b) dispersion problem at high filler loading and c) problem in traditional compounding of thermoplastics in order to offer fabrication of a variety of value-added grades. This technology is also expected to be applicable for other polymers with porous architecture.

List of Publications and Other Achievements

Bulbul Maira

A) <u>Publications</u>

1. New Reactor Granule Technology for Highly Filled Nanocomposites: Effective Flame Retardation of Polypropylene/Magnesium Hydroxide Nanocomposites
   <u>Bulbul Maira</u>, Patchanee Chammingkwan, Minoru Terano and Toshiaki Taniike, Macromolecular Materials and Engineering, **2015**, 300, 679-683.

2. Reactor Granule Technology for Fabrication of Functionally Advantageous Polypropylene Nanocomposites with Oxide Nanoparticles
   <u>Bulbul Maira</u>, Patchanee Chammingkwan, Minoru Terano and Toshiaki Taniike, Composites Science and Technology, **2017**, 144, 151-159.

3. Templated Synthesis of Nano-Sized Silica in Confined Amorphous Space of Polypropylene
   Kengo Takeuchi, <u>Bulbul Maira</u>, Minoru Terano and Toshiaki Taniike, Composites Science and Technology, **2017**, 140, 1-7.

4. Versatile Strategy for Fabrication of Polypropylene Nanocomposites with Inorganic Network Structures based on Catalyzed in-situ Sol-Gel Reaction during Melt Mixing
   Kei Kaneko, Nitin Yadav, Kengo Takeuchi, <u>Bulbul Maira</u>, Minoru Terano, Toshiaki Taniike, Composites Science and Technology, **2014**, 102, 120-125.

B) <u>Domestic Conferences</u>

1. **Oral Presentation**: Fabrication and properties of highly filled PP/Al$_2$O$_3$ nanocomposites based on reactor granule technology; <u>B.Maira</u>, P. Chammingkwan, M. Terano and T. Taniike, **27th Materials Life Society**, Hikone, Japan, 14-15 July, 2016.

2. **Oral Presentation**: Versatile new reactor granule technology for fabrication of polyolefin-based nanocomposites and its application to PP/Al$_2$O$_3$ nanocomposites; <u>B.Maira</u>, P. Chammingkwan, M. Terano and T. Taniike, **The SPSJ 65th Symposium on Macromolecules**, Yokohama, Japan, 14-16 September, 2016.

B) <u>International Conferences</u>

1. **Poster presentation:** New reactor granule technology for fabrication of polypropylene/magnesium hydroxide nanocomposites with improved dispersion and properties; <u>B.Maira</u>, P. Chammingkwan, M. Terano and T. Taniike, **JAIST Japan-India Symposium on Materials Science 2015**, Nomi, Japan, 2-3 March, 2015.

2. **Oral Presentation:** Fabrication of functionally advantageous polyolefin-based nanocomposites by employing new reactor granule technology; <u>B.Maira</u>, P. Chammingkwan, M. Terano and T. Taniike, **10th International Symposium on Weatherability**, Ota, Japan, 2-3 July, 2015.

3. **Oral and Poster Presentation**: New reactor granule technology for fabrication of functionally advantageous highly filled nanocomposites; <u>B.Maira</u>, P. Chammingkwan, M. Terano and T. Taniike, **The World Polyolefin Congress 2015 (WPOC 2015**), **Tokyo**, Japan, 23-27 November, 2015.

4. **Poster Presentation:** Fabrication of functionally advantageous highly filled nanocomposites by employing new reactor granule technology; B.Maira, P. Chammingkwan, M. Terano and T. Taniike, **Pacifichem 2015**, Honolulu, USA, 15-20 December, 2015.

5. **Poster Presentation:** Versatile new reactor granule technology for fabrication of polyolefin-based nanocomposites and its application to PP/Al_2O_3 Nanocomposites; B.Maira, P. Chammingkwan, M. Terano and T. Taniike, **The 4th Blue Sky Conference on catalytic olefin polymerization**, Sorrento, Italy, 27 June-1 July, 2016.